1973

Rock fragmentation by subsurface thermal inclusions - a finite element study

Mahendrakumar Ramkrishna Patel

Department: Mechanical and Aerospace Engineering

ROCK FRAGMENTATION BY SUBSURFACE THERMAL INCLUSIONS - A FINITE ELEMENT STUDY

by

MAHENDRAKUMAR RAMKRISHNA PATEL, 1947-

A DISSERTATION

Presented to the Faculty of the Graduate School of the

UNIVERSITY OF MISSOURI-ROLLA

In Partial Fulfillment of the Requirements for the Degree

DOCTOR OF PHILOSOPHY

in

MECHANICAL ENGINEERING

1973

Jerry F. Lehnhoff
Advisor

Clark R Barker

Peter G. Hansen

R. J. Pence

ABSTRACT

Although rock tunneling machines are being used extensively with performance and cost advantages over traditional drill and blast methods, their usefulness for hard rock excavation is far from being practical due mainly to the inability of present day mechanical cutters to penetrate these rocks economically. Among various novel techniques that are being investigated, internal heating methods seem to be the most promising. This investigation is concerned with a feasibility study of thermal rock fragmentation using heat to create in-depth thermal inclusions.

The three-dimensional problem of in situ rock fragmentation involves parallel rows of equidistant holes drilled to a constant depth. Thermal inclusions are created at the bottoms of these holes. The nature of the temperature and resulting stress field is such that the rock is first fractured along the line of a series of holes. A second and very important fracture occurs on a plane perpendicular to the hole axes passing through the thermal inclusion. This fracture is parallel to the working face and makes possible the removal of a layer equal to the depth of the thermal inclusions.

Two two-dimensional models were obtained by passing cutting planes through and perpendicular to the hole axes. These models were used to study the process parameters; hole diameter, hole spacing and hole depth. Hard rock was characterized as a linearly elastic, homogeneous, isotropic brittle material, and the problem was formulated within the framework of the linear, uncoupled theory of

thermoelasticity. For the temperature analysis, average thermal properties were used, whereas thermoelastic properties for stress analysis were allowed to vary with the temperature. Temperature and stress results were obtained through finite element approximations. A finite element code was developed for the transient thermal stress studies. Fracture predictions are based on the Griffith and the McClintock-Walsh modified Griffith fracture criteria.

Hole spacing and the melt-free depth were found to be the most influencial parameters governing the fracture. Also, the optimum melt-free depth was found to be related to the hole spacing and thus, the fragmentation configuration can be optimized by a proper choice of the single parameter, the hole spacing.

The optimum location of the subsurface fracture parallel to the working face and the fracture time were found to be associated with hole depth at least equal to half the difference between the hole spacing and the hole diameter with the thermal inclusions concentrated at the very base of the holes. Although any further increase in the hole depth was found to have a negligible effect on the location and the fracture time of the parallel cracks, it will mean that the heat source will have a greater burden against which to open cracks between the holes. The optimum hole depth therefore seems to be one associated with very small melt length and a melt-free depth equal to approximately half the difference between the hole spacing and the hole diameter.

For the optimum location of the parallel fracture of Dresser basalt, the dimensionless fracture time ratio, t_f^*, was found to be

related to the dimensionless fracture length ratio, L^*, according to the equation, $t_f^* = L^{*2.7}$.

This power relationship suggests that the optimum fragmentation configuration should involve small hole spacings.

The theoretically predicted fracture patterns and the fracture length - fracture time relationships were found to be in good agreement with those observed in field tests.

ACKNOWLEDGEMENTS

The author wishes to express sincere appreciation to his advisor, Dr. Terry F. Lehnhoff for his guidance and helpful suggestions which contributed greatly to this research. Gratitude is also due to the Ph.D. advisory committee members, Drs. G. B. Clark, P. G. Hansen, C. R. Barker, and A. J. Penico. Thanks are also extended to Dr. H. D. Keith of the Department of Engineering Mechanics and the personnel of the Computer Science Center for their helpful suggestions and cooperation during the course of the numerical analysis phase of this research.

The author is deeply grateful to the Rock Mechanics and Explosives Research Center, the Department of Mechanical Engineering, and the Department of Engineering Mechanics for the financial support provided in the form of Graduate Research and Teaching Assistantships.

Special appreciation is extended to Mr. Jaw K. Wang who is responsible for the figures, and finally, to my wife Mina for her unending encouragement throughout the course of this work.

TABLE OF CONTENTS

Page

ABSTRACT.....ii

ACKNOWLEDGEMENTS.....v

LIST OF ILLUSTRATIONS.....viii

LIST OF TABLES.....xi

NOMENCLATURE.....xii

I. INTRODUCTION.....1

II. ROCK CHARACTERISTICS AND APPROXIMATIONS.....12

A. General Classification.....12

B. Nonlinearity Considerations.....13

1. Stress-strain Behavior.....14

2. Homogeneity and Isotropy.....15

3. Crack Effects.....16

4. Temperature Effects.....17

a. Thermoelastic Properties.....18

b. Fracture Mechanisms.....23

C. Fracture Theories.....24

1. Griffith Theory.....24

2. McClintock-Walsh Modification.....27

D. Properties Used in Analytical Studies.....29

1. Temperature Analysis.....30

2. Stress Analysis.....33

3. Fracture Predictions.....36

Table of Contents (continued) Page

III. MATHEMATICAL FORMULATION AND METHOD OF ANALYSIS.....38
A. Heat Conduction Problem.....38
B. Stress Problem.....43
C. Fracture Analysis.....46
D. Summary.....49
IV. SLOT MODEL ANALYSES.....50
A. Grid Size Effects.....52
B. Melt Depth Studies.....52
C. Convection Depth Studies.....61
D. Hole Diameter and Spacing Studies.....72
1. Temperature Field Characteristics.....73
2. Fracture Length Effects.....77
E. Fracture Length - Fracture Time Relation.....78
V. HOLE MODEL ANALYSIS.....91
A. Temperature Analysis.....92
B. Stress and Fracture Analysis.....94
VI. CONCLUSIONS AND RECOMMENDATIONS.....103
BIBLIOGRAPHY.....109
VITA.....114
APPENDICES
A. STRESS CODE, TRATSA - INPUT INSTRUCTIONS AND PROGRAM LISTING.....115
B. FRACTURE CODE - INPUT INSTRUCTIONS AND PROGRAM LISTING.....143
C. FIELD TEST RESULTS.....153

LIST OF ILLUSTRATIONS

Figure — Page

1.1 Three Dimensional Hole Configuration for Thermal Rock Fragmentation....5

1.2 Slot Configuration for Displacement Relief....6

1.3 Two Dimensional Plane Models....8

1.4 Typical Section for Hole Model Analysis....9

1.5 Typical Section for Slot Model Analysis....10

2.1 Thermal Conductivity of Holocrystalline Rocks....19

2.2 Specific Heat Value of High-SiO_2 Rock Types....21

2.3 Average Linear Expansion of Igneous Rocks....22

2.4 Variation of Conductivity of Dresser Basalt with Temperature....31

2.5 Variation of Diffusivity of Dresser Basalt with Temperature....31

2.6 Fragmentation Potential of Dresser Basalt at Elevated Temperatures....35

2.7 Nonlinearity Coefficient of Dresser Basalt at Elevated Temperatures....35

3.1 Nomenclature for Plane Models....39

4.1 Typical Finite Element Grid for the Slot Model Analysis....53

4.2 Temperature Distribution, Model 1A-1, t = 60 sec....55

4.3 Temperature Distribution, Model 1A-2, t = 60 sec....56

4.4 Temperature Distribution, Model 1A-3, t = 60 sec....57

4.5 Temperature Distribution, Model 1A-1, t = 120 sec....58

List of Illustrations (continued)

Figure Page

4.6 Temperature Distribution, Model 1A-2, t = 120 sec.....59

4.7 Temperature Distribution, Model 1A-3, t = 120 sec.....60

4.8 Fracture Zones, Model 2A.....63

4.9 Fracture Zones, Model 2A-1.....64

4.10 Fracture Zones, Model 2A-2.....65

4.11 Fracture Zones, Model 2B.....66

4.12 Fracture Zones, Model 2B-1.....67

4.13 Fracture Zones, Model 2C.....68

4.14 Fracture Zones, Model 2C-1.....69

4.15 Fracture Zones, Model 2C-2.....70

4.16 Temperature Distribution, Model 1A.....74

4.17 Temperature Distribution, Model 2B.....75

4.18 Temperature Distribution, Model 3C.....76

4.19 Fracture Zones, Model 3A.....79

4.20 Fracture Zones, Model 3B.....80

4.21 Fracture Zones, Model 3C.....81

4.22 Fracture Time - Spacing Curves for Slot Models.....82

4.23 Fracture Zones, Model 11A.....83

4.24 Fracture Zones, Model 13B.....84

4.25 Fracture Zones, Model 13C.....85

4.26 Fracture Zones, Model 1A.....86

4.27 Dimensionless Fracture Time - Length Relationship.....90

5.1 Typical Finite Element Grid for Hole Model Analysis.....93

List of Illustrations (continued)

Figure Page

5.2 Temperature Distribution, Model 22A.....95

5.3 Temperature Distribution, Model 22B.....96

5.4 Temperature Distribution, Model 22C.....97

5.5 Fracture Zones, Model 22A.....98

5.6 Fracture Zones, Model 22B.....99

5.7 Fracture Zones, Model 22C.....100

5.8 Fracture Time - Spacing Curves for Hole Models.....102

C.1 Three- and Four-Hole Field Test Configurations.....155

C.2 Four-Hole Field Test and Typical Resulting Excavation.....156

C.3 View of an Excavation After Removal of a Fragmented Block...156

LIST OF TABLES

Table — Page

I. Property Data Used in Temperature Analysis of Dresser Basalt....32

II. Property Data Used in Stress Analysis of Dresser Basalt....33

III. Properties of Basalt Used for Fracture Predictions....37

IV. Parametric Description of Slot Models....51

V. Fracture Times for Slot Models with $a_c \simeq L/2$....87

VI. Fracture Length and Fracture Time Ratios for Slot Models with Convection Depths Approximately Equal to Half the Fracture Length....89

VII. Parametric Description of Hole Models....92

NOMENCLATURE

A = Hole depth, in.

a = Melt depth, in.

a_c = A - a, Melt-free or convection depth, in.

c = Specific heat, cal/gm-°C; Hole spacing, in.

d = Hole diameter, in.

E = Young's modulus, psi

h = Surface convection coefficient, cal/cm^2-sec-°C

k = Conductivity, cal/cm-sec-°C

L = c - d, fracture length, in.

T = Temperature, °C

T_m = Melt temperature, °C

t = Time, sec.

t_f = Fracture time, sec.

x,y = Spacial coordinates

α = Coefficient of thermal expansion, 1/°C

κ = Diffusivity, cm^2/sec.

μ = Internal coefficient of friction between the crack faces

μ_f = Fracture surface coefficient of friction

ν = Poisson's ratio

ρ = Density, gm/cm^3

σ_1 = Major principal stress component, psi

σ_3 = Minor principal stress component, psi

σ_c = Compressive strength of material, psi (-)

σ_n = Normal stress component, psi

σ_t = Tensile strength of material, psi (+)

CHAPTER I

INTRODUCTION

Rock fragmentation is a basic requirement in mining and tunneling operations. A selection of a suitable method for fragmentation is based, among other factors, on economic and practical operating requirements. Rock tunneling machines are being used extensively in both soft and medium-hard rock conditions with performance and cost advantages over traditional drill-and-blast methods which suffer from being cyclic in nature, and also from overbreak into walls, and noise problems. However, these machines have not yet been found practical for operation in the relatively hard rocks due mainly to the inability of present day mechanical cutters to penetrate these rocks economically. New methods of rock removal either independent or usable in conjunction with these machines have therefore been under investigation. A great amount of work is currently being done to examine the possibility of using surface and internal heating methods for efficiently and economically removing the rock.

Heat can be used to weaken, spall, and/or melt rock. When heat sources are used to excavate hard rock by melting, very large quantities of thermal energy are required, and for removal of rock by spallation the process is usually limited to types of spallable rocks composed of a minimum of ten percent quartz [1,2]*. The combination of thermal weakening/spalling and mechanical disintegration appears to offer a promising potential for hard rock excavation. Thus, many of

*Numbers in brackets designate references.

the current investigations of heat-assisted rock fragmentation are aimed at evaluating the effectiveness of various modes of heating in terms of their weakening effects on hard rocks rather than rock fragmentation by thermal energy alone [3,4].

Various methods of drilling and breaking rock by thermal means are described by Maurer [5]. Included among these methods are jet piercing (flame jet), microwave radiation, induction and electric arc heating, nuclear heating (penetration), plasma jets, electron beams, and lasers. Carstens [6] reviewed several of these methods in 1972, and described an additional method, proposed by Thirumalai [7], of forming an internal thermal inclusion and fracturing rock. Considerable research has been accomplished in the past four years, particularly on electron beams [8], lasers [9,10], flame jets [3,11-13], high temperature penetrators [14], and resistance wire and electric arc heaters [15]. Of these various surface and internal heating methods, those involving the internal thermal inclusion are shown to be most promising for the near future [7,15].

Thirumalai [7] was the first to report on a method of formation of a controlled internal thermal inclusion, in this instance by dielectric heating. Laboratory test blocks of charcoal granite and Dresser basalt, somewhat larger than one foot on a side were successfully fragmented without melting by localized heating below 600°C, the heated volume being less than 2 percent of the total rock volume. However, Jasper quartzite blocks could not be fragmented because of their poor response to dielectric heating.

This drawback was successfully overcome by Clark et al. [15] who employed high energy output electric heaters to form the thermal inclusion by inducing local melting. In the initial phase of this current research, coiled wire resistance heaters made of Kanthal wire operating at 1000°C were found to fracture hard granite when they were placed in pneumatically drilled holes, but heaters failed after short term usage. Electric arcs from carbon electrodes were found to generate effective thermal inclusions in solid granite.

Thermal inclusions using the electric arcs in multiple holes have been found to create thermal stress fields which will fracture over distances of two feet or more at reasonable electrical energy levels. Tests to date have yielded promising results for application.

The objective of this thesis investigation is to theoretically supplement the thermal fragmentation project described above, and to provide guidelines for the optimization of significant process parameters.

Theoretical Models

The cost of experimentally studying the various parameters of most engineering systems justifies simplified theoretical studies which provide guidance for the optimal design of such systems. It is often of value to be able to confirm theoretically certain unusual phenomena which have been observed experimentally. The mechanics of the thermal mechanical rock fragmentation system considered here are typical in that full scale tests are difficult and expensive.

The actual fragmentation system is three-dimensional. Figure 1.1 shows a semi-infinite region with equally spaced holes. The holes are drilled to a constant depth over the area where rock is to be removed. Heat sources are placed at the bottoms of the drilled holes. The resulting thermal inclusions (heated zones) cause two types of fractures, one of which is along planes containing the axes of the rows of holes. A more important fracture occurs parallel to the working face (perpendicular to the hole axes) at approximately the depth of the inclusions. This fracture pattern makes possible the removal of rectangular blocks of rock, the block dimensions being determined by the hole spacing and the depth of the thermal inclusions. To facilitate fracture and removal of the rock, free surfaces in the form of slots as shown in Fig. 1.2 are required. The slots can possibly be cut by several different means. Drilling tangent or over lapping holes is one method which has been explored. Other possible methods include water jets, electron beams, plasma jets, lasers and other novel techniques. Employing heaters for pyramid cuts or in a spiral round similar to the way explosives are used is possible. However, the theoretical studies assume no displacement relief.

A complete theoretical analysis of the mechanics of the process requires a transient temperature, thermal stress and fracture study of the three-dimensional geometry shown in Fig. 1.1. The problem is nonlinear in the sense that the thermal and elastic properties of most rocks are highly dependent on temperature.

To study the fracture or fragmentation problem two alternatives to the method selected have been considered. The first and best

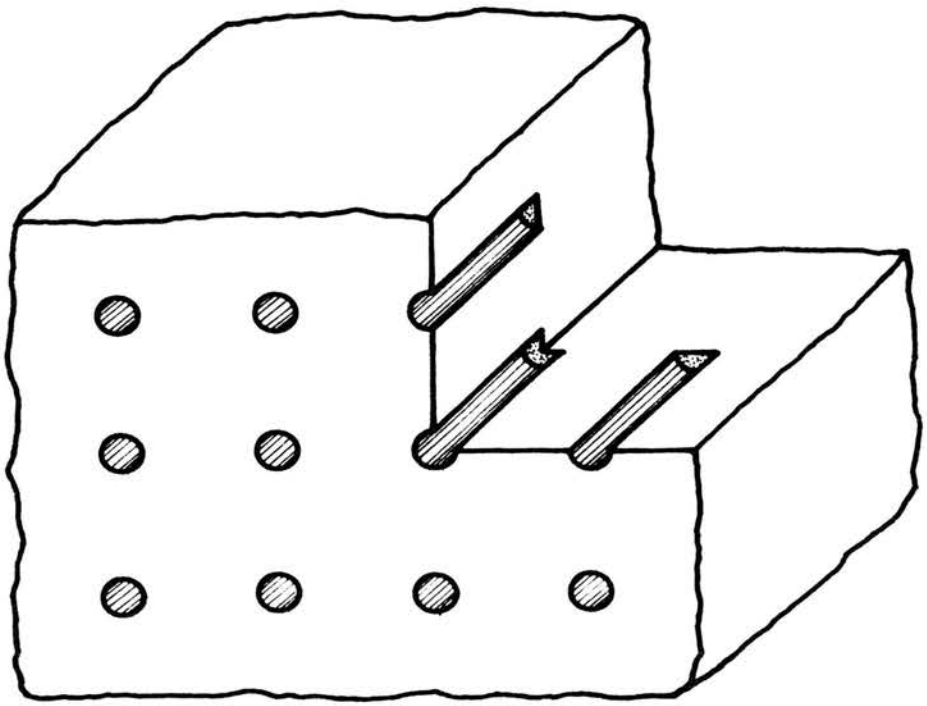

FIG. 1.1 THREE DIMENSIONAL HOLE CONFIGURATION FOR THERMAL ROCK FRAGMENTATION

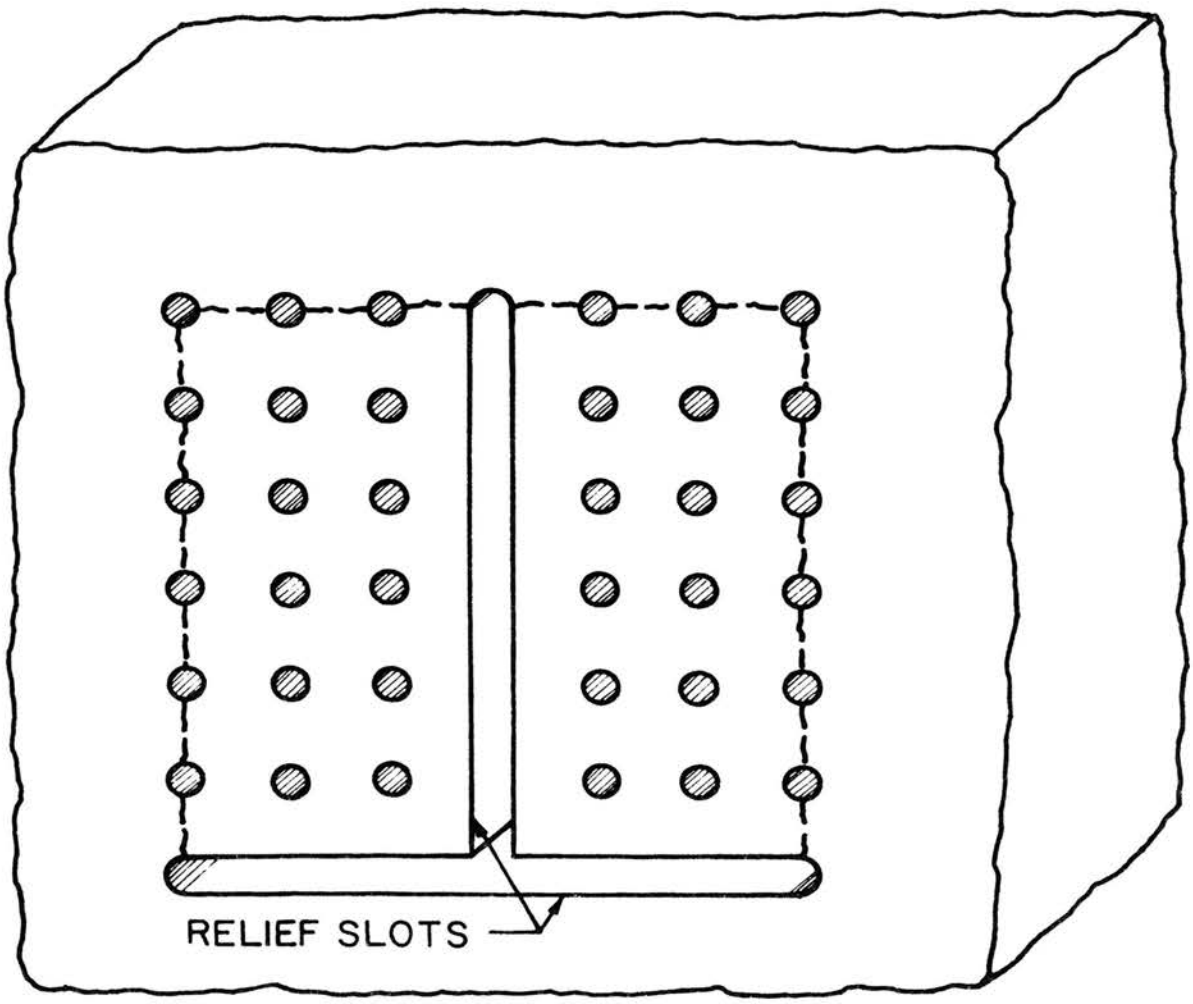

FIG. I.2 SLOT CONFIGURATION FOR DISPLACEMENT RELIEF

alternative from the viewpoint of accuracy would have been to study the actual three-dimensional geometry with anisotropic properties and temperature dependent boundary conditions. For the three-dimensional geometry the finite element method could have been used to study most of the parameters which affect fracture. Three-dimensional codes capable of performing the calculations would have had to be developed. The second alternative would have been to treat a single hole and heater in a semi or half space. If the interactions between the individual stress fields can be neglected, the stress at any point in the rock can be found by adding the contributions to the total stress at that point of each of the surrounding holes.

The approach used allows the displacement boundary conditions to supply the interaction between the stress fields. Consider the hole pattern shown in Fig. 1.1. This pattern can be assumed to extend indefinitely in all directions, providing numerous planes of symmetry normal to the working face. Over each of these planes of symmetry, material displacements do not take place perpendicular to the plane. Thus, considering the location of these planes of symmetry and the significant stresses the two plane models, parallel and perpendicular to the working face, as shown in Fig. 1.3 can be used as a first approximation to study the significant process parameters. In this investigation these models are referred to as the hole and the slot model respectively. The shaded areas in Figs. 1.4 and 1.5 show the typical sections of these models used for the theoretical analysis.

Based on the characteristics of hard, crystalline rocks, the analysis is performed using isotropic, homogeneous, temperature-

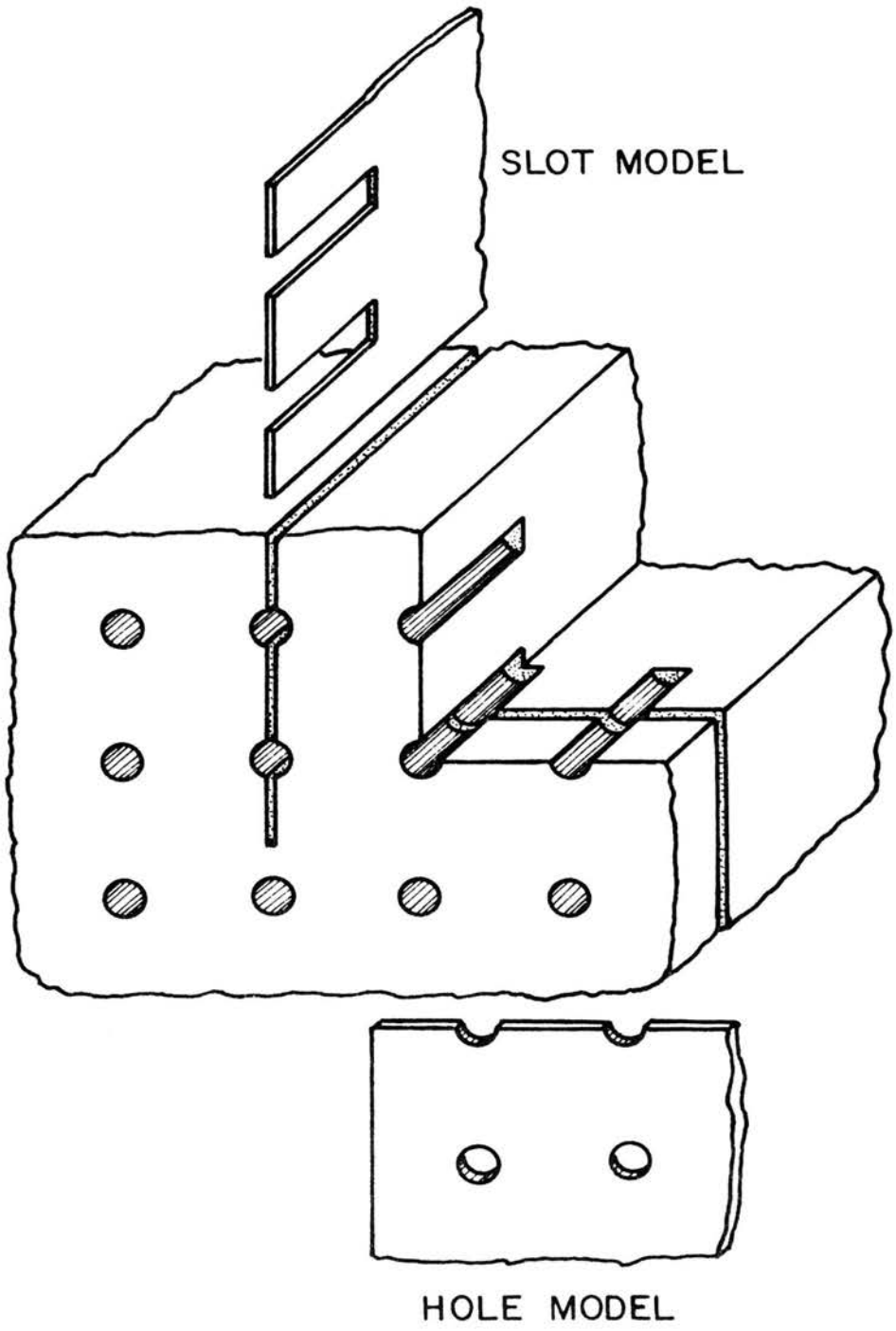

FIG. 1.3 TWO DIMENSIONAL PLANE MODELS

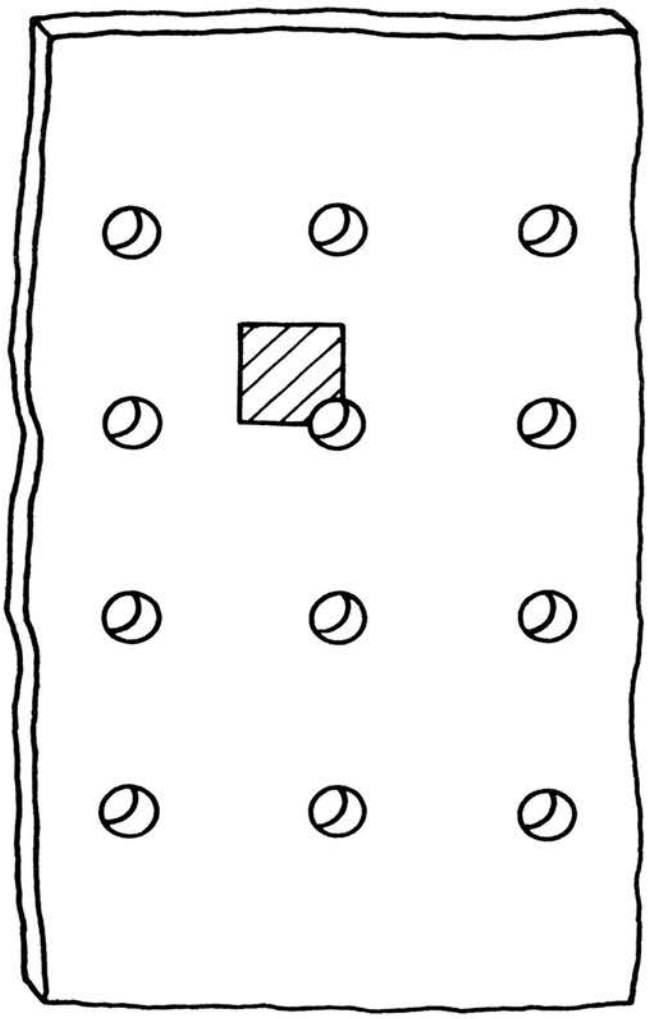

FIG. I.4 TYPICAL SECTION FOR HOLE MODEL ANALYSIS

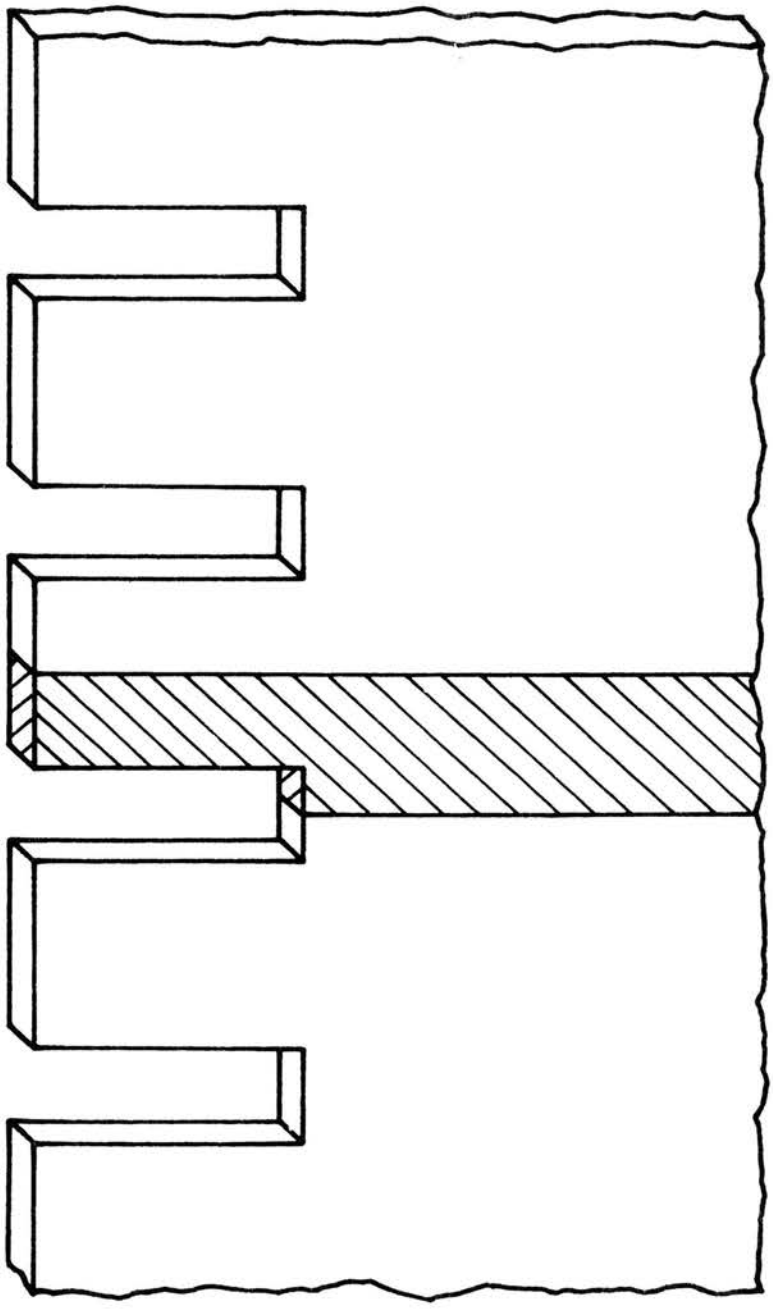

FIG. I.5 TYPICAL SECTION FOR SLOT MODEL ANALYSIS

dependent thermal and thermoelastic material properties. However, the available conduction code could handle only constant thermal properties. For this reason, Dresser basalt was selected as a particular rock type for the analysis. The thermal properties of Dresser basalt show only mild variations with temperature and also, all of the other properties of Dresser basalt necessary for the analysis were readily available. The thermoelastic properties in the stress solution, have been treated as functions of temperature.

The influence of the hole diameter, hole depth and spacing has been explored using the two plane models. The slot model has been used to study the fracture that occurs parallel to the working face of the tunnel or excavation. This fracture passes generally along the bottom of the holes, and depends on the nature of the thermal inclusions. The model is a good indicator of the effect of hole spacing as well as the effect of variations in the heated length. The hole model has been used to study the fracture that occurs between holes on a plane containing the hole axes and provides information about the effect of different hole diameters and spacings on this fracture.

Based on the slot and the hole model studies, optimum parameters for the most desirable fracture pattern are suggested. The fracture patterns predicted by using the optimized process parameters are then compared with the results of typical field tests in App. C. In view of computer time and storage considerations, the typical dimensions used for the theoretical studies were kept two to three times smaller than those used in the field tests, and the value of the coefficient of thermal expansion was higher by one order of magnitude than the actual value for basal

CHAPTER II

ROCK CHARACTERISTICS AND APPROXIMATIONS

Rocks are, in general, complex materials with inherent inhomogeneity and anisotropy as well as temperature-dependent material properties. For rock related studies one must also consider, among other factors, effects of porosity, moisture content, microcracks, bedding and joints, stress relief and stress absorption. An exact thermal stress analysis with all of these factors will be extremely difficult even for the simplest one-dimensional geometry. Simplifying assumptions are, therefore, necessary in order to obtain a workable solution. A description of general characteristics of different kinds of rock is, thus, in order.

A. General Classification [16]

The most general rock classification system is based on the mode of origin. Rocks are divided into three main groups: igneous rocks, sedimentary rocks, and metamorphic rocks.

Igneous rocks originate from solidification of hot, molten material below the earth's crust. These are very hard, massive rocks with granular nonporous structure and exhibit very high compressive strength. Their tensile strength is many times smaller than their compressive strength, yet their tensile strength is higher than the tensile strength of most other rocks.

The most predominant characteristic of sedimentary rocks is stratification or bedding. As a result, they possess strong transversely isotropic properties, and have much less compressive strength than the igneous rocks.

The term "metamorphism" denotes an aging process which brings about a complete change in the original rock characteristics as a result of very long, continuous action of pressure, temperature, and moisture and chemical reactions of atmospheric gases. Most metamorphic rocks possess the highly crystalline texture of igneous rocks with a parallel structure which closely resembles the stratification of sedimentary rocks. Fracture generally occurs due to cleavage along these planes. Metamorphic rocks that do not possess the cleavage planes usually have hard, massive structure with compressive strength on the same order as granite. Most hard metamorphic rocks exhibit some characteristics resembling closely those of igneous rocks. Quartzite is a well known example of this type.

Since this investigation is concerned with thermal fragmentation of hard rocks, mathematical models will be based on properties characteristic of igneous rocks.

B. Nonlinearity Considerations

As mentioned in the beginning of this chapter, approximations are necessary in order to obtain workable solutions for the two-dimensional analytical models. These approximations will be based on the following three major factors:

i. influence on fracture stresses,

ii. complications involved in theoretical studies, and

iii. accuracy of available property data.

Fracture stresses are influenced differently by different nonlinearity related factors. Material nonhomogeneity, for example,

will cause internal loading whereas a work-hardening stress-strain condition will lead to stress absorption. A similar situation is true regarding the degree of complexity of theoretical analysis. Thus, for example, using finite element methods, material nonhomogeneity and anisotropy can be handled rather easily, whereas the study of crack effects or the influence of rock porosity will require a prohibitively large amount of work. This is true regardless of the fact that, for a particular kind of nonlinearity, certain methods are better than others.

Availability and accuracy of rock properties are perhaps two of the most important factors in the consideration of theoretical analysis. Review of laboratory techniques for measuring rock properties indicates that there are no general specified standards except for a very few mechanical property measurements [17,18]. Besides, rocks are known to exhibit slightly different properties in situ [19]. Also, the characteristics of a given rock type from different geological locations vary considerably. Most measured properties, as a result, show about ±5% deviation from the average value. This deviation, however, is considered to be rather small for engineering purposes, and is usually neglected.

The above considerations are used in approximating the following nonlinear rock characteristics:

1. Stress-strain Behavior

For most hard, crystalline rocks, the stress-strain curve is approximately linear and ends abruptly indicating a brittle failure [20]. Some of the rocks do exhibit a nonlinear behavior. However,

this nonlinearity is attributed to the presence of microcracks which close under confinement [21-24]. The stress-strain behavior of in situ rock can, therefore, be assumed to be linearly elastic.

Griggs, Turner, and Heard [25] conducted an extensive study on the effect of temperature on stress-strain relationships of a variety of rocks. According to their results, most rocks show a steady decrease in yield point with increase in temperature. This effect, however, is not important in the study of rock failure resulting from thermal inclusion. This is due to a number of reasons. First, the stress-strain curves for rocks are usually obtained under uniaxial compression, whereas fracture initiates from tensile stresses that are many times smaller than the yield strength in compression. Also, during the preliminary field tests conducted in this investigation, only a small percent of the fractured rock volume was observed to have experienced any appreciable change in temperature. Thus, the effect of the lowered yield strength is localized in nature, in the close vicinity of the inclusion. However, very high temperatures in this region drastically reduce the elastic resistance of the material.

2. Homogeneity and Isotropy

Hard, crystalline rocks consist mainly of quartz, feldspar, augite, magnetite, and mica. For a given rock type, each constituent, in general, differs from others in both texture and grain size. At the same time, average grain size of a constituent varies with rock types. Most hard, crystalline nonporous rocks possess fine-to-medium grained texture and the normal range of grain size is usually from 0.03 mm to

1.0 mm. Individual crystals are chemically heterogeneous and, in general, possess different physical properties. However, the grain distribution is very random. As a result, on a macroscopic scale, hard rocks usually have homogeneous properties. Any slight heterogeneity will, of course, be quite insignificant for the in situ rock investigations [19].

Anisotropic behavior is pronounced only for sedimentary, stratified rocks and metamorphic rocks which have well defined cleavage planes. These rocks are generally soft to medium hard, and are not included in this analysis. For hard rocks, properties are assumed to be isotropic. As a matter of fact, laboratory measurements are generally obtained in random directions and the properties are then averaged, without recording the variations in individual directions.

3. Crack Effects

Cracks are created in the form of voids as a result of removal of gases and water vapor which are entrapped at high pressure and temperature during rock formation. These voids are extremely small compared to faults and joints and are usually in the form of microcracks in nonporous, hard, dense rocks. Nevertheless, they have very definite effects on rock properties, due mainly to material discontinuity and the pressure of accumulated moisture in the cracks. For example, the initial nonlinearity in the elastic behavior of rock has been shown to be due to the existing microcracks [22-24].

Compressive strength of rocks is observed to decrease with increasing moisture content. Although not completely understood, this weakening effect is believed to result from the internal loading caused by pore pressure. Apart from this weakening effect, cracks act as stress raisers and have a very significant effect on fracture propagation.

As the equations of thermoelasticity are based on the theory of continuum, crack effects are probably the most difficult to study. However, for comparatively nonporous, hard rocks, cracks occupy less than 1% of total volume as compared to 10-20% for highly porous rocks like sandstone and limestone [26]. Hence, for hard rocks which possess a very low apparent porosity, the microcrack effects can be neglected.

4. Temperature Effects

Even though application of heat as a technique to fracture rocks has been used since antiquity, little was known about the mechanisms involved. However, in recent years, a large amount of effort has been put forth on the part of numerous researchers to investigate the mechanisms responsible for thermal fragmentation of rock [1-16,27-30]. Heating devices being considered include such modern techniques as high frequency electric heating, induction and microwave heating, electric arcs, infra-red rays, electron beam, lasers, and plasma jets. Although parameters such as the heat transfer efficiency, energy input rate, and fracture time vary considerably with the mode of heating, the fracture mechanism involved remains unchanged.

As opposed to the mechanical fragmentation mode, the thermal fragmentation mechanism depends on the following:

i. Variation of physical properties with temperature,

ii. Thermal weakening effects as a result of spallation, intergranular crack growth, chemical changes, and expansion of entrapped gases and moisture.

a. Thermoelastic Properties

Properties of importance in the thermal fragmentation analysis of rocks include thermal conductivity, diffusivity, coefficient of thermal expansion, modulus of elasticity, and Poisson's ratio. For most rocks, these properties are highly temperature dependent. This is to be expected since the properties of different rock constituting minerals exhibit varying degrees of temperature dependency. Formulating the closed form thermoelasticity equations and their solution for materials with temperature dependent properties is an extremely difficult task. However, using numerical finite element methods, these effects can be studied without a great amount of difficulty.

Thermal conductivity of most igneous rocks decreases with increasing temperature. Figure 2.1 shows the variation of thermal conductivity for some typical igneous rocks as obtained by Birch and Clark [31].

Diffusivity, in general, is obtained mathematically from the values of conductivity, specific heat, and density. Most hard, non-porous igneous rocks show little variation in density with temperature.

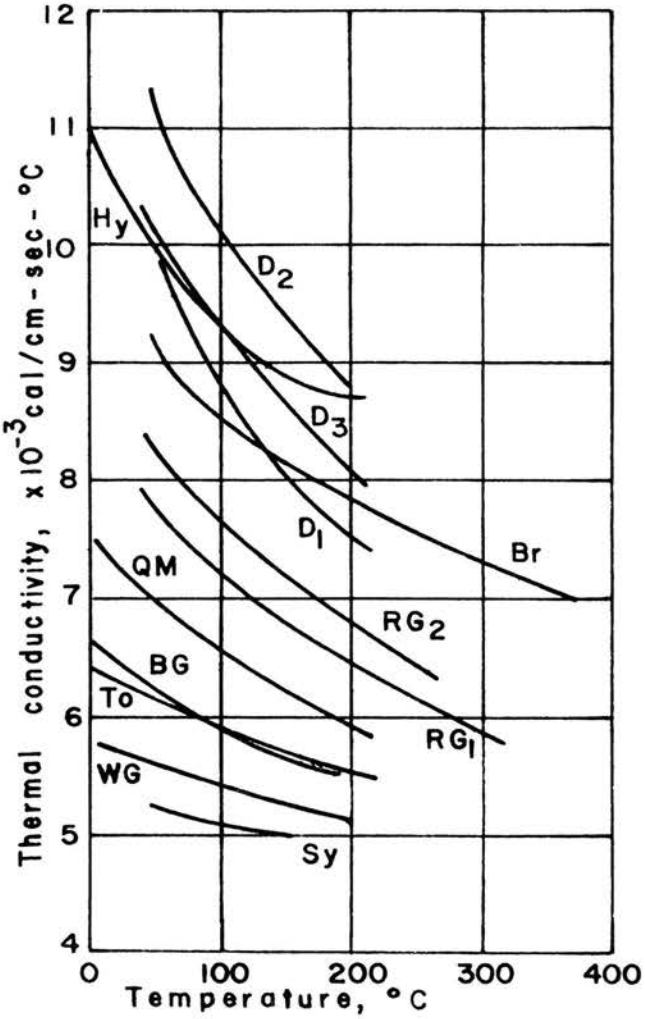

Sy SYENITE, ONTARIO

WG WESTERLY GRANITE

To TONALITE, CALIF.

BG BARRE GRANITE

QM QUARTZ MONZONITE, CALIF.

RG ROCKPORT GRANITE

Br BRONZITITE

Hy HYPERTHENITE

D DUNITE

FIG. 2.1 THERMAL CONDUCTIVITY OF HOLOCRYSTALLINE ROCKS[31]

Mean value of specific heat over the temperature range from 25°C to 625°C were obtained by Geller, et al., [30]. Only a small variation was observed among the specific heats of fourteen rock types tested and the values ranged from approximately 0.23 to 0.25 cal/gm-°C. However, no investigations were made to study the variations in specific heat with temperature.

Temperature dependency of specific heats for six hard rock types was later investigated by Lindroth and Krawza [32]. Tests were conducted at temperatures up to 1000°C. According to this study, temperature dependence of specific heat is strongly influenced by the percentage of quartz content. Results of this study are shown in Fig. 2.2. The break in these curves occurs as a result of a phase change of quartz at approximately 573°C. For rocks containing less than 5% quartz, this break occurs at higher temperatures.

Similar discontinuities can be observed in curves shown in Fig. 2.3, which shows the plot of coefficient of thermal expansion for hard crystalline bodies as a function of temperature. These are part of the results obtained by the Canadian Mines Branch of the Department of Mines and Mineral Surveys which conducted experiments on 37 rock types to determine the variation of linear thermal expansion with temperature [30]. Studies on fusion were also performed. Fusion temperatures of 45 rock types were obtained; fusion temperatures for hard crystalline rocks were observed to lie in the range from 1150°C to 1300°C.

Studies conducted on the effect of temperature on elastic properties of rocks indicate that for hard, nonspallable rocks, both

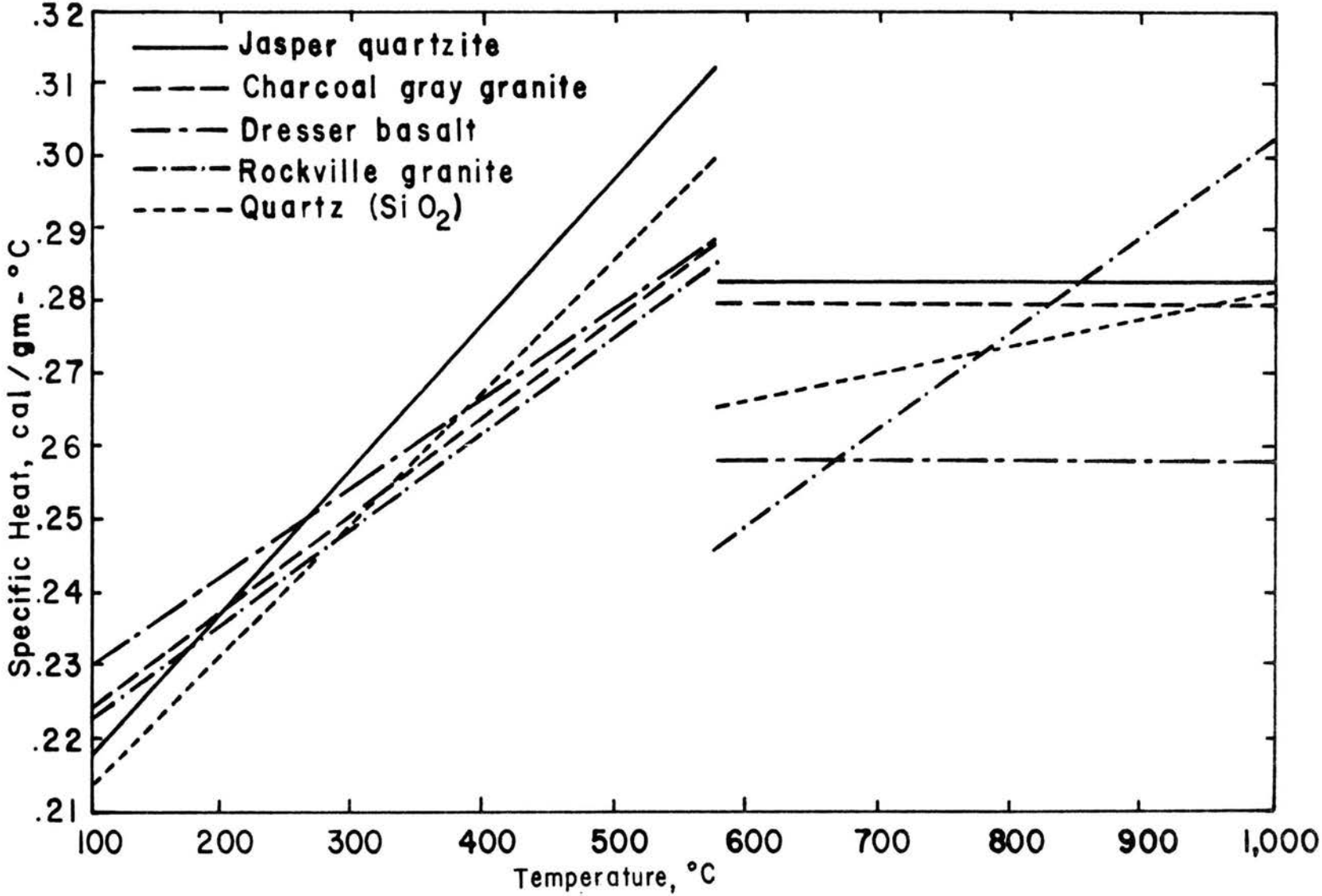

FIG. 2.2 SPECIFIC HEAT VALUE OF HIGH-SiO_2 ROCK TYPES [32]

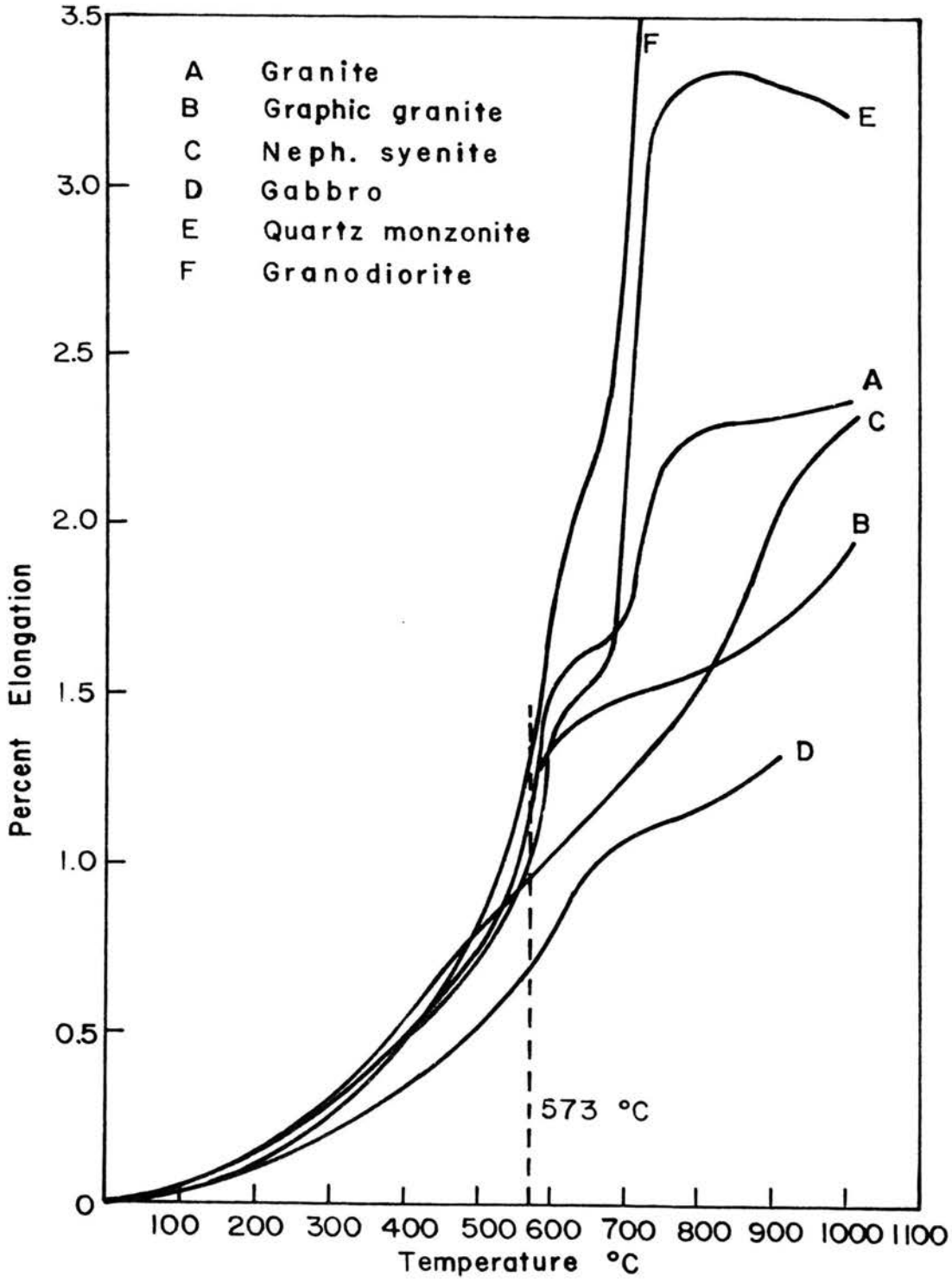

FIG. 2.3 AVERAGE LINEAR EXPENSION OF IGNEOUS ROCKS[30]

Young's modulus and Poisson's ratio show a marked decrease in the vicinity of the fusion temperature. For spallable rocks, however, the upper temperature limit is restricted by the alpha to beta phase transition of quartz, and above this temperature range, only small variations in elastic properties are observed [33-35].

b. Fracture Mechanisms

As opposed to the well defined properties involved in both the temperature and stress analyses, the fracture phenomenon depends on a number of mechanisms for which the variations with temperature have not been described in tabular or graphic form. Little is known about the interactions of various mechanisms involved. Nevertheless, it is well established that temperature has definite weakening effects on rock strength, and the mechanisms responsible include, primarily spallation, intergranular crack growth, chemical changes, and gas and water pocket expansion.

The relative importance of each of these weakening factors depends mainly on the nature of rock; porosity, average grain size, microcracks, and mineral constituents. Except for spallation, relatively little information is available on temperature effects on other mechanisms involved in fracture, mainly due to their inter-relationship.

The term thermal spallation refers to a progressive failure of rock in the form of chips caused by thermal stress. The basic mechanism involved in formation of a spall depends on a sudden increase in the thermal expansion of quartz due to its phase transformation at approximately 573°C. Although it is well established that a certain

percentage of quartz and its phase transition are essential to the inducement of spalling, review of various research efforts on thermal spalling reveals that little agreement exists as to the exact cause of the phenomenon [1,17,30,36-38].

According to Gray [2], spalling can be controlled by proper choice of heating rate. For high heating rates which induce surface melting, spalling effects become trivial. Studies performed by Moavenzadeh, et al., [29] indicate that for igneous rocks complicated crack growth mechanisms have little or no effect on fracture compared to those due to the thermal stress field. Thus, the fracture of rock can be predicted with reasonable accuracy from the knowledge of the stress field alone.

C. Fracture Theories

As discussed above, in thermally induced rock fragmentation studies, the thermal stress field can be regarded as the single major factor responsible for rock failure. Numerous theories have been proposed over the years to relate the stress field to the brittle failure of materials. Of the various theories, the Griffith theory, in its different modified forms, has been the most widely accepted in the field of rock mechanics.

1. Griffith Theory

Griffith's theory evolved through his study of the problem of the tensile strength of glass being much lower than theoretically expected [39]. He suggested that the low tensile strength was due to failure caused by stress concentrations at the tips of minute internal

and surface flaws which have come to be known as Griffith cracks. In formulating this theory, Griffith assumed the material to be a isotropic, homogeneous continuum containing randomly oriented sharp ended elliptical cracks. The mathematical condition for the initiation of a macrocrack was derived based on the energy approach which states that the work done by externally applied forces is equal to the sum of internal strain energy and the surface energy associated with the rupturing of atomic bonds when cracks are formed.

Specific energy is a difficult quantity to evaluate through direct measurements. Hence, the fracture criterion is expressed mathematically in terms of principal stress values. If compressive stresses are taken as negative, the conditions of fracture initiation are given by the following equations.

If

$$3\sigma_1 + \sigma_3 > 0 \tag{2.1a}$$

fracture initiation occurs when

$$\sigma_1 = \sigma_t \quad ; \tag{2.1b}$$

if

$$3\sigma_1 + \sigma_3 < 0 \quad , \tag{2.2a}$$

the condition of fracture initiation is given by

$$(\sigma_1 - \sigma_3)^2 + 8\sigma_t(\sigma_1 + \sigma_3) = 0 \quad . \tag{2.2b}$$

In these equations

σ_1 = major principal stress,

σ_3 = minor principal stress, and

σ_t = uniaxial tensile strength of the material.

For failure governed by Eqs. (2.1), the microscopic crack begins to propagate in its own plane in a direction perpendicular to that of the major principal stress. For failure conditions given by Eqs. (2.2), however, the crack begins to extend in a plane at an angle θ from the minor principal stress axis, given by

$$\cos 2\theta = -\frac{1}{2}\frac{\sigma_1-\sigma_3}{\sigma_1+\sigma_3} \tag{2.3}$$

It should be noted that the fracture criterion given by Eqs. (2.1) and (2.2) was developed for a biaxial stress state. Sack [40] extended Griffith's theory to three dimensions by considering a penny-shaped crack under a triaxial stress state, and concluded that the fracture initiates as a result of growth of cracks that are parallel to the intermediate principal stress direction. Thus, the intermediate principal direction is the most critical crack orientation. However, the magnitude of this principal stress component has no appreciable influence on the crack growth and the Griffith biaxial fracture criterion given by Eqs. (2.1-2.3) can be applied to triaxial stress conditions as well. This result has experimentally been verified by Brace [41] for igneous rocks such as granite.

2. McClintock-Walsh Modification

Experimental verification of Griffith's criterion, however, brought to attention some serious flaws in Eqs. (2.2) and (2.3). Under uniaxial compression ($\sigma_1=0$, $\sigma_3 < 0$), the formula loses its meaning as it implies that the compressive strength of the material is equal to eight times its tensile strength. For most rocks, however, this is not true as the compressive strength is much higher than eight times that in uniaxial tension. Also, under uniaxial compression, according to Eq. (2.3), the most critical cracks would be those at 45° to the stress direction. However, experimental studies by Brace [41] and Bieniawski [42] show that under a compressive stress state, cracks propagate out of their plane in the direction of the major principal compressive stress. These discrepancies required some modification of the Griffith theory for rock failure when one or two of the principal stress components are compressive.

Experimental studies by Brace [41] and Bieniawski [42] served to give an insight into the more complex mechanism involved in rock failure. Based on their experiments, they concluded that when compressive stresses are present, pre-existing Griffith cracks close before the tensile stress at the crack tip reaches the critical value for fracture initiation. To open these closed cracks, higher stresses are required in order to overcome the shear resistance resulting from the interlocking of irregular crack faces. The concept of crack closure was also able to explain the initial nonlinearity in the stress-strain curve of rocks.

McClintock and Walsh [43] were the first to modify the Griffith criterion with consideration given to the effects of crack closure. The fracture criterion in mathematical form given by McClintock and Walsh is as follows:

If

$$\sigma_n = \frac{1}{2}(\sigma_1+\sigma_3) + (\sigma_1-\sigma_3)\cos 2\psi_c < 0 \quad , \tag{2.4a}$$

fracture initiation occurs when

$$\sigma_3 = \sigma_1 \frac{\sqrt{1+\mu^2}+\mu}{\sqrt{1+\mu^2}-\mu} + \sigma_c \tag{2.4b}$$

where

σ_n is the normal stress acting across the crack faces causing the cracks to close,

σ_c is the uniaxial compressive strength of the material,

μ is the internal coefficient of friction between the crack faces, and

σ_1, σ_3 are the major and minor principal stress components, as before.

For this condition of crack initiation, crack propagation direction is given by

$$\tan 2\psi_c = 1/\mu \tag{2.5}$$

where ψ_c is measured from the minor principal stress axis.

Comparison of Eqs. (2.2) and (2.4) shows that the McClintock-Walsh criterion is based on the actual compressive strength of the material and also takes into account the effect of crack closure. Also, note that the original Griffith criterion given by Eqs. (2.1-2.3) is valid whenever $\sigma_n > 0$, so that the normal stress acting across the crack does not cause crack closure.

It should be realized that both Griffith and McClintock-Walsh modified Griffith criteria refer to fracture initiation only, which is not the same as fracture [44]. They do not consider factors such as the energy of plastic deformation; orientation, density, and interactions of existing microcracks; difference between the stress levels causing fracture initiation and those causing the ultimate strength failure; crack propagation velocity and other dynamic effects. Nevertheless, experimental results obtained by Hoek and Bieniawski [45] for a wide variety of rocks show a remarkable agreement with those predicted theoretically by the Griffith and McClintock-Walsh modified Griffith criteria. They, however, replaced the internal crack friction coefficient, μ, by fracture surface coefficient of friction, μ_f, which was obtained experimentally for each rock type tested. For igneous rocks, the value of μ_f has been found to lie between 1.0 and 1.5 [23,41].

D. Properties Used in Analytical Studies

Even though field tests have been conducted on Missouri red granite, for the theoretical analysis, Dresser basalt was found to be more suitable as it contains very little or no quartz. Also, the thermal and elastic properties for basalt as a function of temperature were readily available [1,7,35,46].

1. Temperature Analysis

The available finite element temperature code is not capable of handling temperature dependent thermal properties. However, for Dresser basalt, the thermal conductivity and diffusivity show only small variations with temperature, as shown in Figs. 2.4 and 2.5. The upper limit of 700°C for the temperature range was chosen in view of the fact that the modulus of elasticity for temperatures above 700°C becomes very small, as seen from Table II. The effect of this low value of Young's modulus is that, regardless of the steepness of temperature gradients, in the region where temperatures are higher than 700°C, the stresses will be very small. In other words, the upper limit, 700°C, of the temperature range for curves shown in Figs. 2.4 and 2.5 is taken as the temperature at which the rock becomes plastic. Hence, the nonlinearities in the thermal properties will have a very small effect, if any, on the stresses which contribute to fracture.

In order to simplify the analysis, the assumption of temperature independent properties has been employed in most of the rock related investigations. Under this assumption, properties corresponding to the average temperature of the material are usually selected. This procedure has been shown to yield analytical results well within the range of experimental errors [4,28,47-49].

For this analysis, average values of thermal conductivity and diffusivity were obtained from Figs. 2.4 and 2.5. The input properties for the finite element code, however, are the conductivity, specific heat and specific gravity. Even though the specific heat values as function of temperature were readily available for basalt [32], the

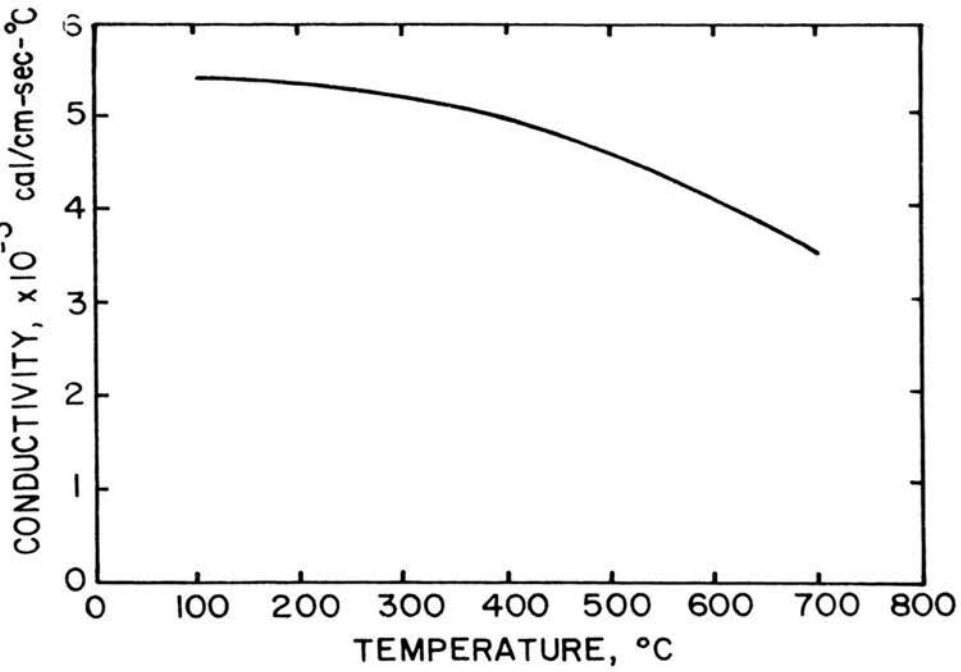

FIG. 2.4 VARIATION OF CONDUCTIVITY OF DRESSER BASALT WITH TEMPERATURE [1]

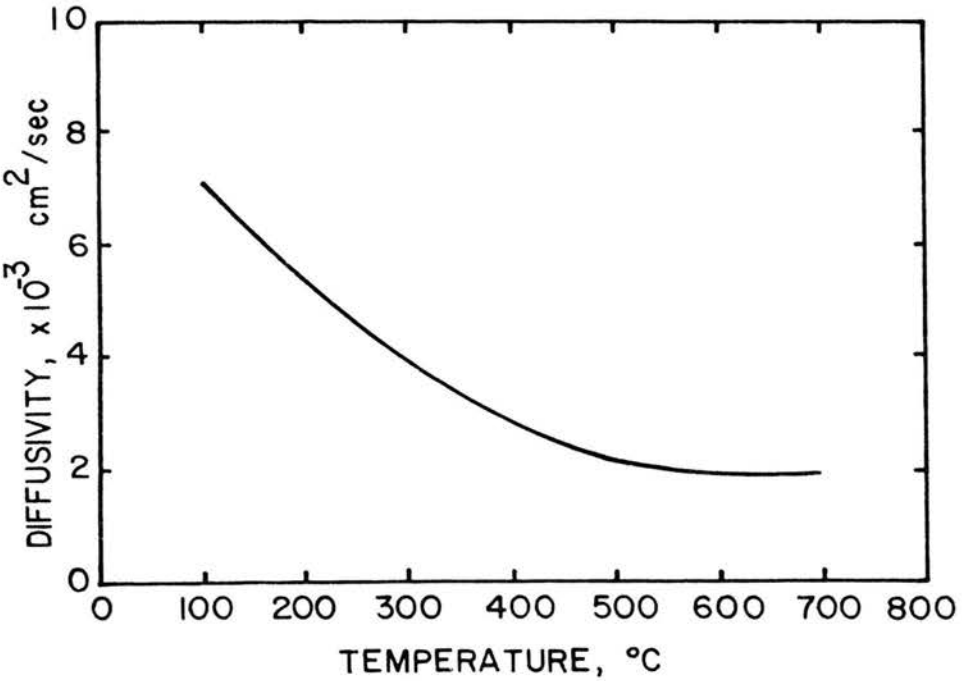

FIG. 2.5 VARIATION OF DIFFUSIVITY OF DRESSER BASALT WITH TEMPERATURE [1]

following procedure was found to be more efficient. The specific gravity of the material was assumed to be constant, equal to that at room temperature. The average value of the specific heat was then obtained from the average values of the thermal conductivity and the diffusivity using the well-known relationship [50]

$$\kappa = \frac{k}{\rho c} \quad *$$

where

κ = average value of thermal diffusivity

k = average value of thermal conductivity

ρ = the specific gravity of material, and

c = the average value of the specific heat.

Values of the properties used for the temperature analysis are tabulated below.

TABLE I

Property Data Used in Temperature Analysis of Dresser Basalt [1,46,51]

Thermal conductivity, k, cal/cm-sec-°C	0.0042
Specific heat, c, cal/gm-°C	0.293
Density, ρ, gm/cm^3	2.97
Melt Temperature, T_m	1250°C
Surface convection coefficient, h, cal/cm^2-sec-°C	0.00021

*For solids, no distinction is generally made between specific heat at constant pressure, c_p, and that at constant volume, c_v. Nevertheless, it should be noted that in this equation c refers to c_p.

2. Stress Analysis

Unlike the temperature analysis, the stress analysis was performed using temperature dependent material properties. This was necessary due to the fact that the variations of the stress related properties with temperature greatly influence, as explained later on, the resulting stress field and consequently, the fracture predictions.

The stress related properties include the coefficient of thermal expansion, α, modulus of elasticity (Young's modulus), E, and Poisson's ratio, ν. Table II gives the values of these properties used in the stress analysis.

TABLE II

Property Data Used in Stress Analysis of Dresser Basalt [7,8,35]

Temperature, T °C	Young's Modulus E, 10^6 psi	Poisson's Ratio ν	Coeff. of Thermal Expansion, α^* 10^{-5}/°C
100	14.5	0.24	2.6
162	14.1	0.23	6.0
287	13.5	0.21	8.2
412	12.6	0.19	10.2
537	10.7	0.145	11.2
610	8.3	0.105	11.7
630	6.4	0.09	11.8
650	4.6	0.07	11.9
670	2.8	0.05	12.0
690	0.9	0.02	12.0

*As mentioned on p. 11, considerable saving in computer time was achieved by using this higher value.

As was mentioned earlier, the rock is assumed to become plastic at 700°C as its elastic resistance for higher temperatures becomes very small.

In order to explain the strong influence of the stress related properties on the probability of fracture, the concept of fragmentation potential was introduced by Thirumalai [7]. This concept is based on the observation that the thermal load vector is proportional to the factor

$$F = \frac{E\alpha T}{1 - \nu}$$

and thus, in the absence of mechanical loading, the resulting stress field depends directly on F [52].

In the nondimensional form, Thirumalai defines the fragmentation potential as

$$F^* = \frac{F}{F_{max}}$$

where F_{max} denotes the maximum value of F.

Figure 2.6 shows the variation of F^* with temperature for Dresser basalt. If the properties were assumed to be constant, the variation in F^* would have been linear as shown by the broken line. The difference between the ordinates for the solid and the broken line is an indication of the influence on the stress field of the nonlinear, temperature dependent properties as given in Table II. Another method of predicting whether or not the temperature dependence of the thermo-elastic properties will have a significant effect on the stress field

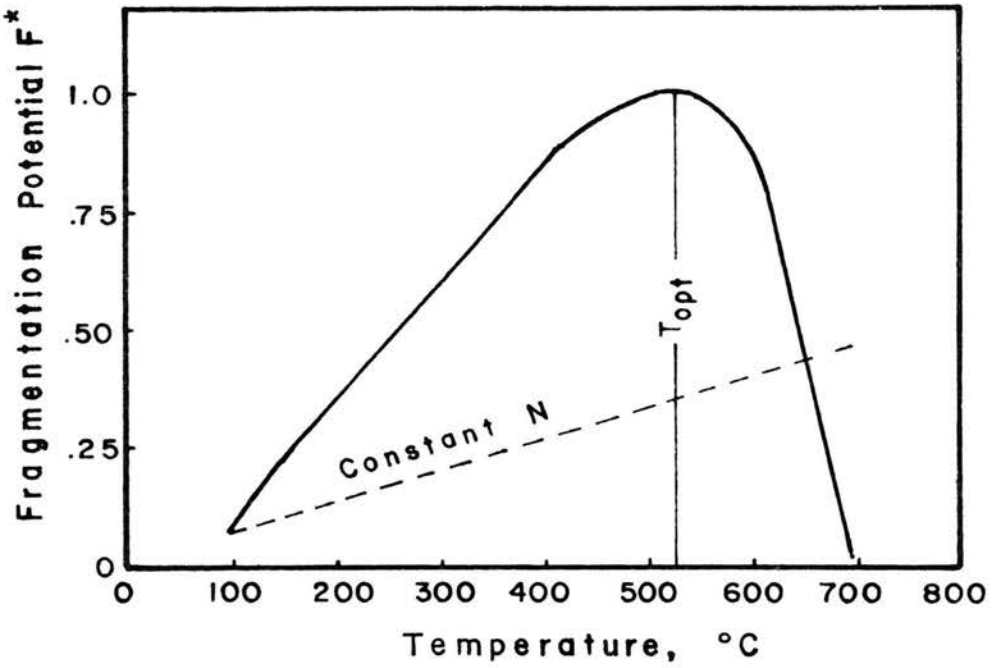

FIG. 2.6 FRAGMENTATION POTENTIAL OF DRESSER BASALT AT ELEVATED TEMPERATURES [7]

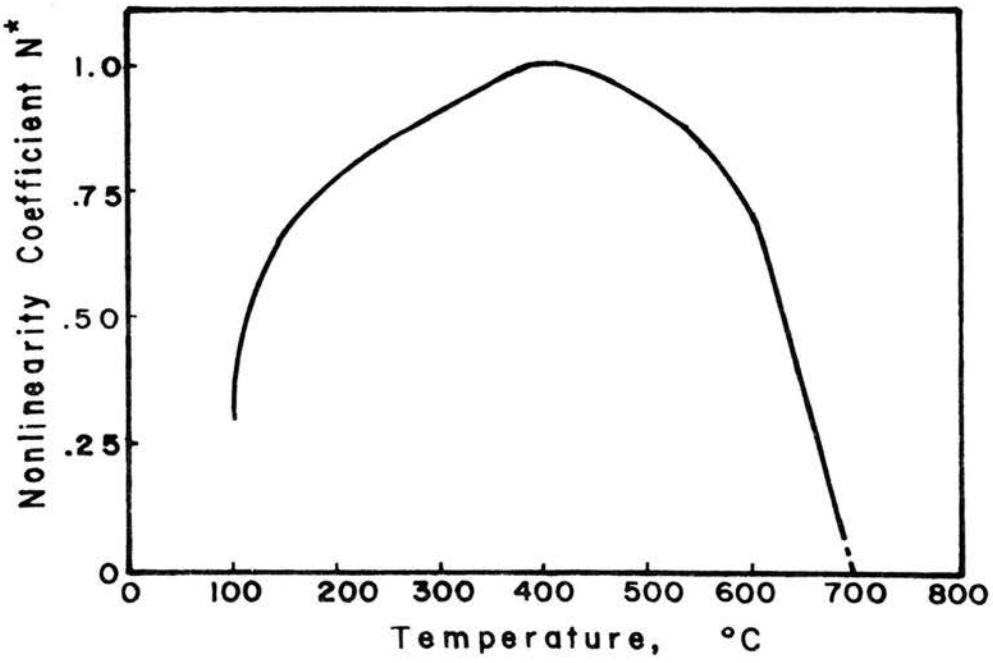

FIG. 2.7 NONLINEARITY COEFFICIENT OF DRESSER BASALT AT ELEVATED TEMPERATURES

is through the use of what will be referred to as the nonlinearity coefficient. This coefficient will be defined as

$$N^* = \frac{N}{N_{max}}$$

where

$$N = \frac{E\alpha}{1 - \nu} \quad ,$$

and N_{max} denotes the maximum value of N.

The usefulness of this definition lies in the fact that, for a homogeneous solid under pure thermal loading it is the variation of N^* which influences the stress field rather than the individual variations of each of the thermoelastic properties. Thus, for materials exhibiting thermoelastic properties, it is possible to obtain quite accurate stress solutions provided the nonlinearity coefficient, N^*, remains fairly constant.

Variation of the nonlinearity coefficient for basalt is shown in Fig. 2.7. The highly nonlinear nature of this curve indicates that for a reasonably accurate solution, the thermoelastic properties should be allowed to vary with temperature in the stress analysis.

3. Fracture Predictions

Fracture analysis is performed based on the Griffith and McClintock-Walsh modified Griffith criteria. Once the principal stresses have been obtained from the stress analysis, the following properties are required in order to predict the initiation of fracture:

uniaxial tensile strength, σ_t, uniaxial compressive strength, σ_c, and the fracture surface coefficient of friction, μ_f, of the material.

Confining pressure is known to increase the strength of the rock. This effect, however, is neglected here since this investigation is concerned with rocks a few feet below the surface of the earth [25].

Temperature, on the other hand, has a weakening effect on the rock strength [25]. This, too, is neglected in view of the localized nature of heating and the observation that the major portion of thermally fractured rock volume experiences only a small average increase in temperature.

Table III gives the properties used in the fracture analysis.

TABLE III

Properties of Basalt Used for Fracture Predictions [23,41,45,53]

Uniaxial tensile strength, σ_t	2,195 psi
Uniaxial compressive strength, σ_c	42,399 psi
Fracture surface coefficient of friction, μ_f	0.9

CHAPTER III

MATHEMATICAL FORMULATION AND METHOD OF ANALYSIS

The three-dimensional thermoelasticity problem and its reduction to three two-dimensional mathematical models were considered in Ch. I. In Ch. II, hard rock characteristics were discussed and simplifying assumptions introduced for theoretical studies. In this chapter, analytical aspects such as mathematical formulation of equations and methods of their solution are considered.

The thermal fragmentation analysis considered here involves relatively low stress levels and very low strain rates as compared to conventional explosive and nuclear blasting techniques. Under these conditions, the effects of thermoelastic coupling are negligible. Thermal inertia effects are also neglected as the time rate of temperature change is very slow. Thus, the general problem can be formulated within the framework of the linear, uncoupled theory of thermoelasticity. For this formulation, the problem becomes explicit, in that solutions can be obtained in two distinct steps; solution to a well-defined heat conduction problem, and solution of the stress problem with known temperature distribution [4,52].

A. Heat Conduction Problem

The geometries for the slot and the hole models considered in this investigation are shown in Fig. 3.1. Parameters used to describe these geometries are as follows:

c = center-to-center distance between the hole (or slot) axes,

d = hole diameter (or slot width),

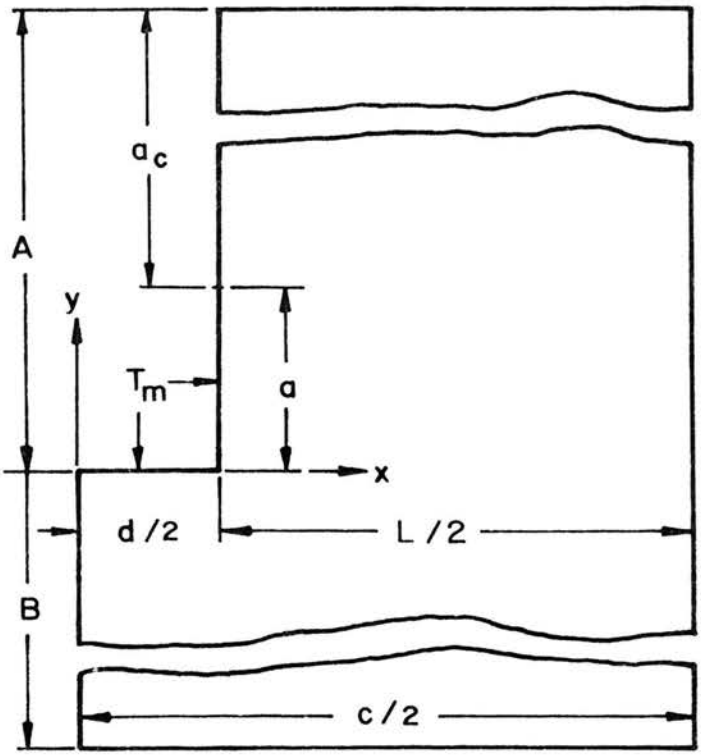

(a) SLOT MODEL

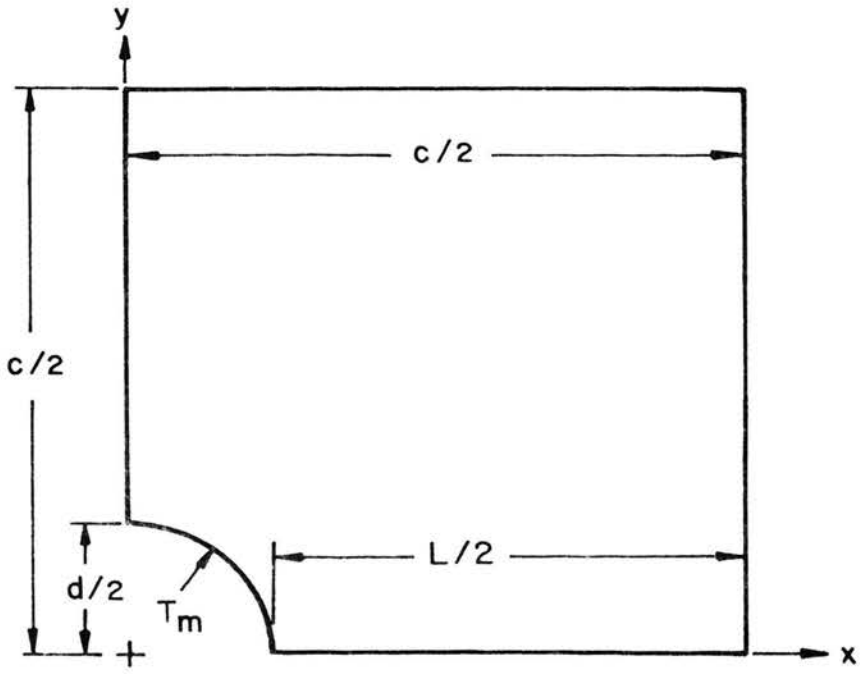

(b) HOLE MODEL

FIG. 3.1 NOMENCLATURE FOR PLANE MODELS

A = total hole (or slot) depth,

a = melt depth,

L = fracture propagation length.

In the subsequent discussion, the remaining hole or slot depth, A-a, is referred to as convection depth, a_c. Parameter B is chosen arbitrarily but large enough so as to satisfy both the traction free and ambient temperature conditions on boundary y = -B of the slot model.

In the absence of internal heat generation, the governing equation of two-dimensional heat conduction for a homogeneous, isotropic solid with constant properties is given by

$$k\left(\frac{\partial^2 T}{\partial x^2} + \frac{\partial^2 T}{\partial y^2}\right) = \rho c \frac{\partial T}{\partial t}$$

where

k = thermal conductivity

ρ = density

c = specific heat, and

T = T(x,y,t) denotes the temperature at point (x,y) at time t.

For notational convenience, the ambient temperature is assumed to be zero so that the initial condition becomes

$$T(x,y,0) = 0 \quad .$$

The boundary conditions for the slot model are:

$$\frac{\partial T}{\partial x} = 0 \quad , \qquad \begin{cases} x = 0 \ , \ y < 0 \\ x = c/2 \end{cases}$$

$$\frac{\partial T}{\partial x} + hT = 0 , \qquad x = d/2,\ y > a$$

$$\frac{\partial T}{\partial y} + hT = 0 , \qquad y = A$$

$$T = T_m , \qquad \begin{cases} 0 \leq x \leq d/2,\ y = 0 \\ x = d/2,\ 0 \leq y \leq a \end{cases}$$

$$T = 0 , \qquad y = -B \ .$$

The boundary conditions for the hole model are:

$$\frac{\partial T}{\partial x} = 0 , \qquad \begin{cases} x = 0,\ y < d/2 \\ x = c/2 \end{cases}$$

$$\frac{\partial T}{\partial y} = 0 , \qquad \begin{cases} x > d/2,\ y = 0 \\ y = c/2 \end{cases}$$

$$T = T_m , \qquad x^2 + y^2 = d^2/4 \ .$$

In the above equations, T_m denotes the melt temperature of the material and h is the coefficient of convection heat transfer.

Solution Techniques

A great deal of work has been done on solving problems of unsteady state or transient heat conduction [50,54-57]. Analytical tools include such classical techniques as separation of variables, integral transforms, Green's functions and those based on variational principles. The integral methods introduced by Goodman [58] and the Galerkin's

variational method [59] are widely used to obtain approximate closed form solutions. Each method has some advantages over the others; however, each has its own limitations and the choice of the method to solve a particular problem depends largely on the nature of the problem itself.

With the advent of high-speed, large scale digital computers, the approximate numerical finite difference and finite element methods have become more popular due to their ease of application and capability of handling today's highly nonlinear, complex problems.

Even though the temperature problem considered in this investigation is linear in that constant average thermal properties are used, the boundary conditions are quite complex. Also, for the stress analysis part, properties are allowed to vary with temperature which makes obtaining a closed form solution extremely difficult. Thus, closed form temperature solutions will be of little advantage and since a two-dimensional code was readily available, the numerical finite element solution was chosen.

Application of the finite element method for the solution of problems governed by a general quasi-harmonic differential equation is discussed by Zienkiewicz [60]. The well-known Laplace and Poisson equations are particular cases of the general quasi-harmonic equation and govern such frequently encountered problems as those of heat conduction, seepage flow, distribution of electromagnetic potential, and torsion and bending of prismatic members. The finite element conduction code used in this analysis was developed based on the formulation given by Wilson and Nickell [61]. Details of this code are proprietary in nature and hence are not given here [62].

B. Stress Problem

The problem of linear, uncoupled thermoelasticity involves fifteen equations with fifteen unknowns; six stress components, six strain components, and three displacement components. The field equations in index notation are as follows [52]:

Equilibrium equations:

$$\sigma_{ij,j} + f_i = 0$$

Stress-strain relations:

$$\sigma_{ij} = \delta_{ij}\lambda\varepsilon_{kk} + 2\mu\varepsilon_{ij} - \delta_{ij}(3\lambda+2\mu)\alpha T$$

Strain-displacement relations:

$$\varepsilon_{ij} = 1/2(u_{i,j}+u_{j,i})$$

where

σ_{ij} = the stress tensor
ε_{ij} = the strain tensor
u_i = the displacement vector
f_i = the body force vector
δ_{ij} = the Kronecker delta
α = the coefficient of thermal expansion, and
λ,μ = Lame's constants .

It should be noted that the stress tensor, σ_{ij}, and the strain tensor, ε_{ij}, are both symmetric, that is,

$$\left.\begin{aligned}\sigma_{ij} &= \sigma_{ji}\\ \varepsilon_{ij} &= \varepsilon_{ji}\end{aligned}\right\} \qquad i \neq j \ .$$

Also, since six strain components are expressed in terms of only three displacement components, the following compatibility relations must be satisfied:

$$\gamma_{prm}\gamma_{qsn}\varepsilon_{rs,mn} = 0$$

where

γ_{ijk} is the alternating tensor.

Plane Theory of Thermoelasticity

For simply connected regions, in the absence of body forces, the general formulation given above simplifies for the plane theory of thermoelasticity to the solution of the biharmonic equation

$$\nabla^2\nabla^2 F + cE\nabla^2(\alpha T) = 0$$

where

$\nabla^2 = \dfrac{\partial^2}{\partial x^2} + \dfrac{\partial^2}{\partial y^2}$, the Laplacian

$$c = \begin{cases} 1, \text{ plane stress} \\ \dfrac{1}{1-\nu} \text{ , plane strain} \end{cases}$$

ν = Poisson's ratio

E = Young's modulus, and

α = coefficient of thermal expansion.

Once the Airy stress function F is determined, the stresses can be obtained from the following relations:

$$\sigma_x = \frac{\partial^2 F}{\partial y^2}$$

$$\sigma_y = \frac{\partial^2 F}{\partial x^2}$$

$$\tau_{xy} = - \frac{\partial^2 F}{\partial x \partial y} \cdot$$

It is important to note that the solution to the biharmonic equation is to be obtained subject to the boundary conditions. Since both the slot and the hole models considered in this investigation involve mixed boundary conditions, that is, specified tractions as well as specified displacements, solution of the biharmonic equation in itself becomes quite complicated. Further complications are introduced due to the temperature variations of the thermoelastic properties, E, ν, and α. No attempt was therefore made to obtain closed form solutions. Rather, approximate numerical solutions were sought using the finite element method which due to its generality of application provides a powerful tool for the solution of complex structural problems with arbitrary geometries and nonlinear material properties.

Numerous finite element codes have been developed in recent years for the solution of elasto-plastic and thermal stress problems. However, no suitable code was available for the transient thermoelastic stress analysis. The available codes for thermoelastic

analysis are quasi-static in nature and can handle stationary temperature distributions only. This means that for a given problem geometry, the temperature distribution at each time step must be run separately through the stress program to determine the stress distribution as a function of time. This procedure becomes highly inefficient as the program recomputes the entire stiffness matrix and load vector for each of the sets of temperature data.

A new finite element code was, therefore, developed for the transient thermal stress analysis. This code is identified by the acronym "TRATSA" (TRAnsient Thermal Stress Analysis) and can be used for plane or axisymmetric bodies with temperature-dependent material properties. The code is based on theoretical formulations given by Zienkiewicz [60] and Jones and Crose [63]. These formulations assume linear displacement between nodes, resulting in constant stress elements. Both triangular and quadrilateral elements can be used. The input instructions and the program listing are given in Appendix A.

C. Fracture Analysis

The fracture predictions made in this investigation are exploratory in nature and are based on the stress field which is obtained by assuming the material to remain a continuum. In practice, however, initiation of a crack will change the temperature field which, in turn, effects the stresses. Cracks also tend to relieve the stresses, but at the same time, they also act as stress raisers. A rigorous treatment of the problem would require progressive introduction of additional convection and traction free boundary conditions with the creation of new fracture surfaces.

If the propagation of a crack is to be followed, the numerical treatment of the thermoelasticity problem becomes coupled in the sense that once the crack initiation is predicted from the known stress field, one must go back and recompute the temperature distribution for the next time step allowing for the newly developed fracture surfaces. For an extensive investigation such an approach becomes impractical due to the amount of work involved in the reformulation of the problem at each time step and the resulting prohibitively large amount of machine time. Apart from this, for problems not involving dynamic fracture, there is little justification in using a progressive fracture approach as the crack propagation of nondynamic nature, in actual practice, is largely governed by the orientation of the pre-existing microcracks and the interactions between them; factors for which no theoretical knowledge is available.

The fracture predictions in this analysis are based on the Griffith and the McClintock-Walsh modified Griffith criteria. These fracture theories are themselves approximate as they are derived from an energy formulation and neglect the effects of stress concentrations and the interactions between the cracks. These theories, therefore, can at best be considered statistical in nature. This is evidenced by the results of Lauriello [4] and Bieniawski [42] who obtained "statistically" good correlations between the experimentally observed fracture fields and those predicted theoretically using the Griffith and the modified Griffith fracture criteria.

Fracture Propagation Studies

During the preliminary analysis, it was found that, predicting the initiation of a crack and following its propagation even under

the assumption that the presence of a crack does not effect the temperature and stress fields, requires a rather large number of stress runs with very small time steps. Stress runs with large time steps, on the other hand, result in large fracture zones giving no indication whatsoever of the actual crack propagation path. This observation necessitated some sort of approximate procedure that could serve as a compromise between the two extremes and would yield practically comprehensible propagation data.

A procedure was devised based on a concept referred to hereafter as the concept of fracture intensity level. With this concept, the crack can be predicted to lie within a small narrow band rather than a whole large fractured zone as obtained from the stresses using large time steps. The fracture intensity level is defined in terms of the stress magnitude in excess of that necessary for fracture. Thus, a fractured element, A, having a higher excess stress than some other fractured element, B, will be identified by a fracture intensity level higher than that of element B.

This procedure, of course, does not eliminate the trial and error method necessary in finding the solution associated with the complete fracture of the solid; that is, solution when fracture reaches a free surface. Once this solution is obtained, excess stresses associated with fractured elements are computed. The total range from minimum to maximum excess stress magnitude is divided into a number of intervals and labeled in terms of the fracture intensity levels. The computer code is written to plot the fractured elements together with their respective stress intensity levels. From the plotted output,

it is possible to trace the approximate crack propagation path; with the crack initiating at the point of the highest stress intensity level and progressing in the direction of decreasing fracture levels.

D. Summary

The thermal fragmentation analysis is performed in three steps. The first step involves the temperature solutions obtained by using a finite element conduction code. Average thermal properties are used in this part of the analysis. The temperature results are then used as input into the finite element stress code TRATSA. Thermo-elastic properties are allowed to vary with temperature for the stress analysis. Principal stresses are computed and read through the fracture code. Fracture predictions are based on the Griffith and the McClintock-Walsh modified Griffith criteria. The solid is assumed to remain a continuum and the effects of crack initiation on temperature and stress fields are neglected. The concept of fracture intensity level, based on the stress magnitude in excess of that required for fracture was introduced to obtain an approximation to the fracture propagation path.

CHAPTER IV

SLOT MODEL ANALYSES

As mentioned in Ch. I, the slot model is obtained by passing a cutting plane along a series of holes and observing the geometry that is projected on the cutting plane. This model was designed for the parametric study of the fracture which occurs on a plane perpendicular to the hole axes passing approximately through the thermal inclusions. This fracture is parallel to the working face and makes possible the removal of a layer equal to the depth of the thermal inclusions. In the subsequent discussion this subsurface fracture, due to its orientation with respect to the working face, is referred to as the parallel fracture. The significance of the process parameters which are the hole diameter, hole depth, hole spacing and the depth of heating on the actual removal of the layer can be approximated by studying their influence on the parallel fracture. The slot model studies, therefore, are of primary importance.

In order to study the significant process parameters, twenty different slot models were analyzed. Effects of hole diameter and hole spacing were studied by using three different values of each; the combinations giving nine different fracture lengths. Effects of convection depth and melt depth were investigated using various combinations of these values for a given hole diameter and hole spacing. Parametric description of these models is given in Table IV.

TABLE IV

Parametric Description of Slot Models

Model	Hole Diam d, in.	Spacing c, in.	Fracture Length L = c-d	Melt Depth a, in.	Conv. Depth a_c = A-a
1A	1.0	4.0	3.0	0.5	1.5
1A-1				2.0	0.0
1A-2				2.0	2.0
1A-3				4.0	0.0
1B	1.0	8.0	7.0	0.5	3.0
1C	1.0	12.0	11.0	0.5	5.0
2A	2.0	4.0	2.0	0.5	1.0
2A-1				1.2	0.8
2A-2				0.5	0.1
2B	2.0	8.0	6.0	0.5	3.0
2B-1					0.1
2C	2.0	12.0	10.0	0.5	5.0
2C-1					3.0
2C-2					0.1
3A	1.5	4.0	2.5	0.5	1.5
3B		8.0	6.5		3.0
3C		12.0	10.5		5.0
11A	2.0	5.0	3.0	0.5	1.5
13B		8.5	6.5		3.0
13C		12.5	10.5		5.0

A. Grid Size Effects

Accuracy of the finite element solution depends largely on the size of the elements; the smaller the element size, the more accurate the solution. However, computer time increases with an increase in the number of elements. Hence, it is necessary to adjust the finite element grid so that acceptable solutions can be obtained economically. Fairly large elements can be used in the areas where low stresses are expected, whereas regions of high stress concentrations should be divided into very fine grids. Thus, the problem geometry and the boundary conditions should be given primary consideration in drawing the finite element grid. For thermal stress problems, the magnitude of the temperature gradient must also be taken into consideration as it greatly influences the stress field.

For the slot model analysis, effects of element size and time increment were investigated. A value of 0.2 seconds for the time increment for a typical grid shown in Fig. 4.1 was found to yield quite accurate results. Size of the smallest elements used in this grid is 0.025 in. square.

B. Melt Depth Studies

The stress state in the elastic rock surrounding the heater and molten rock inclusion depends on the temperature field and mechanical constraints in the form of specified displacement boundary conditions. Due to the poor thermal conductivity of rocks, the resulting thermal gradients are very steep. This requires very small sized elements for a reasonably accurate analysis. It is necessary, therefore, to

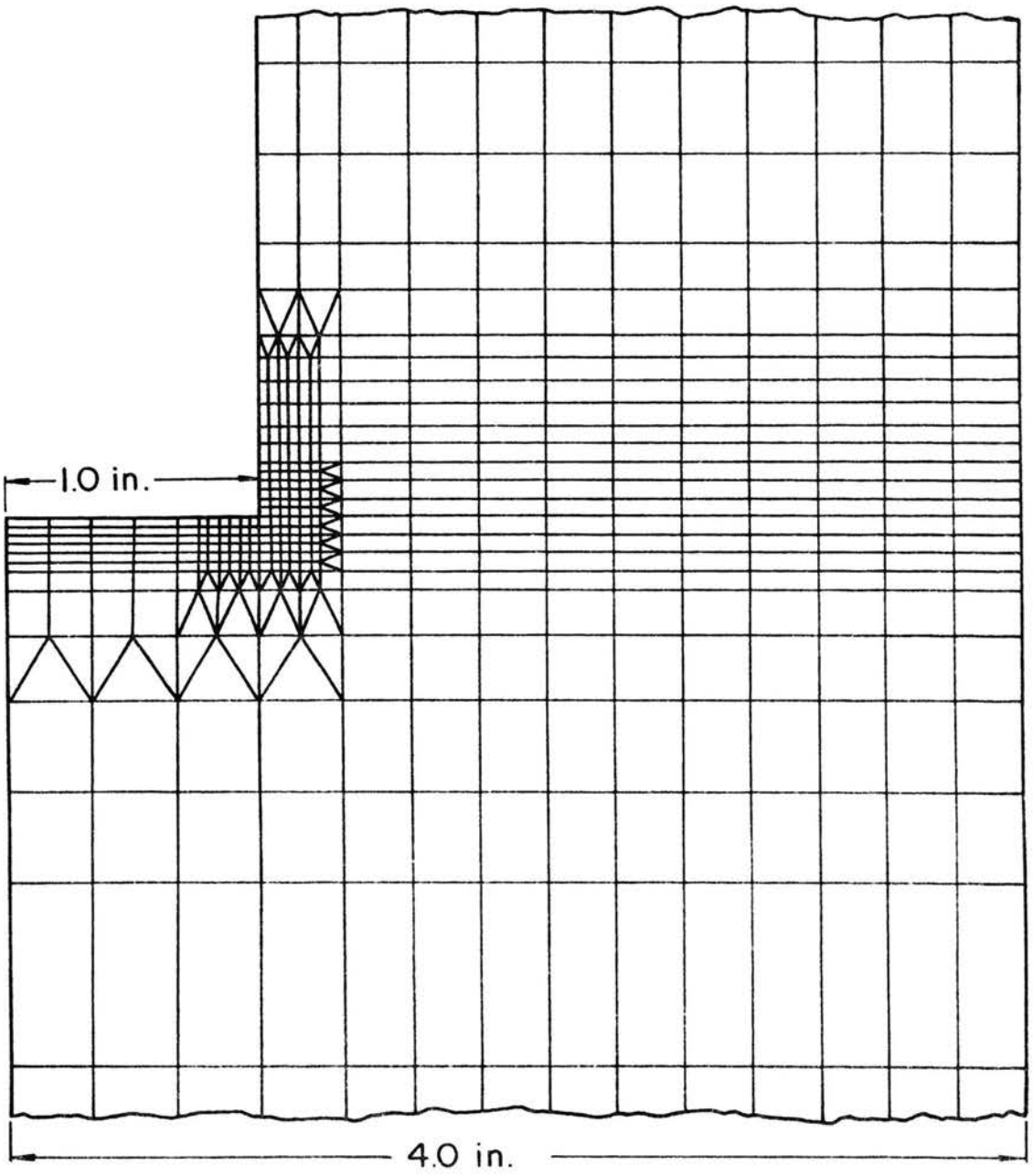

3.4.1 TYPICAL FINITE ELEMENT GRID FOR THE SLOT MODEL ANALYSIS

reduce the semi-infinite problem geometry to a finite region for numerical treatment.

The experimentally observed fractures occur in the vicinity of the slot base. This location for the secondary fractures is highly desirable from an economical viewpoint. Hole depths used in the field tests varied from 12.0 in. to about 30.0 in. and the thermal inclusions were observed to be in the range from 4.0 in. to 12.0 in. in length. These values were much too high to be used for the numerical finite element analysis. However, for a given geometry under identical mechanical constraints, the stress field in an area depends only on the temperature field in that area. Thus, it is possible to obtain a reasonably accurate stress field in the vicinity of the slot base by using small melt depths provided the temperature field in this area remains fairly constant for different melt depths.

Effects of different melt depths and convection depths on the temperature field in the vicinity of the slot base were investigated using models 1A-1, 1A-2, and 1A-3. Parametric description of these models is given in Table IV.

Results of these studies are plotted in Figs. 4.2-4.7 which show the temperature plots for two different time values. Temperature contours are plotted in increments of 100°C except for the 50°C contour. The melt temperature used in the analysis was 1250°C. Comparison of these results show that the temperature field in the vicinity of the slot base does remain fairly constant for different combinations of melt depth and convection depth values. However, it should be realized that for the above statement to be true, there exists a lower limit on

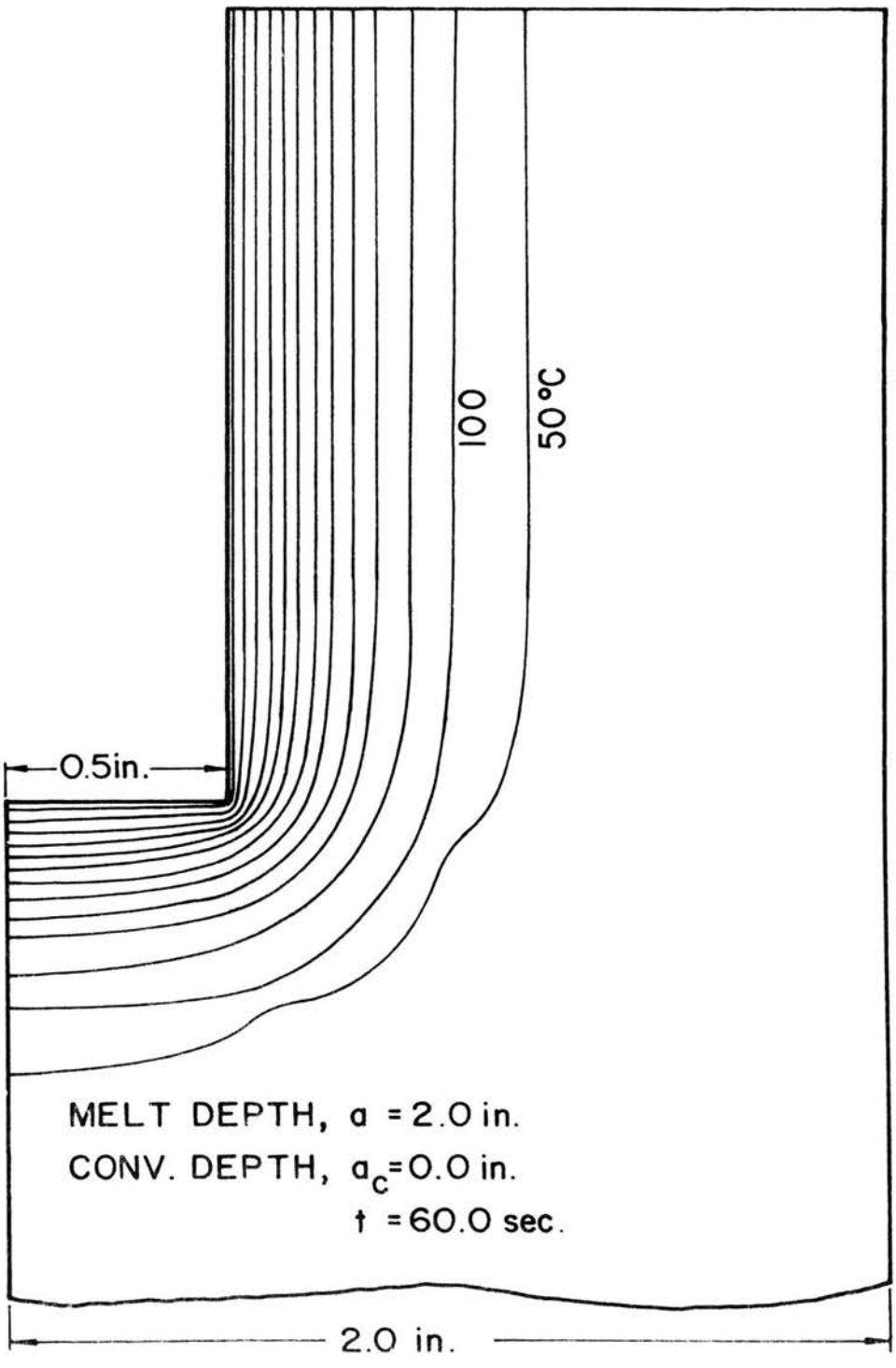

FIG. 4.2 TEMPERATURE DISTRIBUTION, MODEL IA-1, t=60 sec.

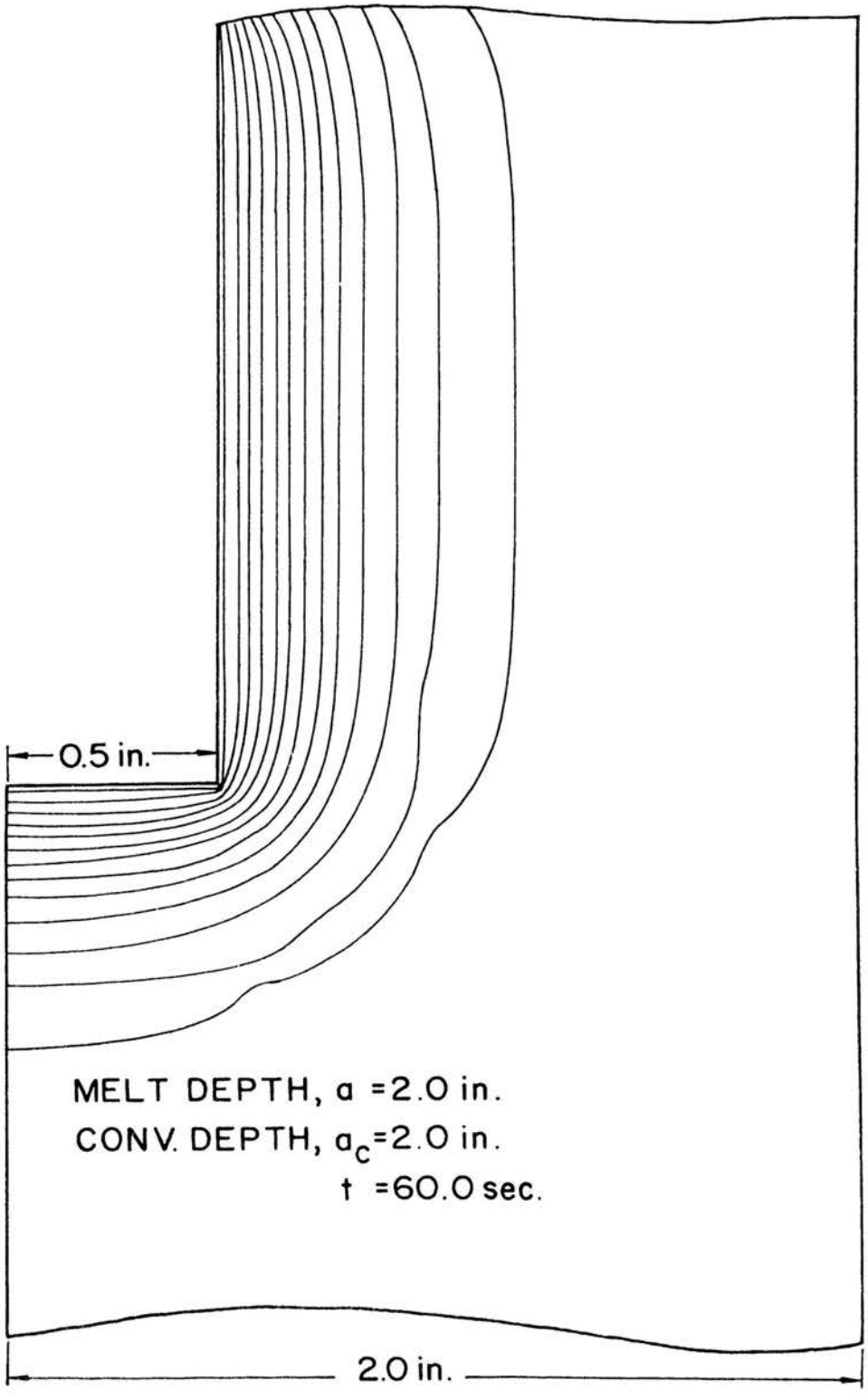

FIG. 4.3 TEMPERATURE DISTRIBUTION, MODEL 1A-2, t=60 sec.

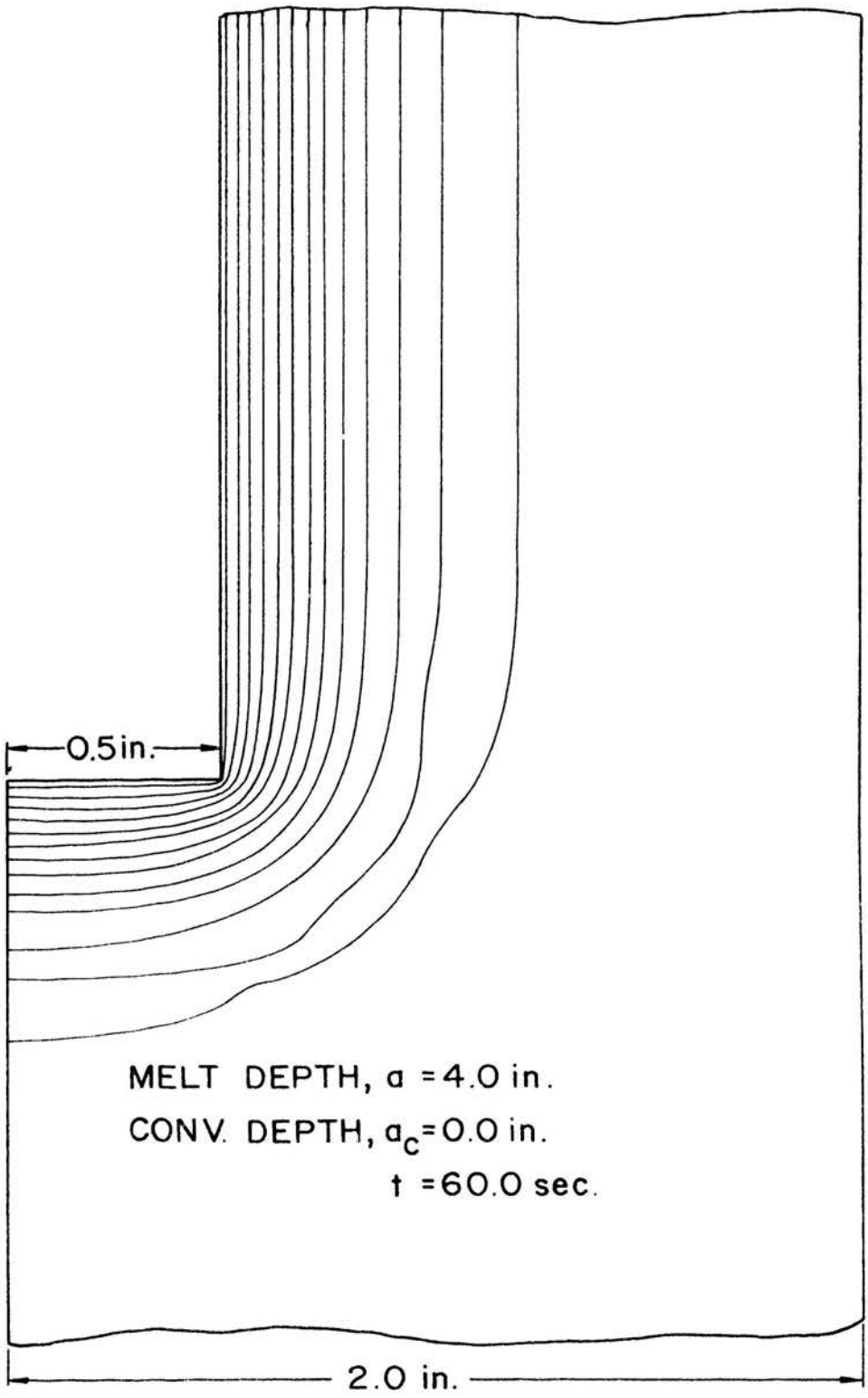

FIG. 4.4 TEMPERATURE DISTRIBUTION, MODEL IA-3, t =60 sec.

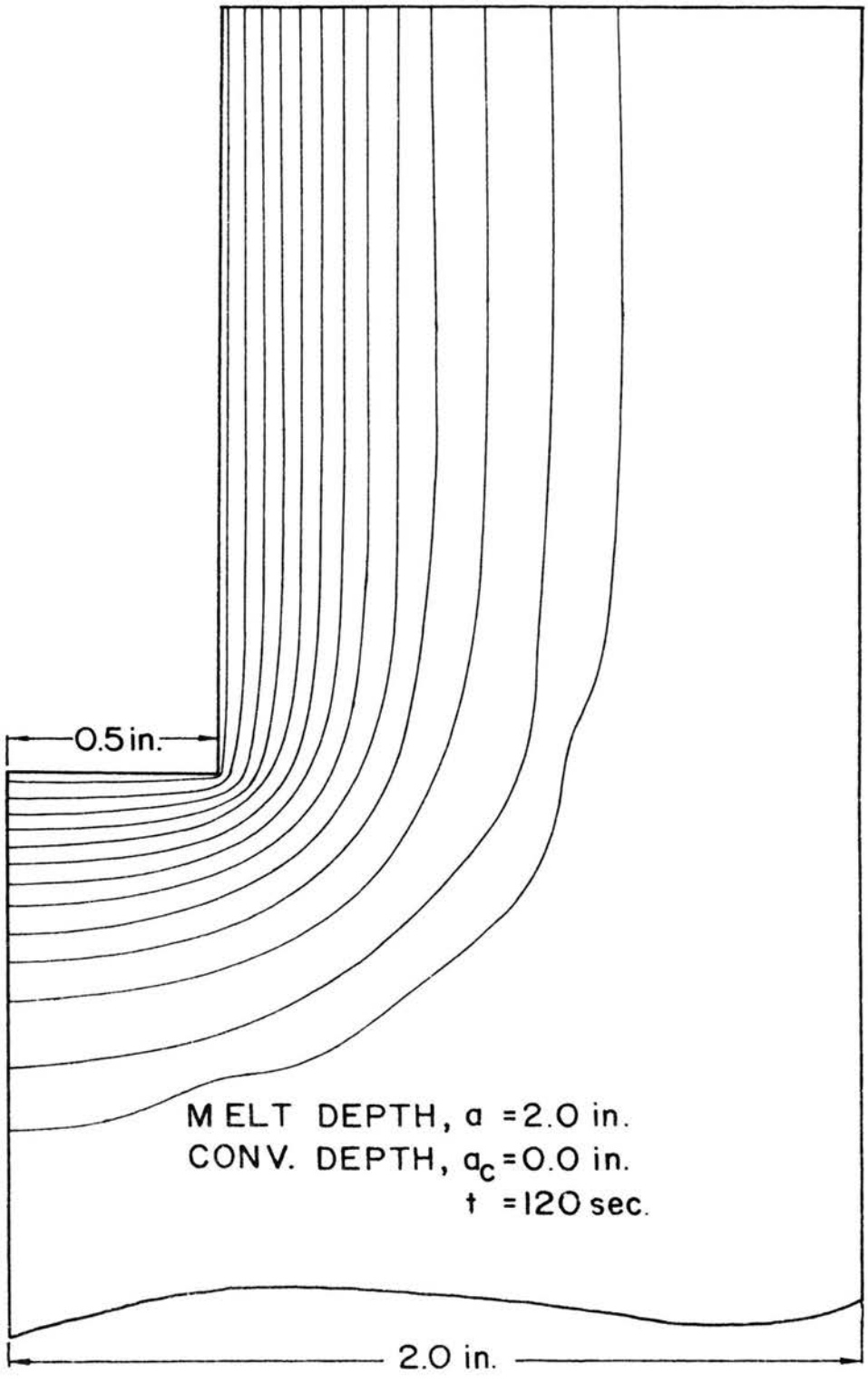

FIG. 4.5 TEMPERATURE DISTRIBUTION, MODEL 1A-1, t = 120 sec.

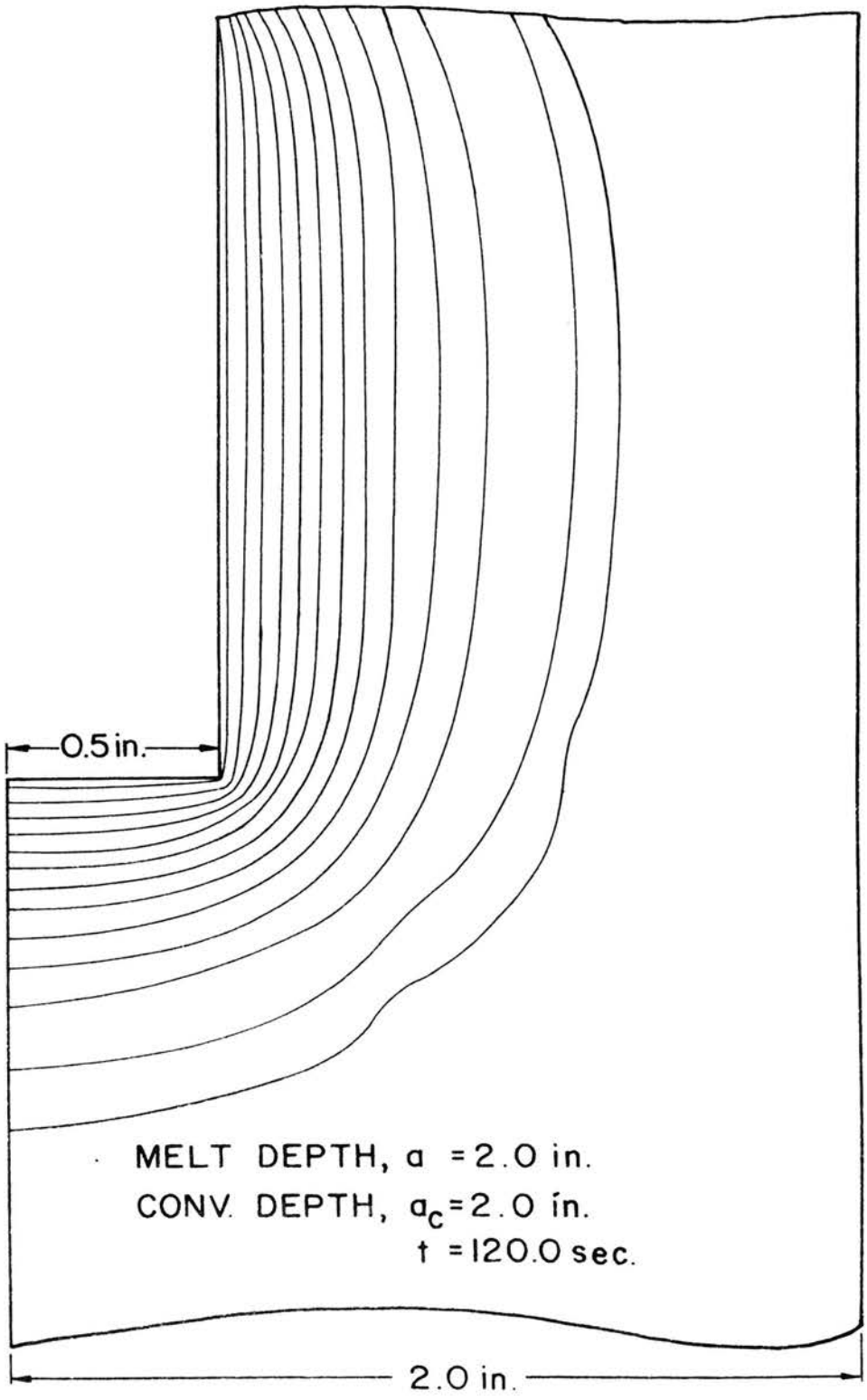

FIG. 4.6 TEMPERATURE DISTRIBUTION, MODEL 1A-2, t=120 sec.

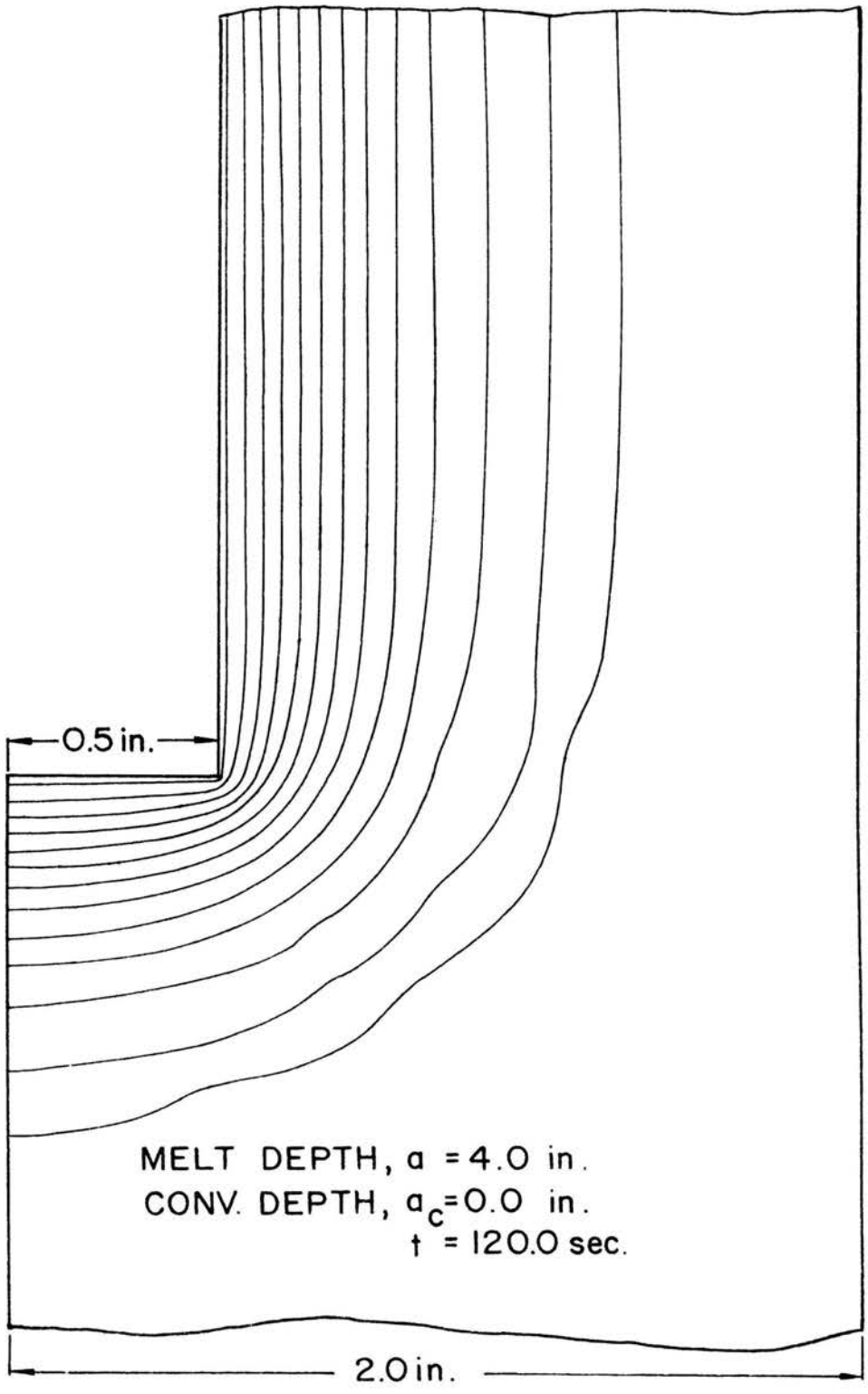

FIG. 4.7 TEMPERATURE DISTRIBUTION, MODEL 1A-3, t=120 sec.

the value of the melt depth, a. A value of 0.5 in. was found to be sufficiently high in order to obtain an invariant temperature field in the immediate surrounding of the slot base. The subsequent analysis was, therefore, completed using a melt depth value of 0.5 in.

C. Convection Depth Studies

As seen from the results shown in Figs. 4.2 - 4.7, the temperature distribution in the vicinity of the slot base is independent of the convection depth. However, for small melt depths, the stress field in this region is highly dependent on the convection depth. This effect results from two factors. Although the temperature distribution as seen from Figs. 4.2 - 4.7 is approximately one-dimensional in the melt-depth section, thermal gradients near the point of transition from melt condition to convection condition are highly localized. These highly localized gradients give rise to very high stress concentrations. Also, due to the localized heating, the thermal expansion of this area is restrained by the relatively large cold zone. This thermally induced constraint induces very high compressive stresses in the heated zone and tensile stresses in the cold zone. For a given temperature distribution, the severeness of the thermal constraint increases with increase in the volume of the cold zone, up to a certain critical value. Once the cold zone volume reaches this critical value, any further increase has no effect on the stress field. For the slot models, since the volume of the cold zone depends directly on the convection depth, there exists a critical value of the convection depth beyond which any increase in

the convection depth has no significant effect on the fracture inducing stresses.

The convection depth studies were conducted using models 2A, 2A-1, 2A-2; 2B, 2B-1; and 2C, 2C-1, 2C-2. The hole diameter for these models was kept constant. Three values of hole spacing were considered, giving three different fracture lengths. For models of equal fracture length, convection depths were varied, the highest value being approximately equal to half the fracture length. Parametric description of these models is given in Table IV.

The results of these studies are shown in Figs. 4.8 - 4.15. In view of the assumption that the material above 700°C has no elastic resistance, the problem geometry is modified using the 700°C isotherm. The fracture completion time is denoted by t_f, and the probable fracture zones at this time are shown by the cross-hatched area. The doubly cross-hatched area shows the fracture zone governed by the McClintock-Walsh modified Griffith criterion, Eqs. 2.4. The remainder of the fracture zone is governed by the original Griffith criterion, Eqs. 2.1 and 2.2. In the subsequent discussion, the two types of fracture zones are referred to as the McClintock-Walsh zone and the Griffith zone, respectively.

The McClintock-Walsh zone is associated with very high compressive stress components. For very small or no convection depths, the fracture is characterized by a McClintock-Walsh zone in the high temperature region followed by a small Griffith tension zone in the low temperature area and a large secondary McClintock-Walsh zone extending to the line of symmetry. The increase in the cold zone

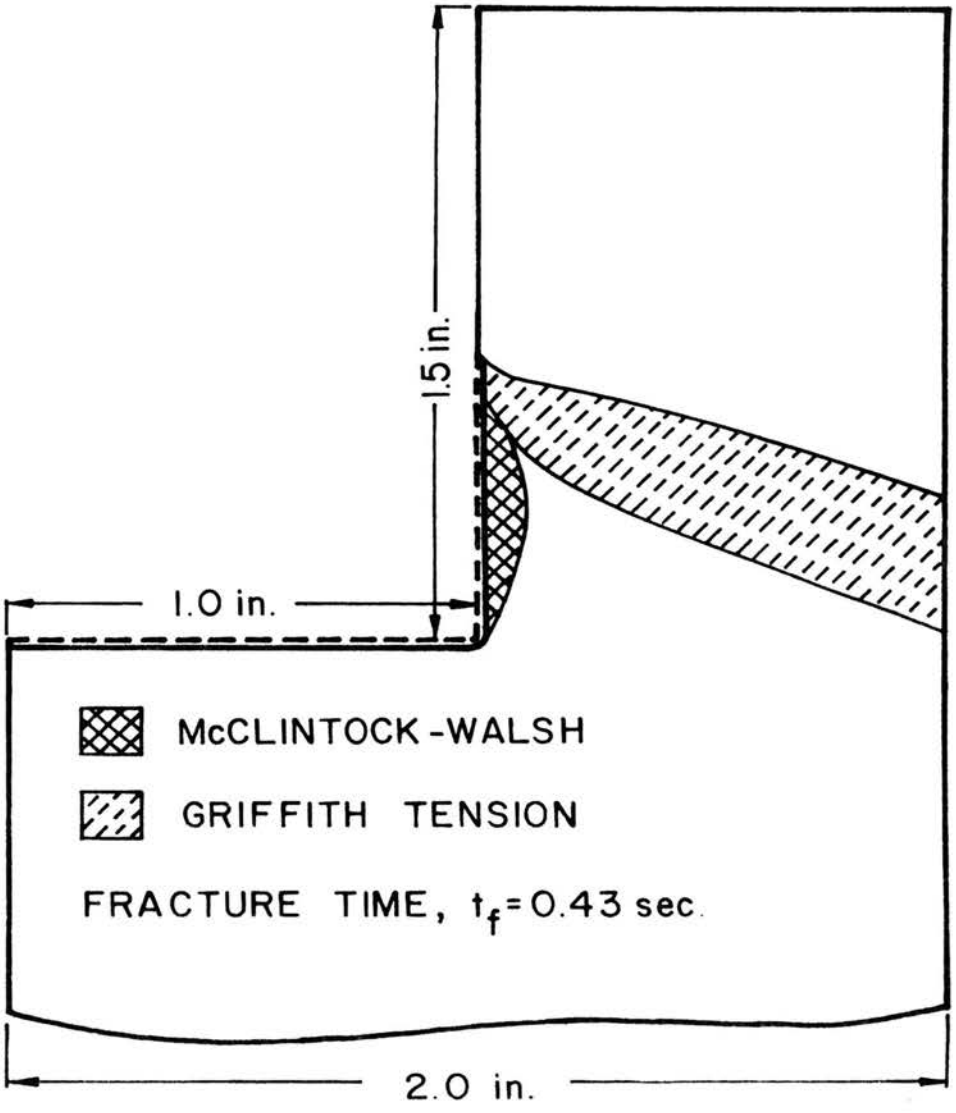

FIG. 4.8 FRACTURE ZONES, MODEL 2A

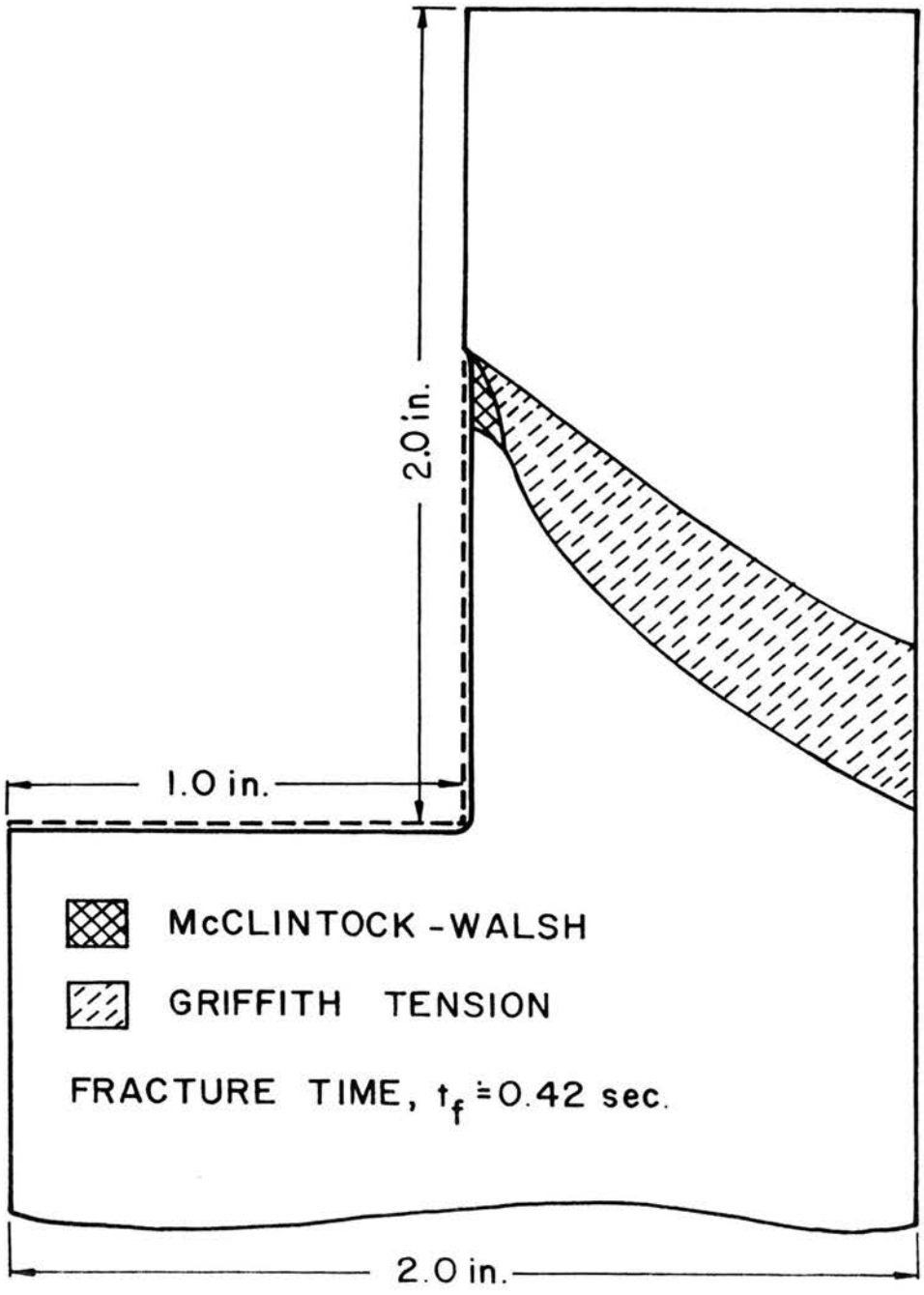

FIG. 4.9 FRACTURE ZONES, MODEL 2A-1

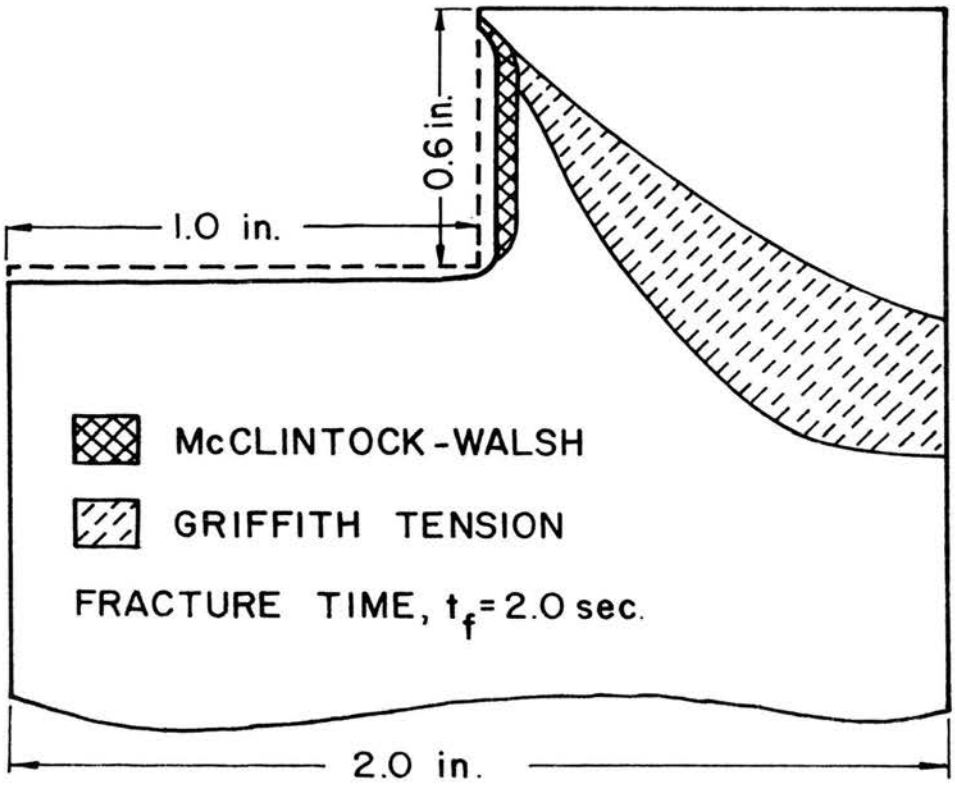

FIG. 4.10 FRACTURE ZONES, MODEL 2A-2

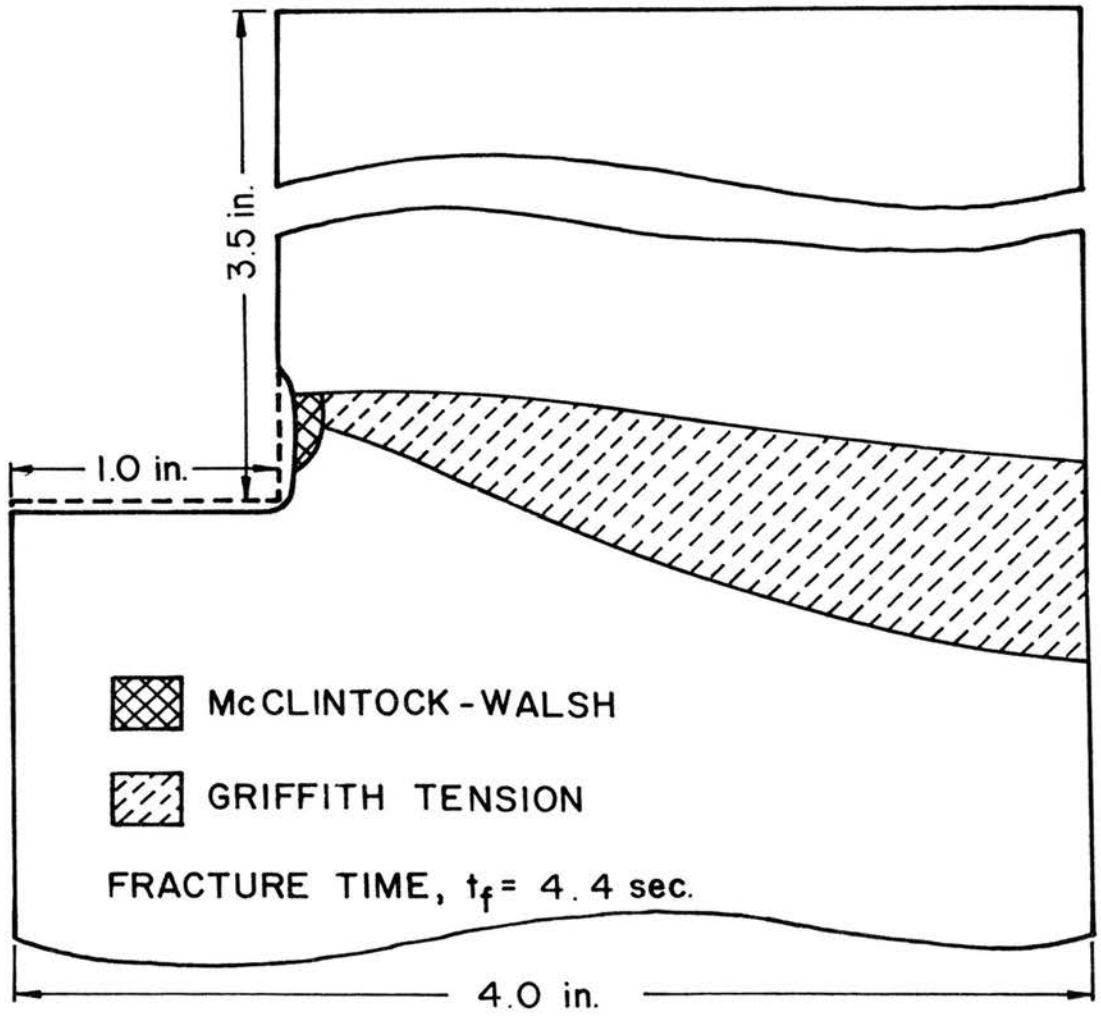

FIG.4.11 FRACTURE ZONES, MODEL 2B

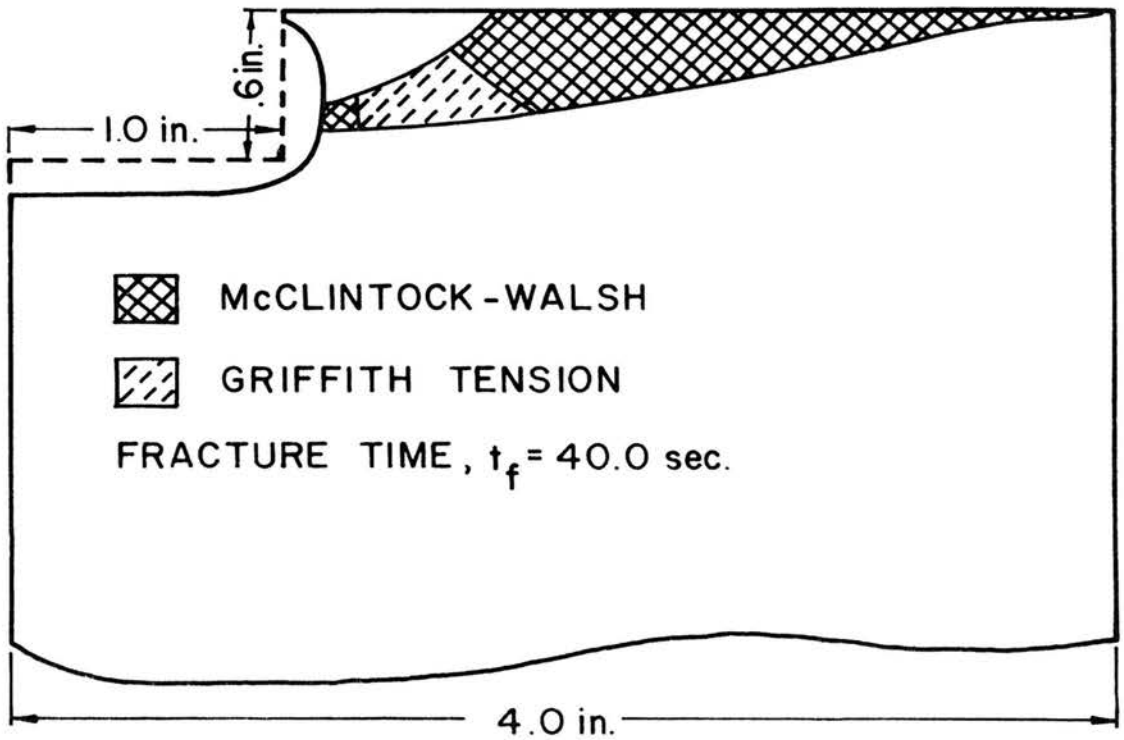

FIG. 4.12 FRACTURE ZONES, MODEL 2B-1

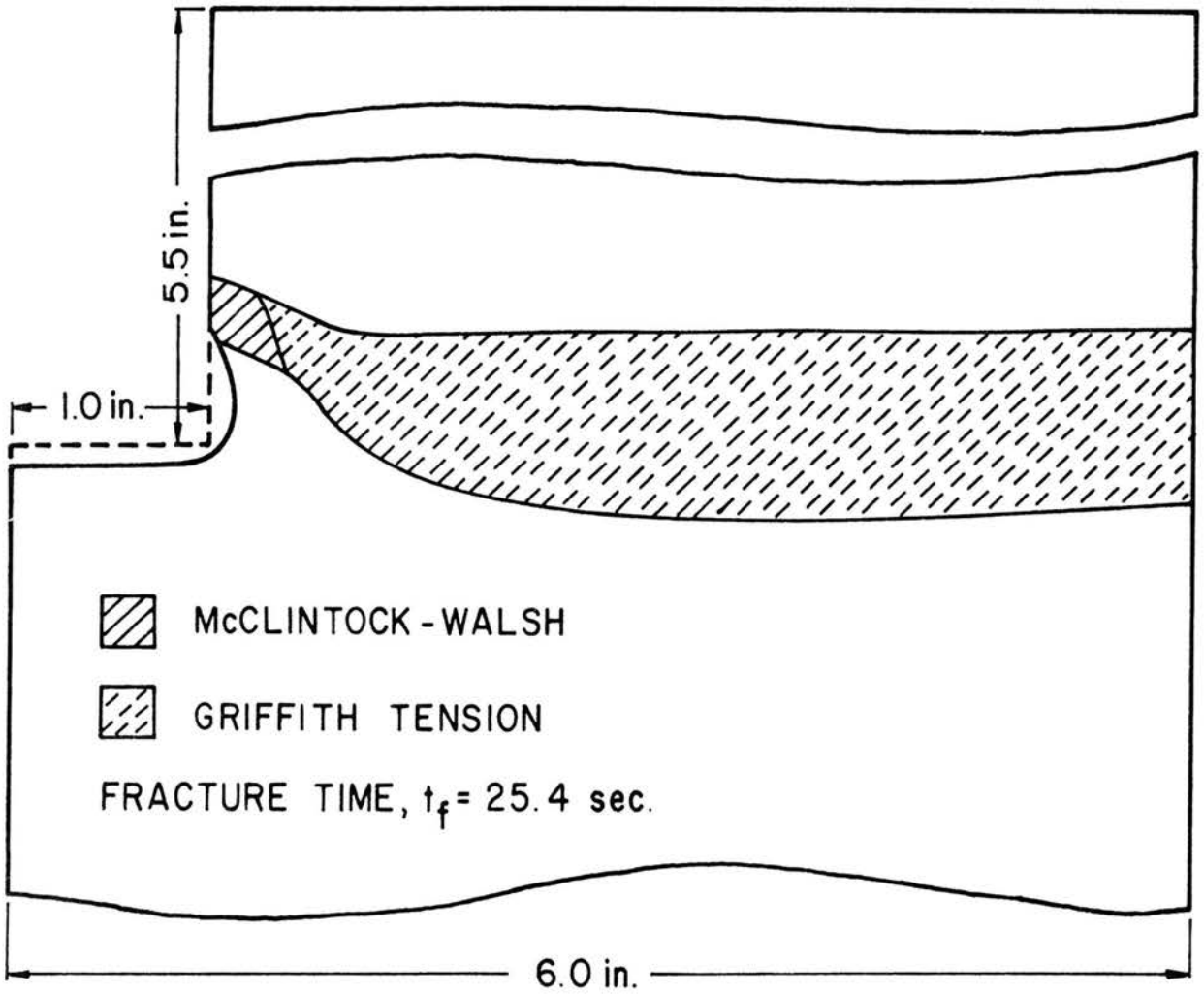

FIG. 4.13 FRACTURE ZONES, MODEL 2C

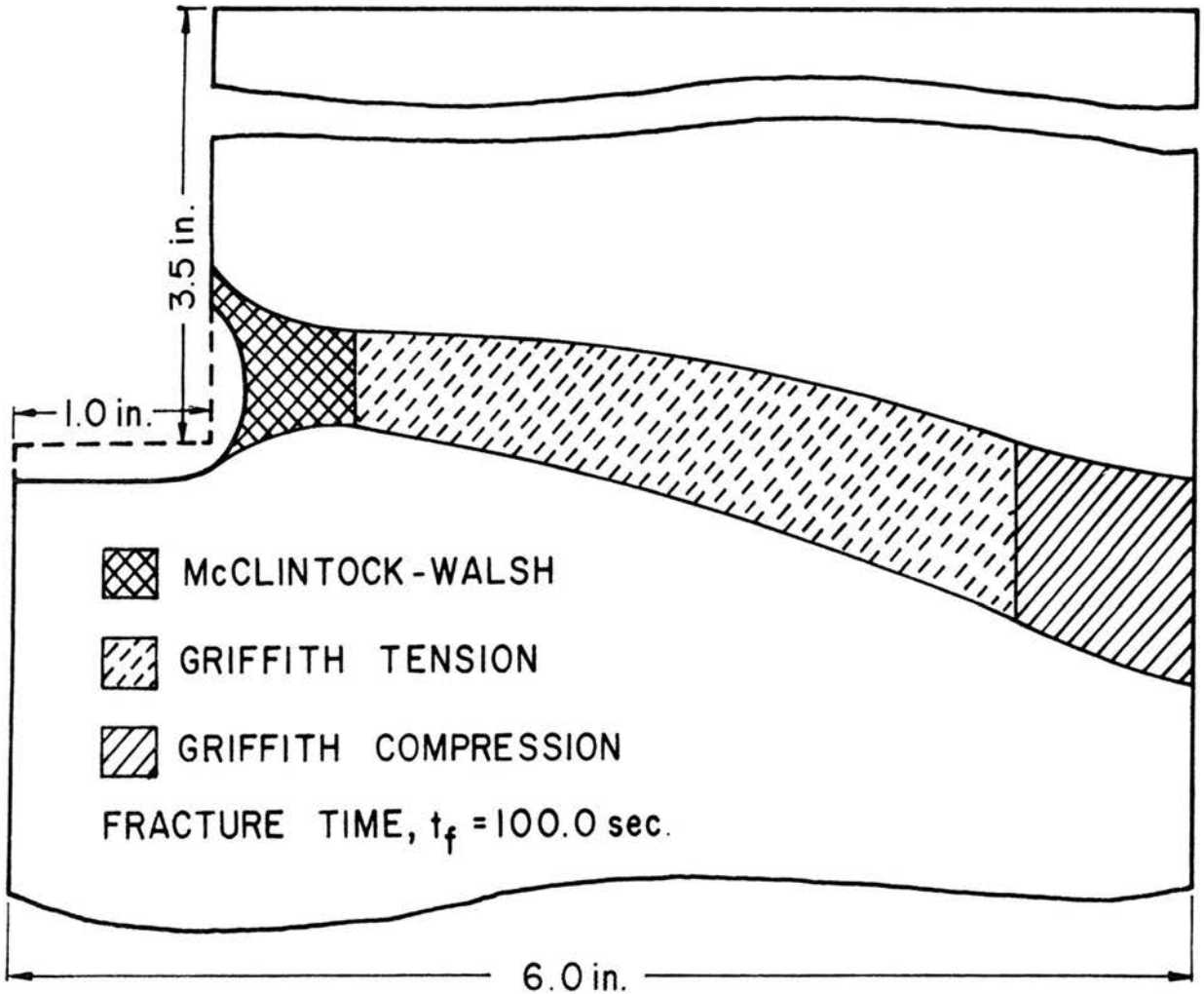

FIG. 4.14 FRACTURE ZONES, MODEL 2C-1

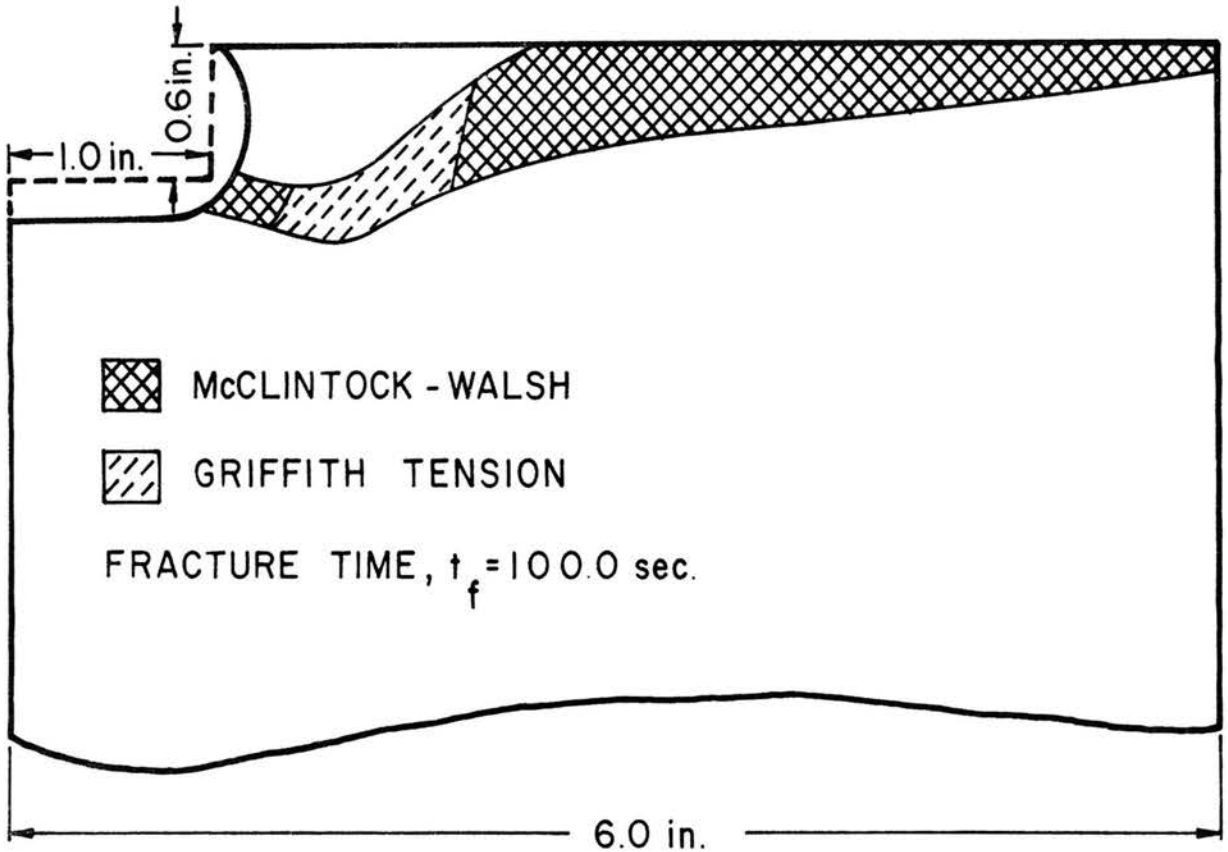

FIG. 4.15 FRACTURE ZONES, MODEL 2C-2

volume and the consequent thermal constraint as a result of the increase in the convection depth has relatively little influence on the McClintock-Walsh zone in the high temperature area and the small Griffith zone immediately following it. This is due to the fact that the stress state in these zones result primarily from the temperature gradients and that changes in the convection depth have very little effect on the temperature field in this region.

The McClintock-Walsh zone in the cold region is, however, greatly influenced by convection depth changes. As the convection depth is increased, the thermal constraint becomes more severe. As a result, the high compressive stress components in the cold region start to decrease in magnitude and the tensile stress components increase sharply. The net effect of these changes in the stress components is that the secondary McClintock-Walsh zone begins to shrink. If the convection depth is continuously increased, a stage is reached when the secondary McClintock-Walsh zone completely disappears and transforms into the Griffith tension zone which now extends to the line of symmetry. In this discussion, the convection depth associated with the completion of the above transformation is referred to as the critical convection depth.

The critical convection depth was found to be approximately equal to half the fracture length. From the results for convection depths approximately equal to the critical value, it is seen that the total fracture zone consists of a small McClintock-Walsh zone in the high temperature region followed by a Griffith tension zone in the low temperature region and extending all the way to the line of symmetry.

For convection depths smaller than the critical value, the fracture time shows only small variations with changes in convection depth. However, as the convection depth approaches the critical value, the McClintock-Walsh zone rapidly transforms into the Griffith tension zone, and because of the tensile strength of the rock being much lower than its compressive strength, the fracture time is drastically reduced. Once the fracture mode transformation is completed, the fracture time shows a negligibly small decrease with any further increase in the convection depth.

The fracture zones in Figs. 4.8 - 4.15 show another very important effect of the convection depth changes. This effect involves the location of the parallel fracture. The optimum location of the parallel fracture requires the crack initiation to occur very close to the hole base and the crack propagation in a plane approximately parallel to the hole base. The fracture zones in Figs. 4.8 - 4.15 indicate that, in order to obtain the optimum location, the thermal inclusion should be concentrated at the very base of the hole while the convection depth should, at least, be equal to half the fracture length, and that any further increase in the convection depth has only a trivial influence on the location of the parallel cracks and the fracture time.

D. Hole Diameter and Spacing Studies

Hole diameter and the hole spacing are, perhaps, the two most significant parameters in the study of rock fragmentation using subsurface thermal inclusions. The hole diameter effects the fracture length as well as the size of the thermal inclusion. The hole

spacing, however, is the more important factor as it directly controls the volume of the rock removed.

In order to investigate the effects of the hole diameter and the hole spacing, nine fracture lengths were considered. Hole spacings of 4.0 in., 8.0 in., and 12.0 in. were used and for each hole spacing, hole diameter values of 1.0 in., 1.5 in., and 2.0 in. were considered.

In Table IV, the models used for the hole diameter and the hole spacing studies are identified as 1A, 1B, 1C; 2A, 2B, 2C; and 3A, 3B, 3C. The melt depth and the convection depth values were selected based on the results of the melt depth and the convection depth studies as described in the beginning of this chapter. The melt depth value was kept constant at 0.5 in. for all models. For a given model, the total hole depth considered was such that the convection depth was approximately equal to the critical value, that is, approximately half the fracture length.

1. Temperature Field Characteristics

The temperature distribution at the time of fracture completion was found to be far from stationary and highly localized in the vicinity of the slot base. Plots of the typical temperature fields at the time of fracture completion are shown in Figs. 4.16 - 4.18. As seen from these plots, the major portion of the fractured volume does not experience any temperature change. Thus, the stresses in this region occur entirely due to the load vector resulting from the thermal constraint. The natural thermal expansion of the high temperature region is resisted by the cold volume. As a consequence of this constraint, the hot region undergoes a compressive loading while the

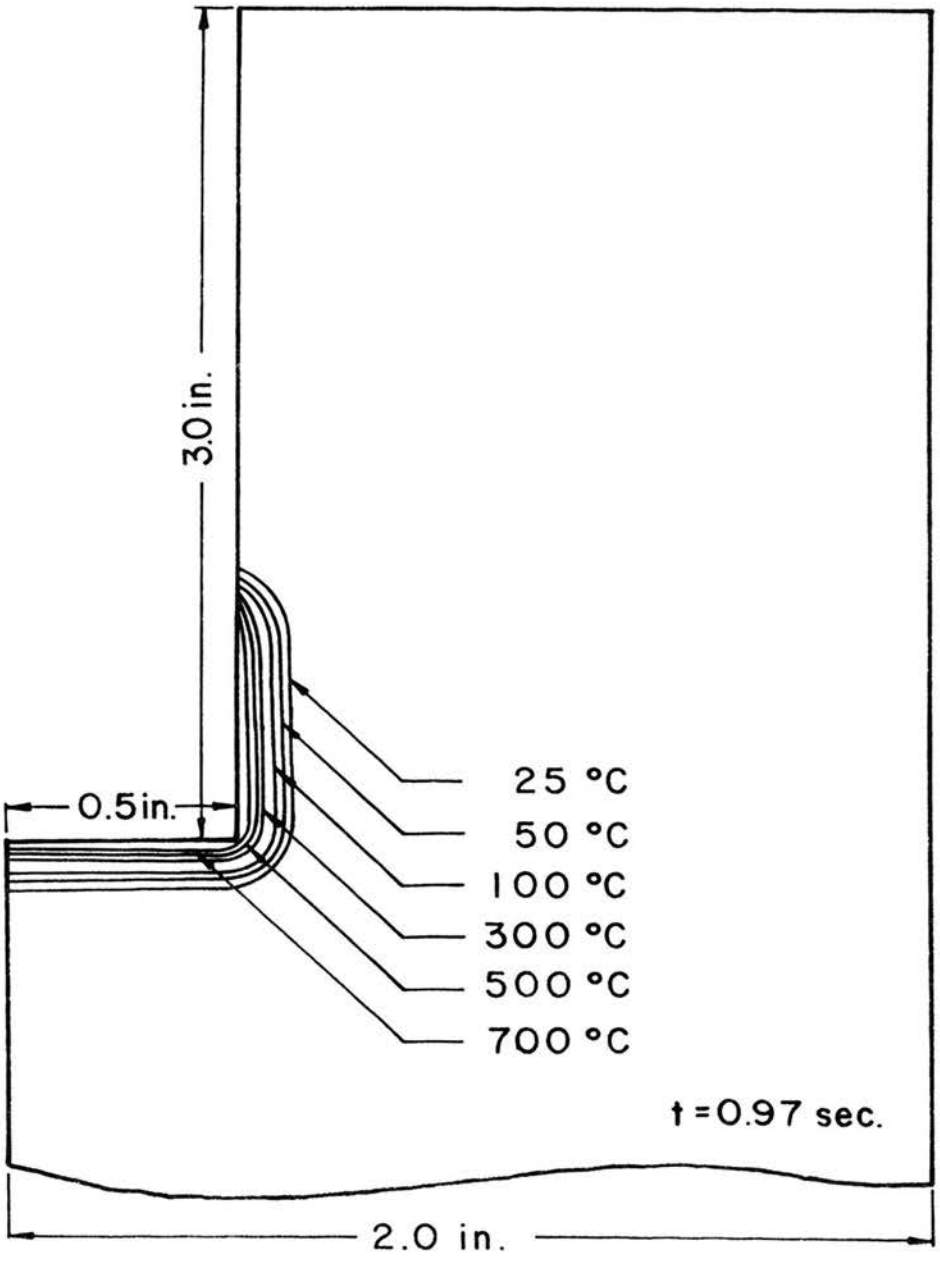

FIG. 4.16 TEMPERATURE DISTRIBUTION, MODEL 1A

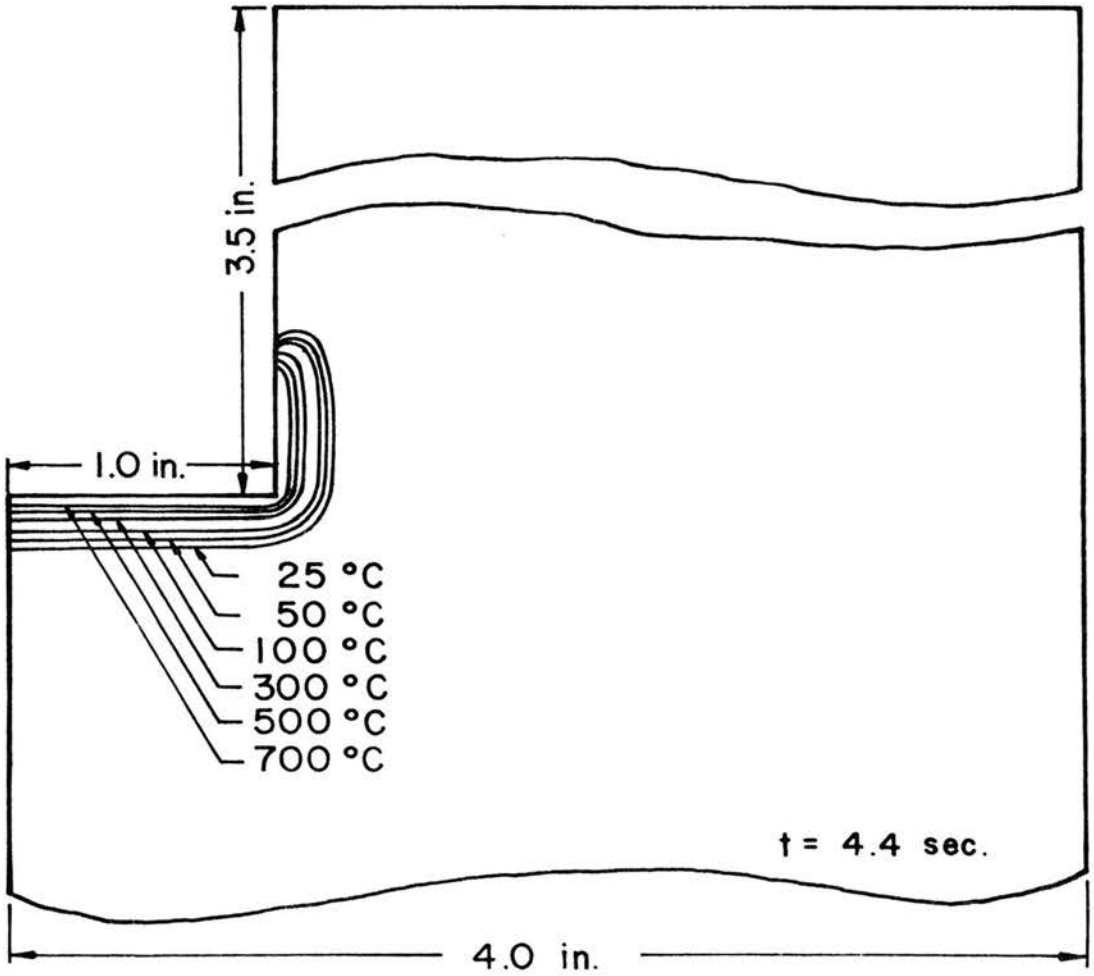

FIG. 4.17 TEMPERATURE DISTRIBUTION, MODEL 2B

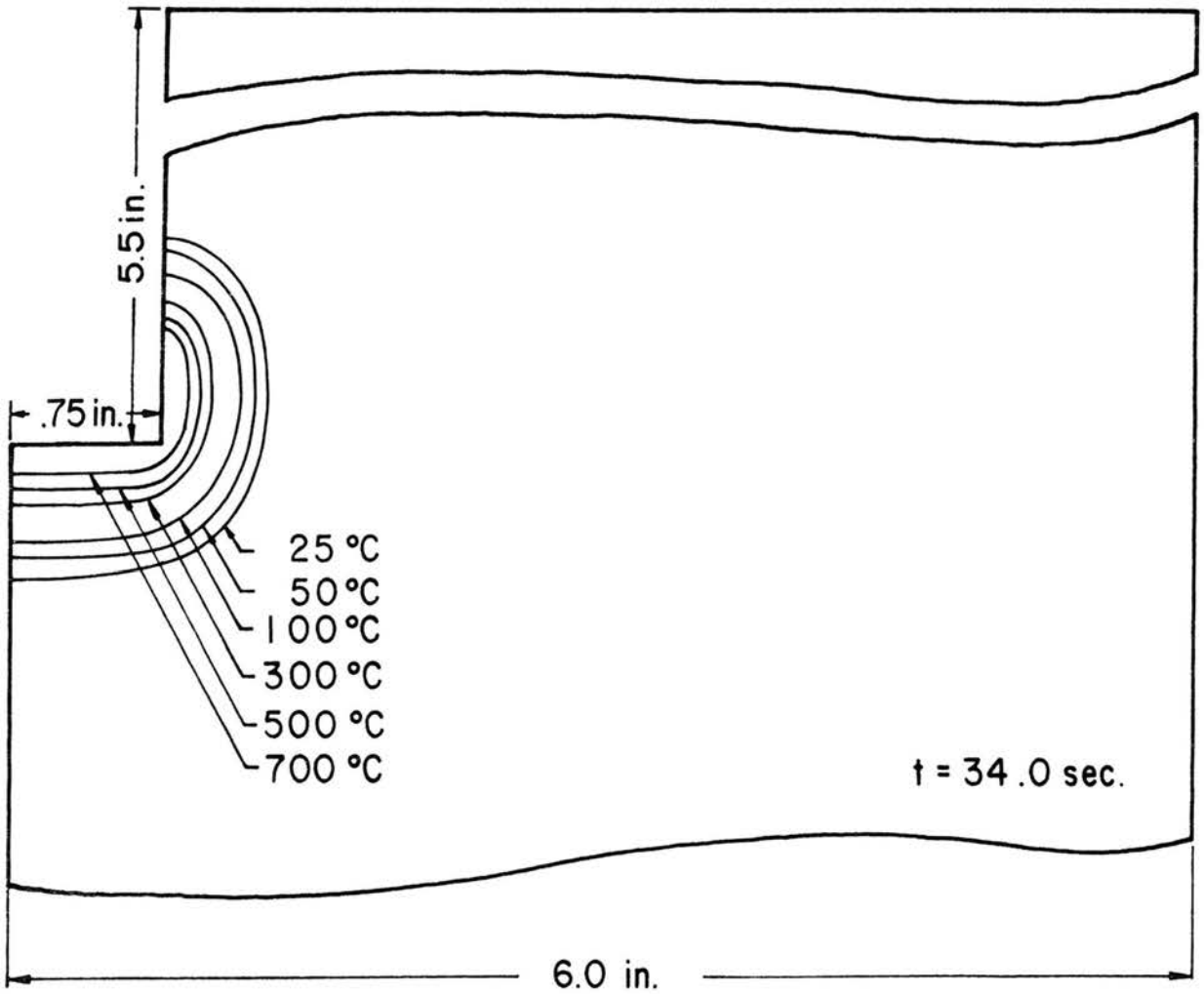

FIG. 4.18 TEMPERATURE DISTRIBUTION, MODEL 3C

cold zone is under a tensile load condition. In view of the equilibrium of forces, the compressive load vector integrated over the entire high temperature region must equal the tensile load vector integrated over the cold zone volume. Since the rock fracture is attributed to the tensile failure because of the tensile strength of rock being much lower than its compressive strength, only a small hot region is required to induce fracture causing stresses in a comparatively large cold zone.

As the hole spacing is increased, the cold zone volume also increases. A higher tensile load vector is therefore necessary in order to cause the fracture inducing stresses in the cold zone. This, in turn, requires a larger natural expansion of the hot region and, therefore, a larger volume of the hot zone and a longer time for fracture completion.

Thus, as the hole spacing is increased, the fracture completion time also increases. However, as seen from Figs. 4.16 - 4.18, the increase in the fracture completion time is much higher than the corresponding increase in the hot zone volume. This is explained by the fact that while the thermal expansion and the resulting force vector are directly dependent on the volume of the hot zone, the volume of the hot zone itself is a complex function of the thermal conductivity and the thermal diffusivity, and for rocks the values of both these properties are extremely low.

2. Fracture Length Effects

From the above discussion, it is clear that while for a given hole diameter, increasing the hole spacing increases the fracture completion time, it must also be true that for a given hole spacing,

the fracture completion time will decrease if the hole diameter is increased. In other words, it is the change in the fracture length that affects the fracture completion time. This is demonstrated by the fracture zone plots shown in Figs. 4.8, 4.11, 4.13, 4.19 - 4.21, and the fracture completion time versus the hole spacing plots shown in Fig. 4.22.

It is possible, therefore, to study the effect of the change in hole diameter on the fracture time by keeping the hole diameter unchanged and changing the hole spacing such that the fracture length will remain the same. Models 11A, 13B, and 13C as described in Table IV were designed in support of this hypothesis. These models were obtained by increasing the diameters of models 1A, 3B, and 3C to 2.0 in. and increasing the hole spacing correspondingly so as to keep the fracture lengths unchanged.

Plots of the fracture zones for models 11A, 13B, and 13C are shown in Figs. 4.23 - 4.25. Comparison of fracture times and the fracture plots of these models with those of models 1A, 3B, and 3C shown in Figs. 4.26, 4.20, and 4.21 confirms the above mentioned hypothesis.

E. Fracture Length - Fracture Time Relation

Results presented for different models indicate that the fracture completion time can be expressed as a function of the single variable, the fracture length. Fracture completion times for models with convection depths approximately equal to the critical convection depth are listed in Table V. Values from this table were used to compute the fracture length ratios and the corresponding fracture completion

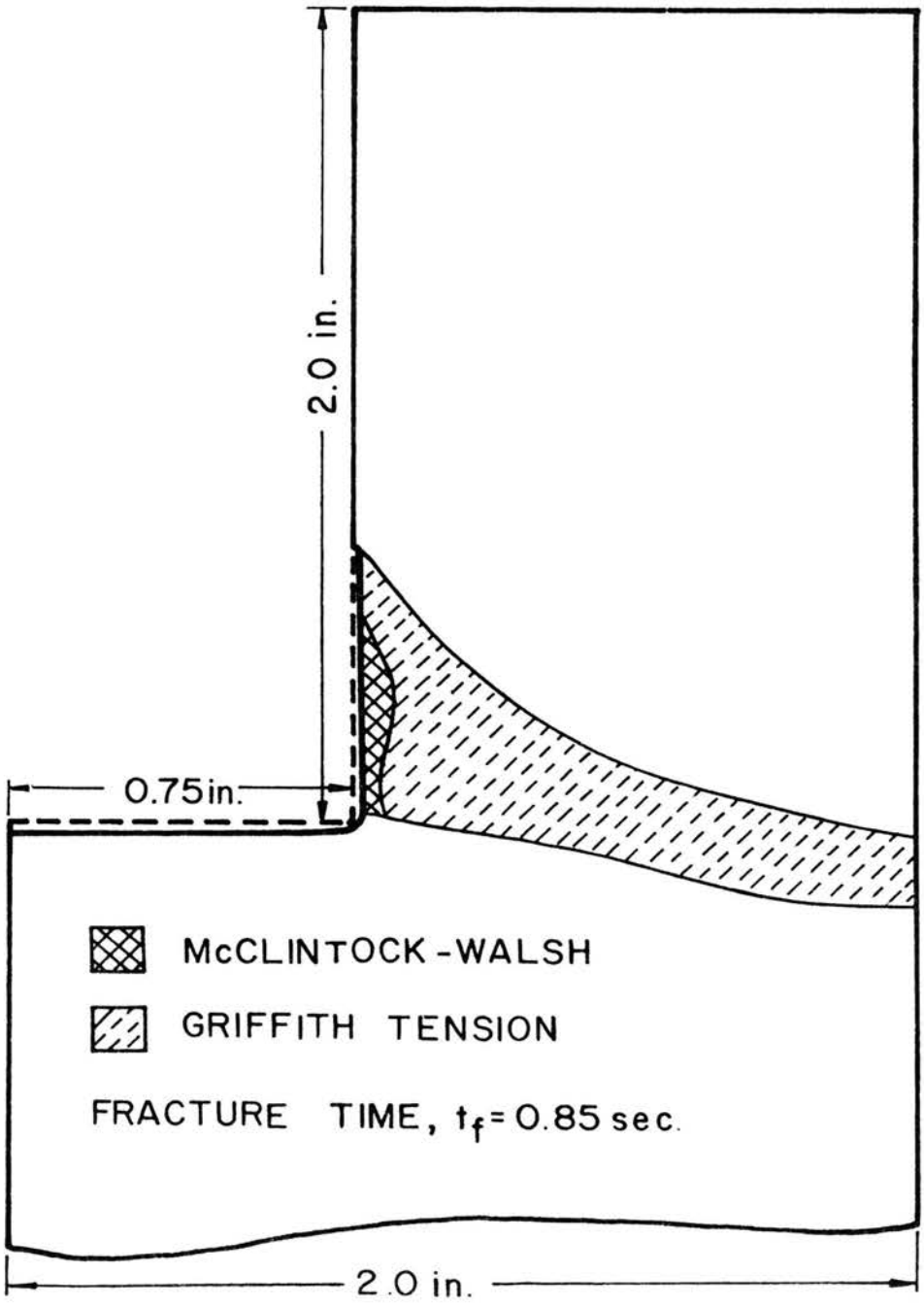

FIG. 4.19 FRACTURE ZONES, MODEL 3A

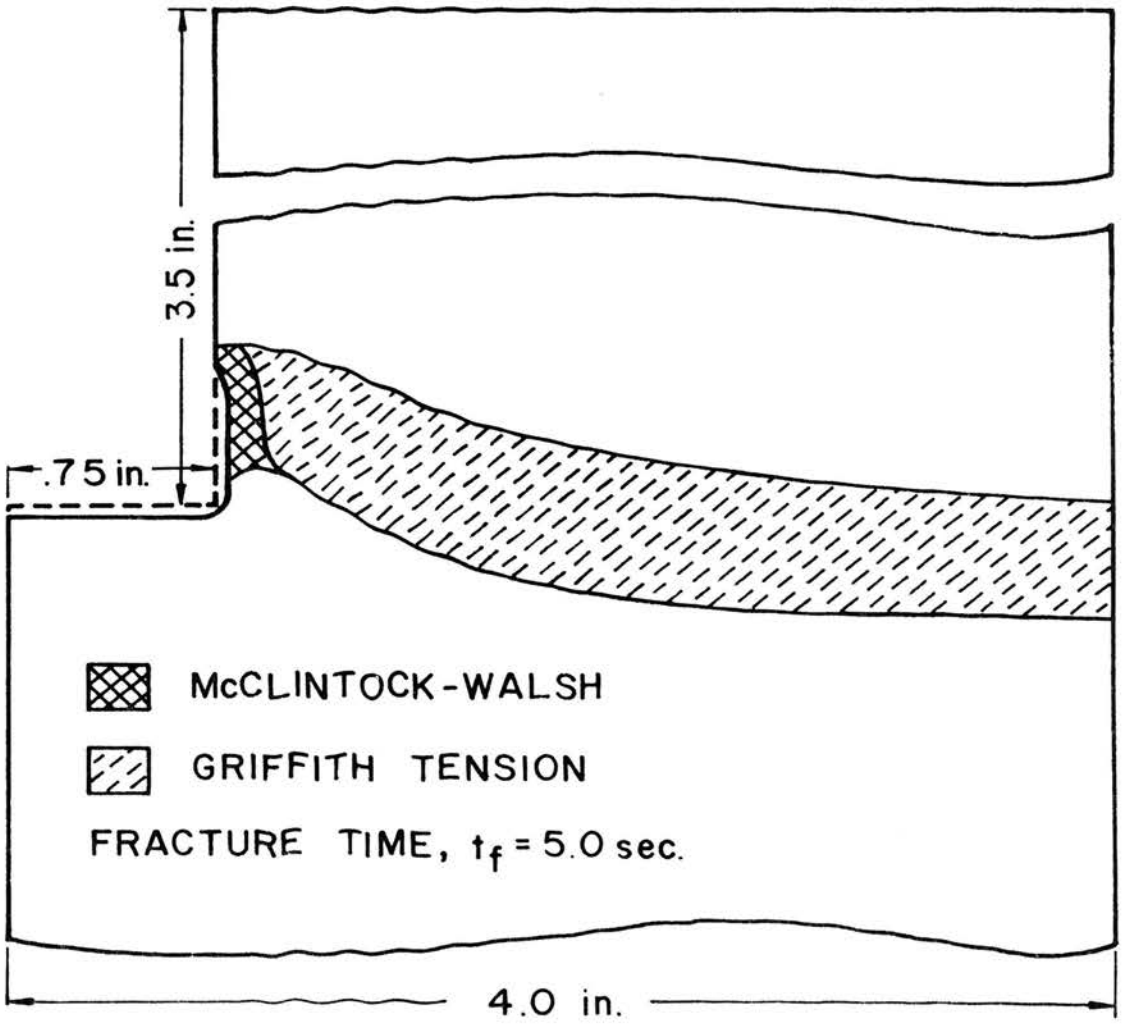

FIG. 4.20 FRACTURE ZONES, MODEL 3B

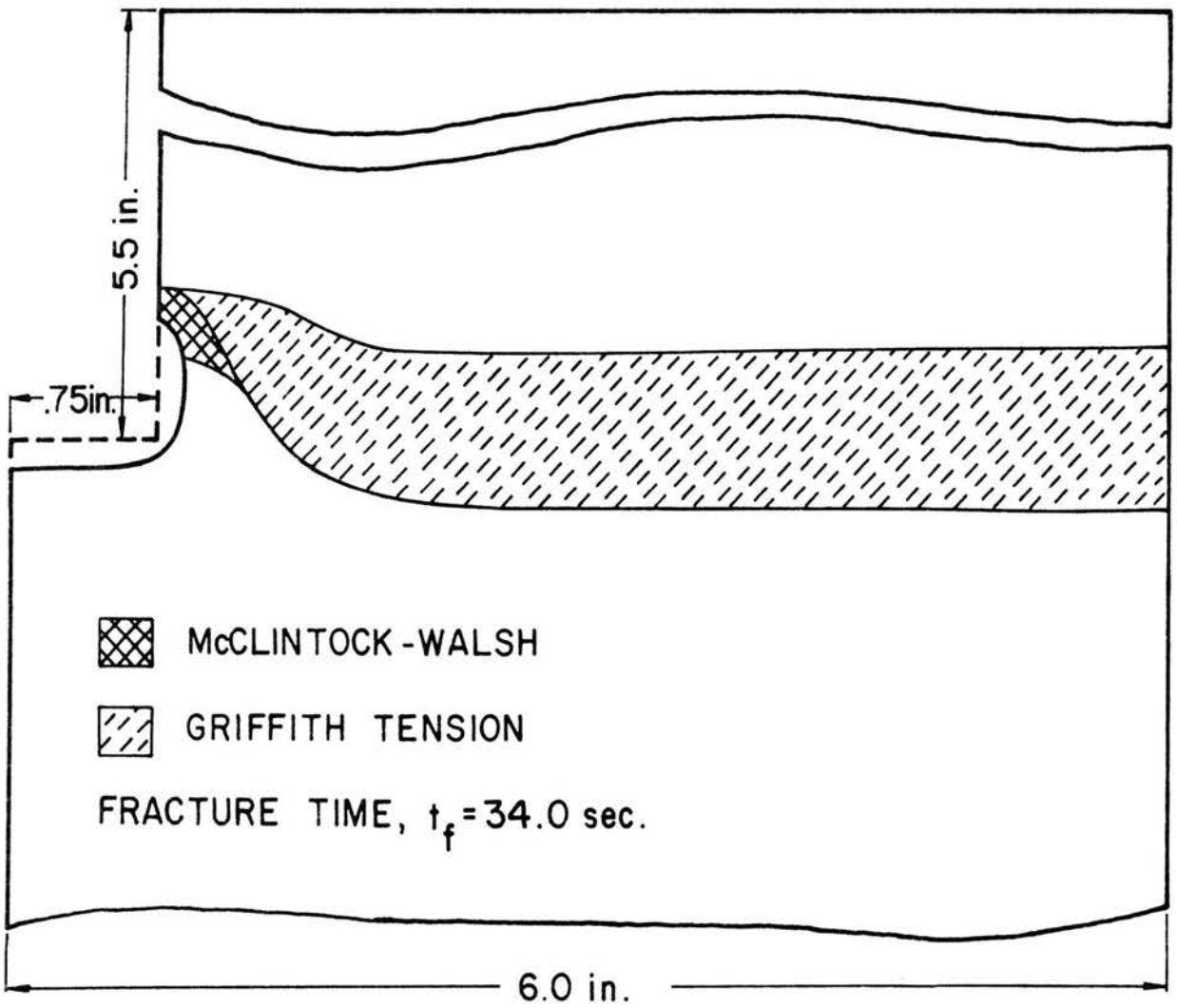

FIG.4.21 FRACTURE ZONES, MODEL 3C

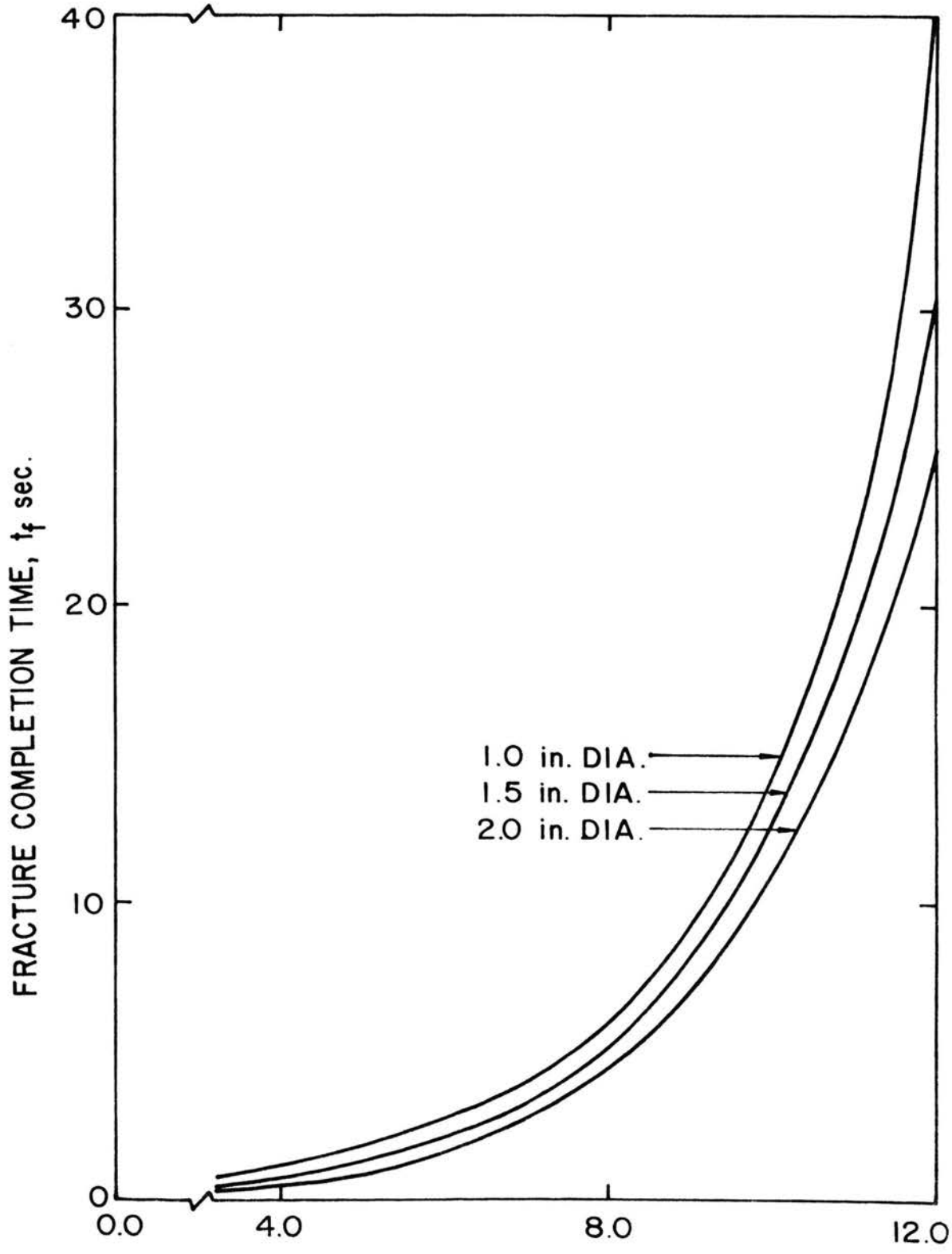

FIG. 4.22 FRACTURE TIME-SPACING CURVES FOR SLOT MODELS

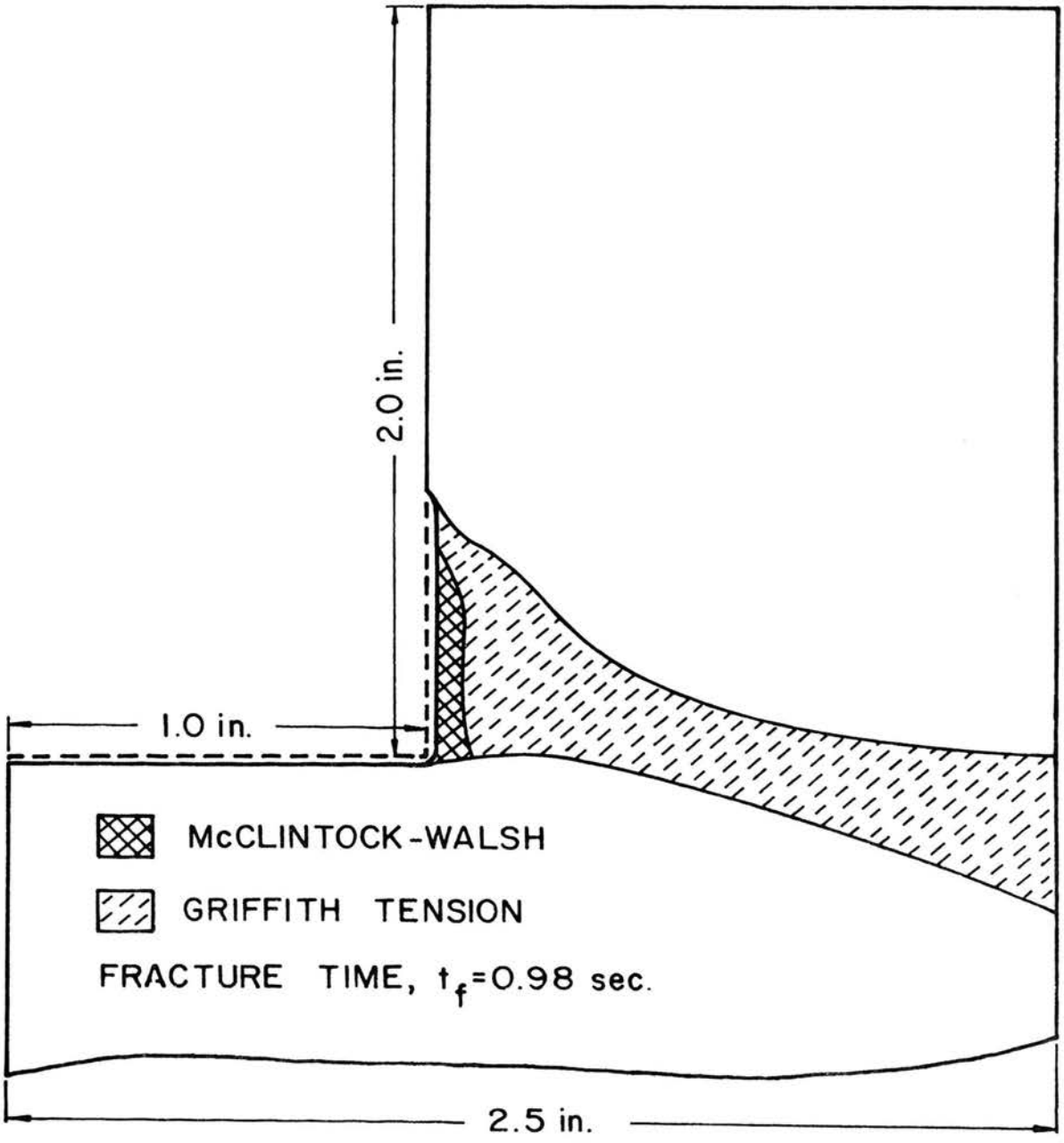

FIG. 4.23 FRACTURE ZONES, MODEL 11A

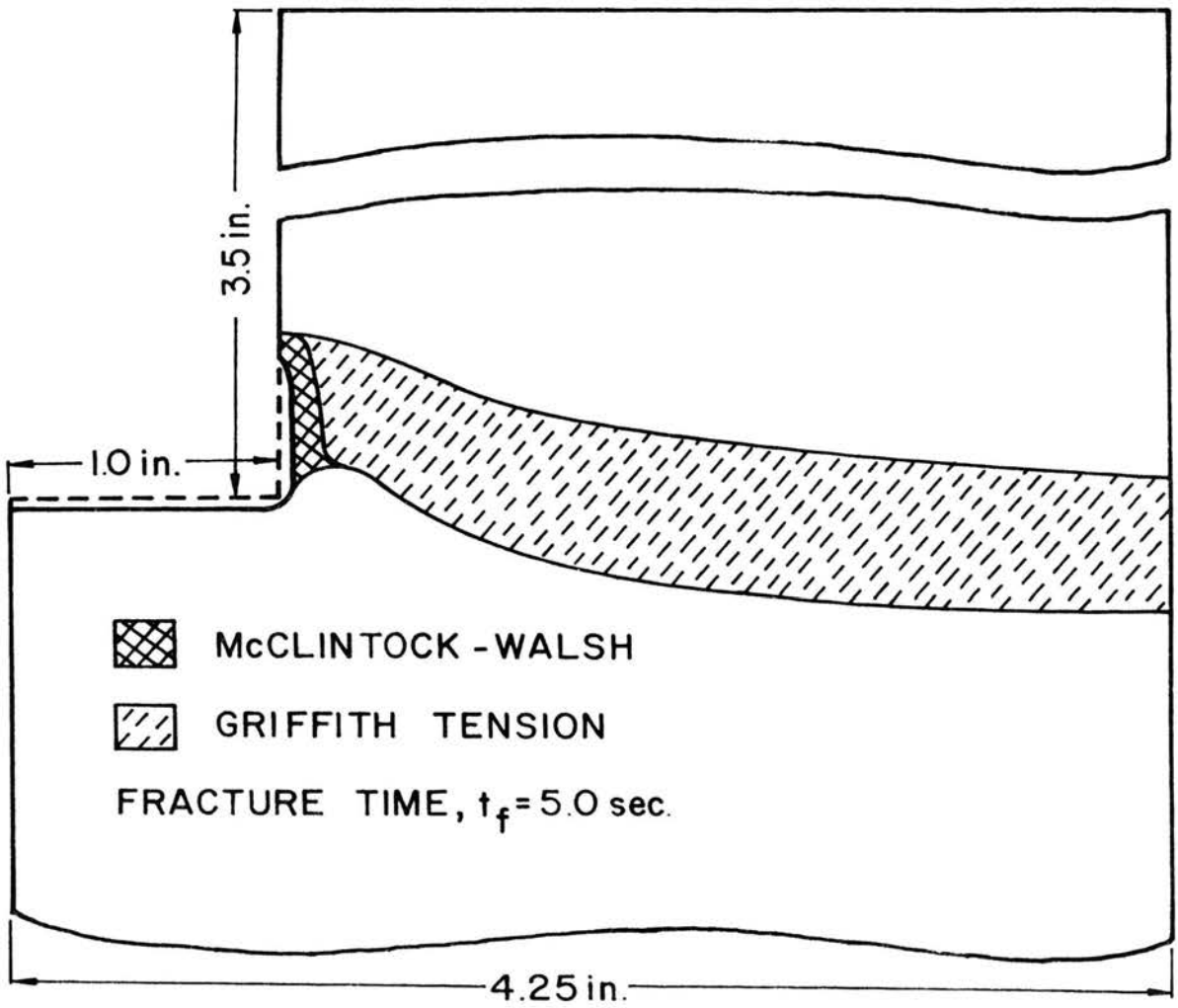

FIG. 4.24 FRACTURE ZONES, MODEL 13B

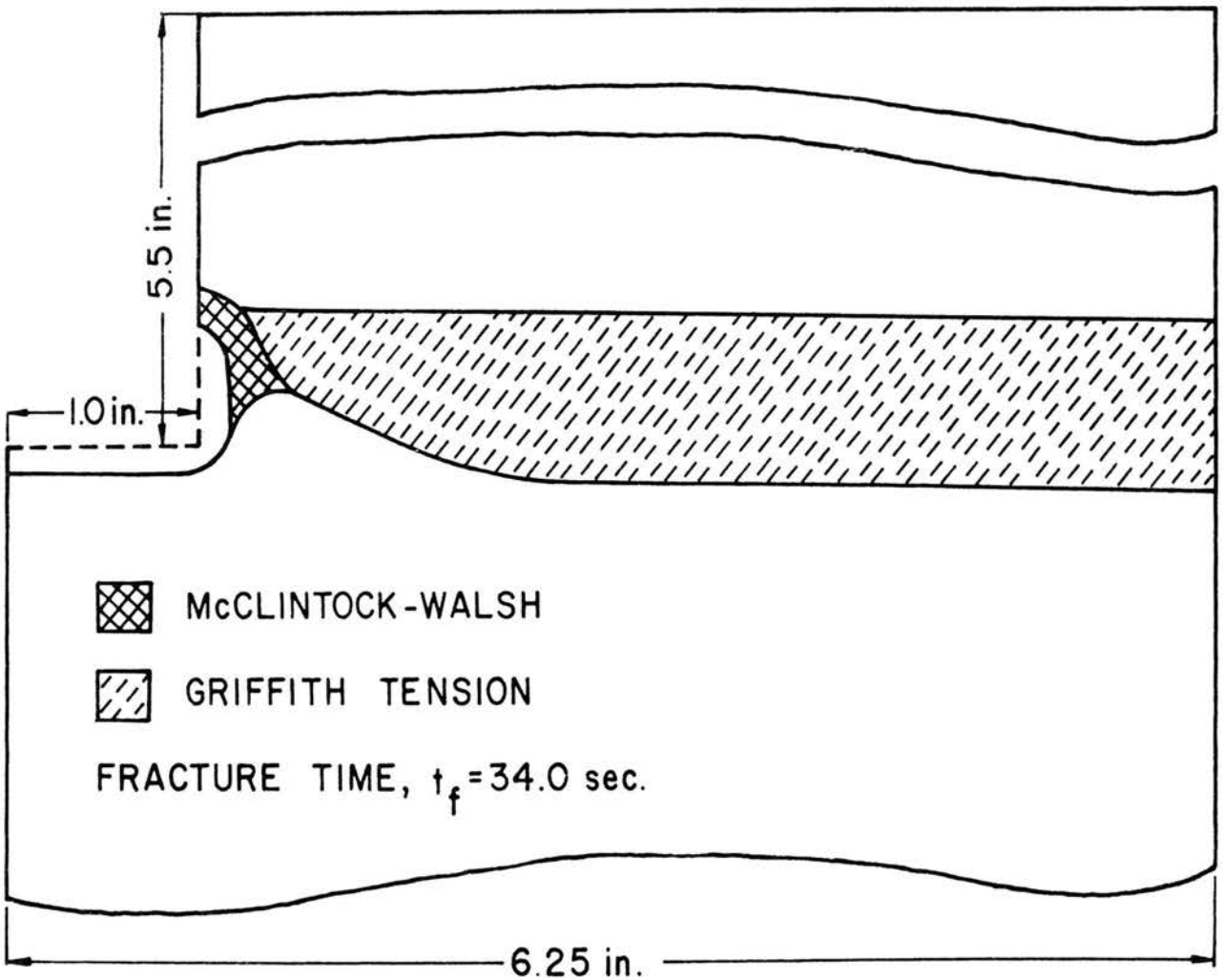

FIG. 4.25 FRACTURE ZONES, MODEL 13C

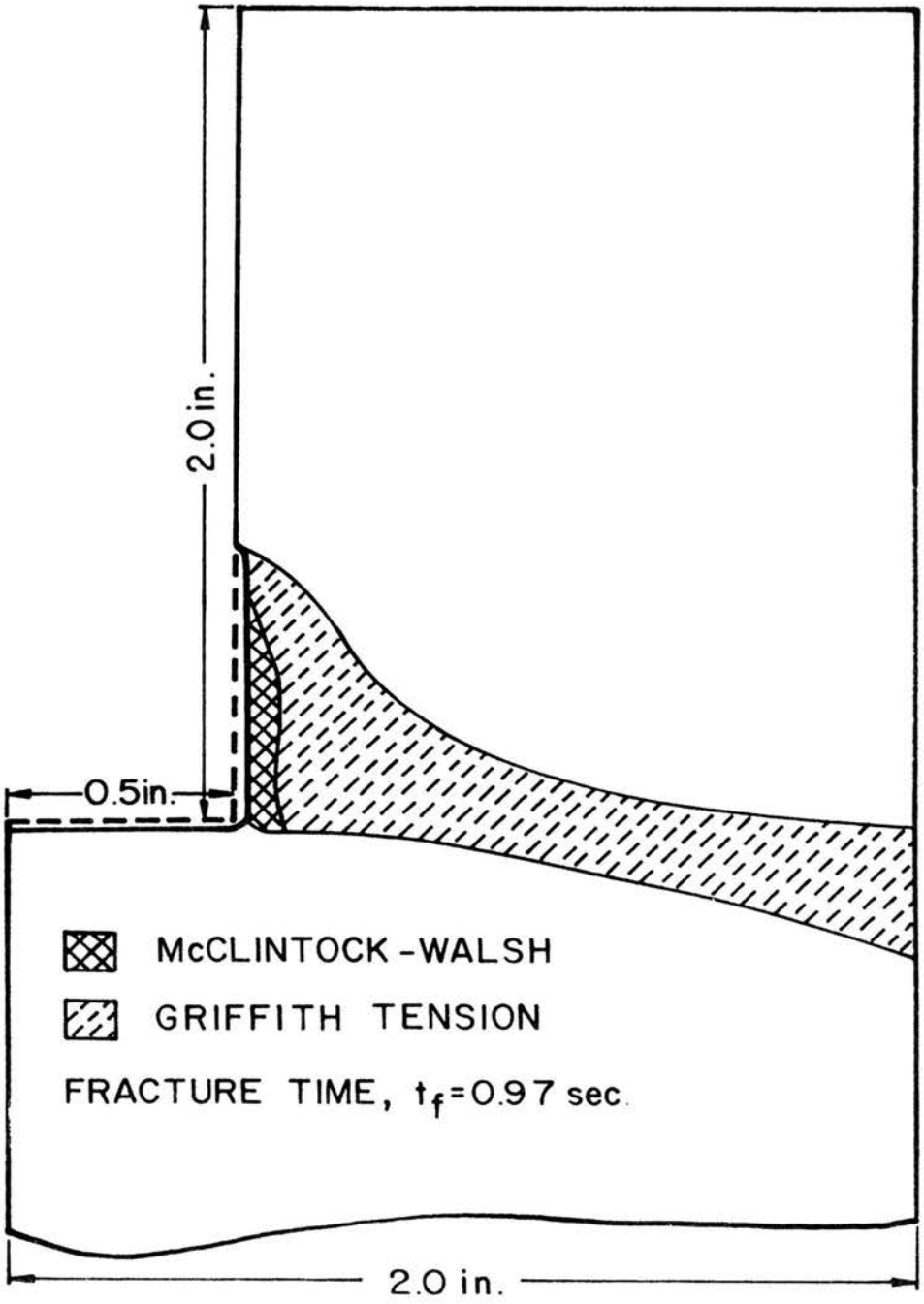

FIG. 4.26 FRACTURE ZONES, MODEL IA

TABLE V

Fracture Times for Slot Models with $a_c \simeq L/2$

Model	Hole Diam. d, in.	Spacing c, in.	Fracture Length L = c-d	Conv. Depth a_c, in.	Fracture Time t_f, sec.
1A	1.0	4.0	3.0	1.5	0.97
1B		8.0	7.0	3.0	5.82
1C		12.0	11.0	5.0	40.6
2A	2.0	4.0	2.0	1.0	0.43
2B		8.0	6.0	3.0	4.4
2C		12.0	10.0	5.0	25.4
3A	1.5	4.0	2.5	1.5	0.85
3B		8.0	6.5	3.0	5.0
3C		12.0	10.5	5.0	34.0
11A	2.0	5.0	3.0	1.5	0.98
13B		8.5	6.5	3.0	5.0
13C		12.5	10.5	5.0	34.0

time ratios are given in Table VI. These values were plotted on a logarithmic scale as shown in Fig. 4.27 from which the following relation was obtained:

$$t_f^* = L^{*2.7} \tag{4.1}$$

where t_f^* is the fracture completion time ratio, and L^* is the fracture length ratio.

The usefulness of Eq. (4.1) lies in the fact that the fracture completion time for any given fracture length can be predicted from the data for a single test.

TABLE VI

Fracture Length and Fracture Time Ratios for Slot Models with Convection Depths Approximately Equal to Half the Fracture Length

Length L_1	Length Ratio $L^* = \frac{L_2}{L_1}$	Time Ratio $t_f^* = \frac{t_2}{t_1}$	Length L_1	Length Ratio $L^* = \frac{L_2}{L_1}$	Time Ratio $t_f^* = \frac{t_2}{t_1}$
2.0	5.5	96.0	6.0	1.83	9.23
	5.25	80.2		1.75	7.23
	5.0	60.0		1.67	5.78
	3.5	13.73		1.16	1.322
	3.25	11.8		1.08	1.136
	3.0	10.38			
	1.5	2.28	6.5	1.69	8.12
	1.25	2.02		1.61	6.8
				1.53	5.09
2.5	4.4	47.4			
	4.2	39.7		1.07	1.165
	4.0	29.7			
	2.8	6.78	7.0	1.57	6.97
	2.6	5.84		1.5	5.84
	2.4	5.14		1.42	4.38
	1.2	1.13			
			10.0	1.1	1.59
3.0	3.67	42.0		1.05	1.34
	3.5	35.2			
	3.33	26.3	10.5	1.04	1.19
	2.33	6.02			
	2.17	5.17			
	2.0	4.55			

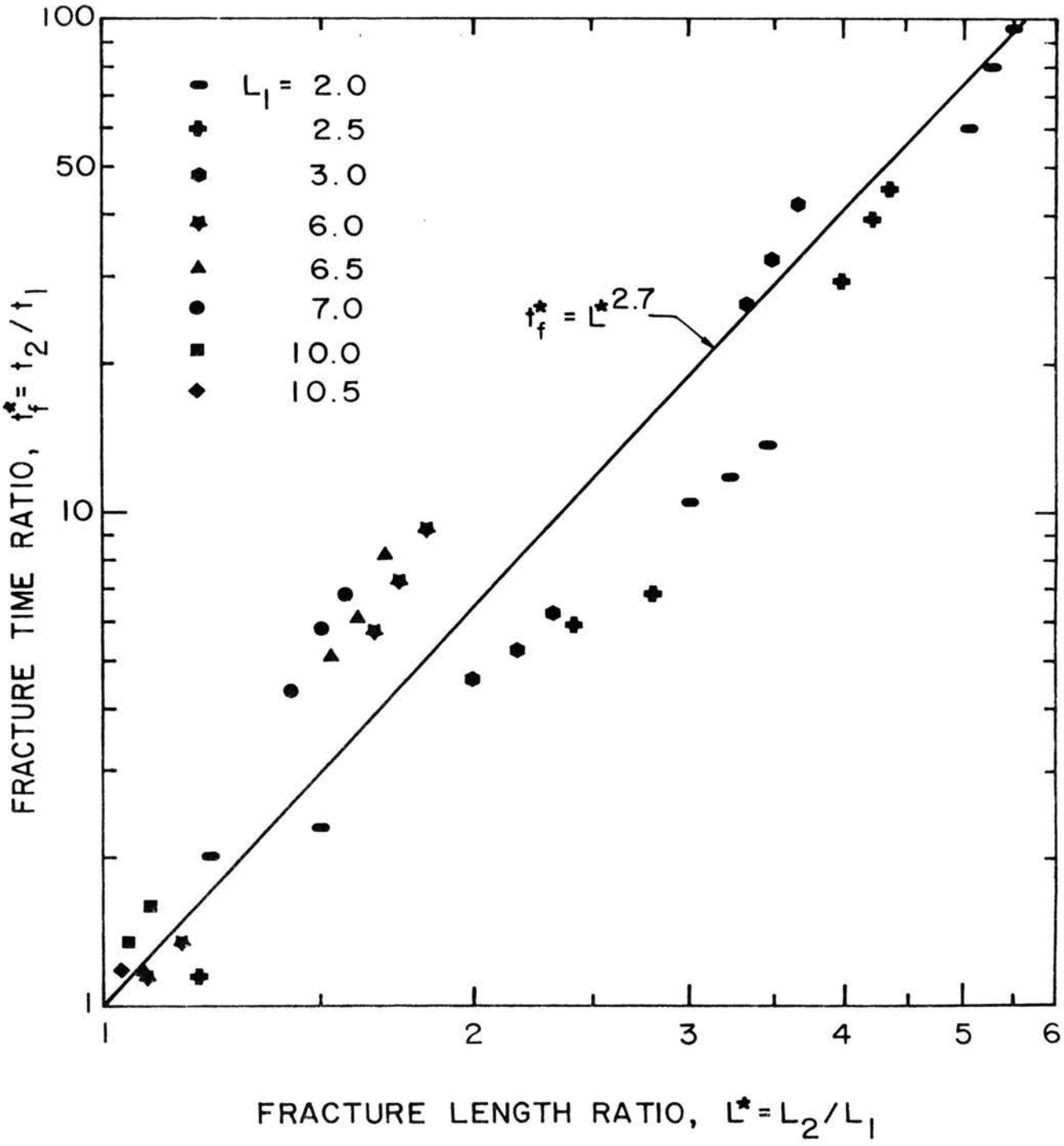

FIG.4.27 DIMENSIONLESS FRACTURE TIME-LENGTH RELATIONSHIP

CHAPTER V

HOLE MODEL ANALYSIS

The hole model was designed to study the influence of the hole diameter and the hole spacing parameters on the fracture which occurs along the line of a series of holes. Because of its orientation with respect to the working face, this fracture in the subsequent discussion is referred to as the perpendicular fracture.

The model is obtained by passing a cutting plane, parallel to the working face, through the center of the thermal inclusions. The geometry of this model is therefore that of a thin uniform plate with a series of holes. For the plane, two-dimensional thermal stress analysis, the variations in the temperature and the stresses across the thickness are neglected. For the actual problem however, this is only true for the melt depth section as the hole is only partially heated, and as shown in the previous chapter, the fracture initiates in the vicinity of the point of transition from the melt condition to the convection condition and propagates to the surface. It was also shown that the fracture times for the parallel fractures using small or zero convection depths were much higher than those obtained by using convection depths approximately equal to or greater than half the fracture lengths. Thus, the results of the hole model analysis given in this chapter are representative of the upper bound solution of the three-dimensional problem with small hole depths heated along their entire length.

The hole model studies were conducted using three values each of the hole diameter and the hole spacing; the combinations giving nine

different fracture lengths as described in Table VII. The hole diameter and the hole spacing values for these models are the same as those for the parallel fracture studies using the slot models. A typical finite element grid used for the hole model analysis is shown in Fig. 5.1.

TABLE VII

Parametric Description of Hole Models

Model	Hole Diameter d, in.	Hole Spacing c, in.	Fracture Length L = c-d
21A	1.0	4.0	3.0
21B		8.0	7.0
21C		12.0	11.0
22A	2.0	4.0	2.0
22B		8.0	6.0
22C		12.0	10.0
23A	1.5	4.0	2.5
23B		8.0	6.5
23C		12.0	10.5

A. Temperature Analysis

As in the case of the slot model studies, the fracture time values for the hole models were observed to be small compared to those associated with the steady-state temperature distribution. As a result, the temperature field at the time of the fracture is highly localized in the vicinity of the melt condition and is independent of the changes in the boundary conditions at the far end. Thus, the

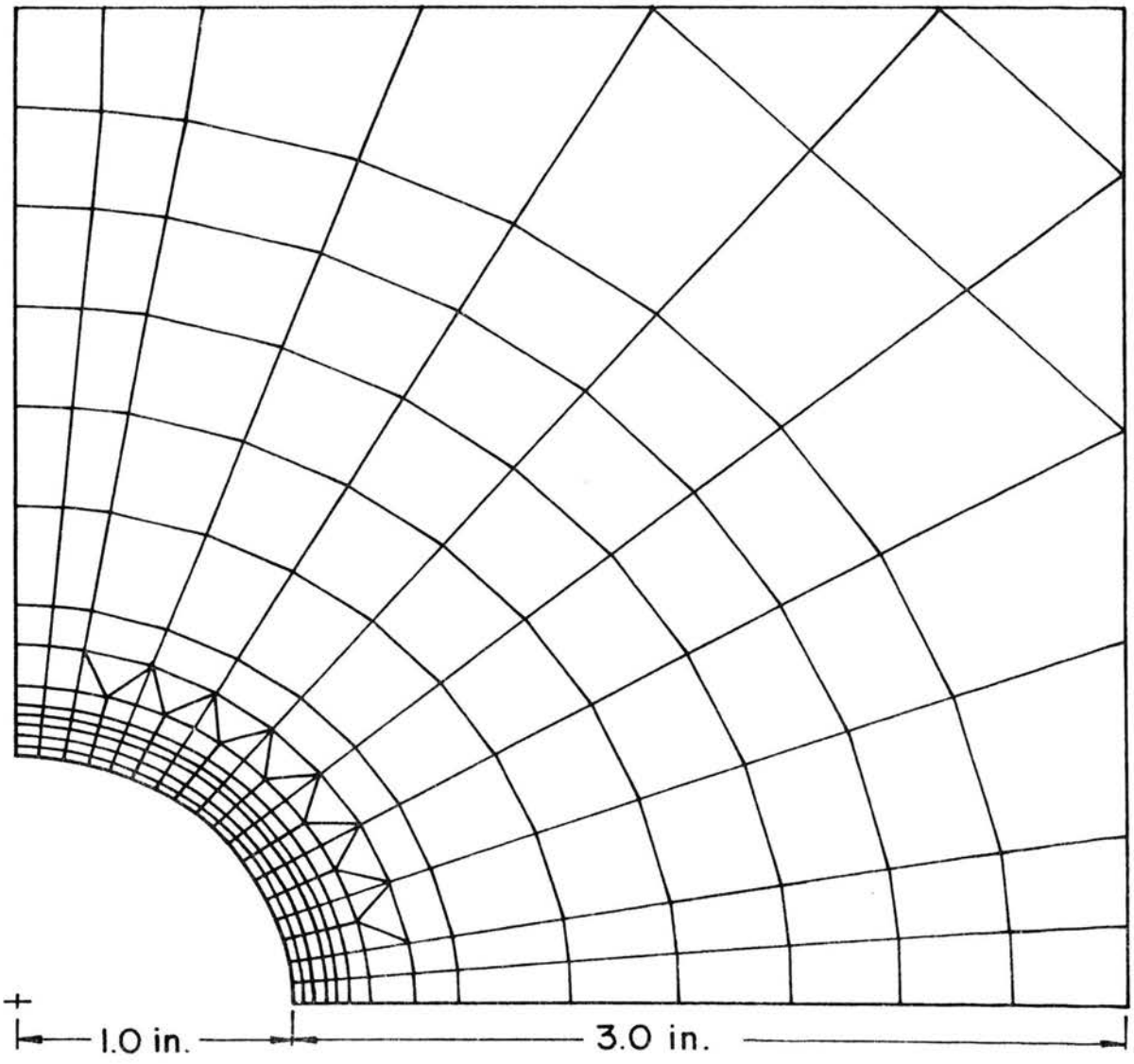

FIG. 5.1 TYPICAL FINITE ELEMENT GRID FOR HOLE MODEL ANALYSIS

hole models are characterized by almost radial, one-dimensional temperature fields as typically illustrated in Figs. 5.2 - 5.4.

B. Stress and Fracture Analysis

Unlike the slot models, where the ratio of the cold zone volume to the hot zone volume varies with the convection depth, the volume ratio for a given hole model is constant. Thus, the fracture plots for the hole models are characteristic of those for the slot models with deep holes heated along their entire depth. For slot models with very small convection depths, it was shown in Ch. IV that the fracture zone consists of a McClintock-Walsh zone in the high temperature region, followed by a small Griffith tension zone and a large secondary McClintock-Walsh zone. Also, the fracture completion times for small convection depth models were found to be much higher than those given in Table V where convection depths used are approximately equal to the critical values. These two observations are also reflected through the hole model analysis as seen from the typical fracture plots shown in Figs. 5.5 - 5.7.

From these results, it can be inferred that the fractures originate in the melt depth section across the holes and propagate to the surface. It can also be observed that, like the slot models, the fracture completion time in the case of the hole models is dependent only on the fracture length, and that the individual variations in the hole diameter and the hole spacing parameters will have no influence on the fracture time provided the fracture length is kept constant. This is obvious from the approximately parallel

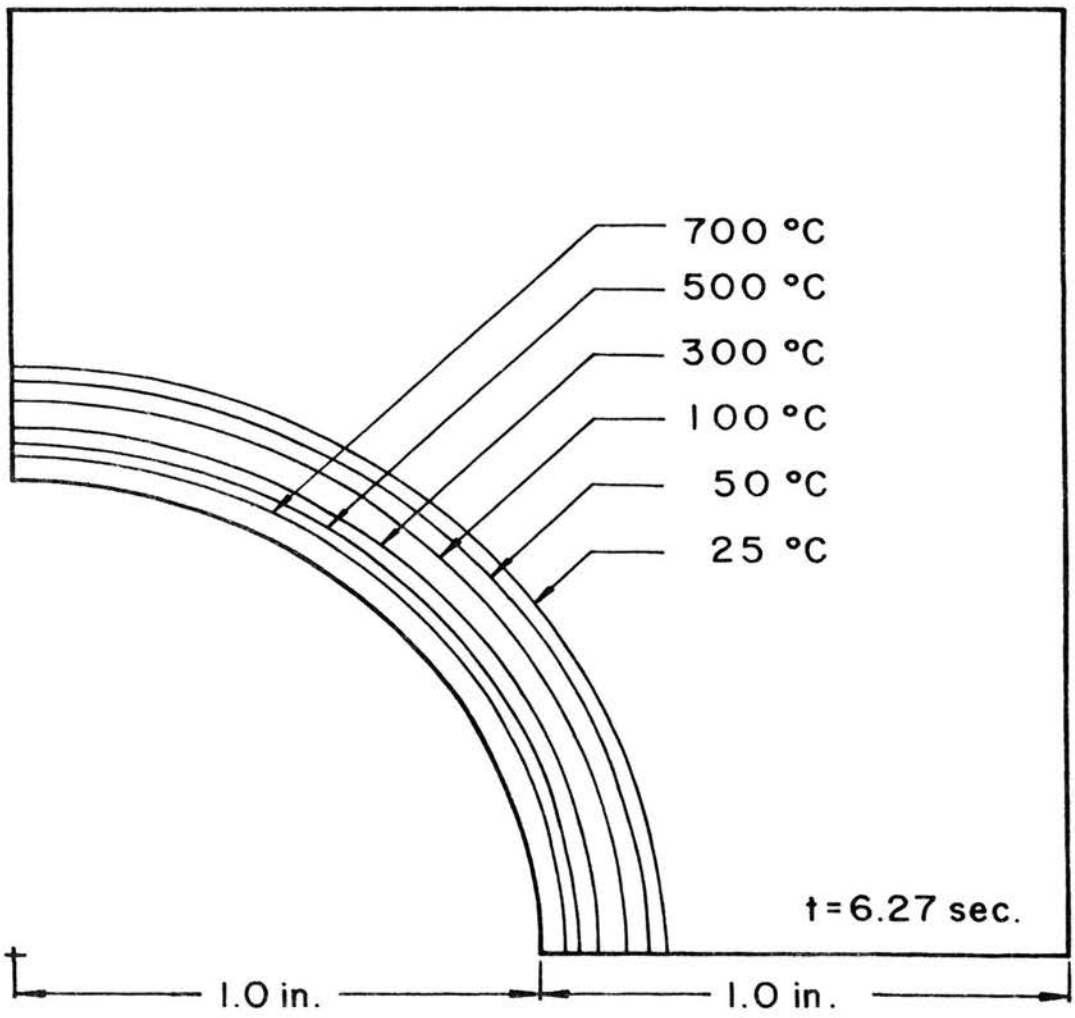

FIG. 5.2 TEMPERATURE DISTRIBUTION, MODEL 22A

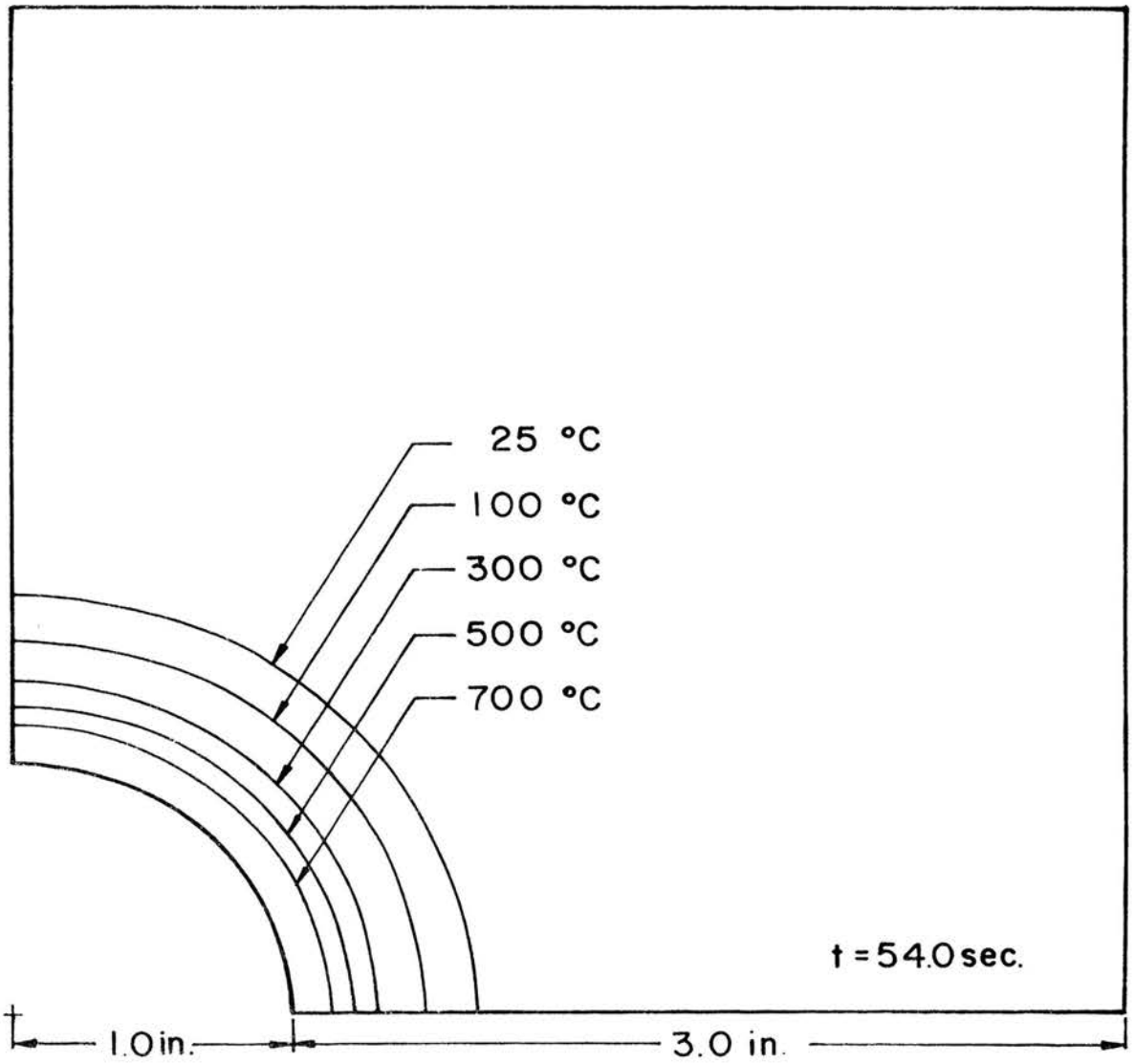

FIG. 5.3 TEMPERATURE DISTRIBUTION, MODEL 22B

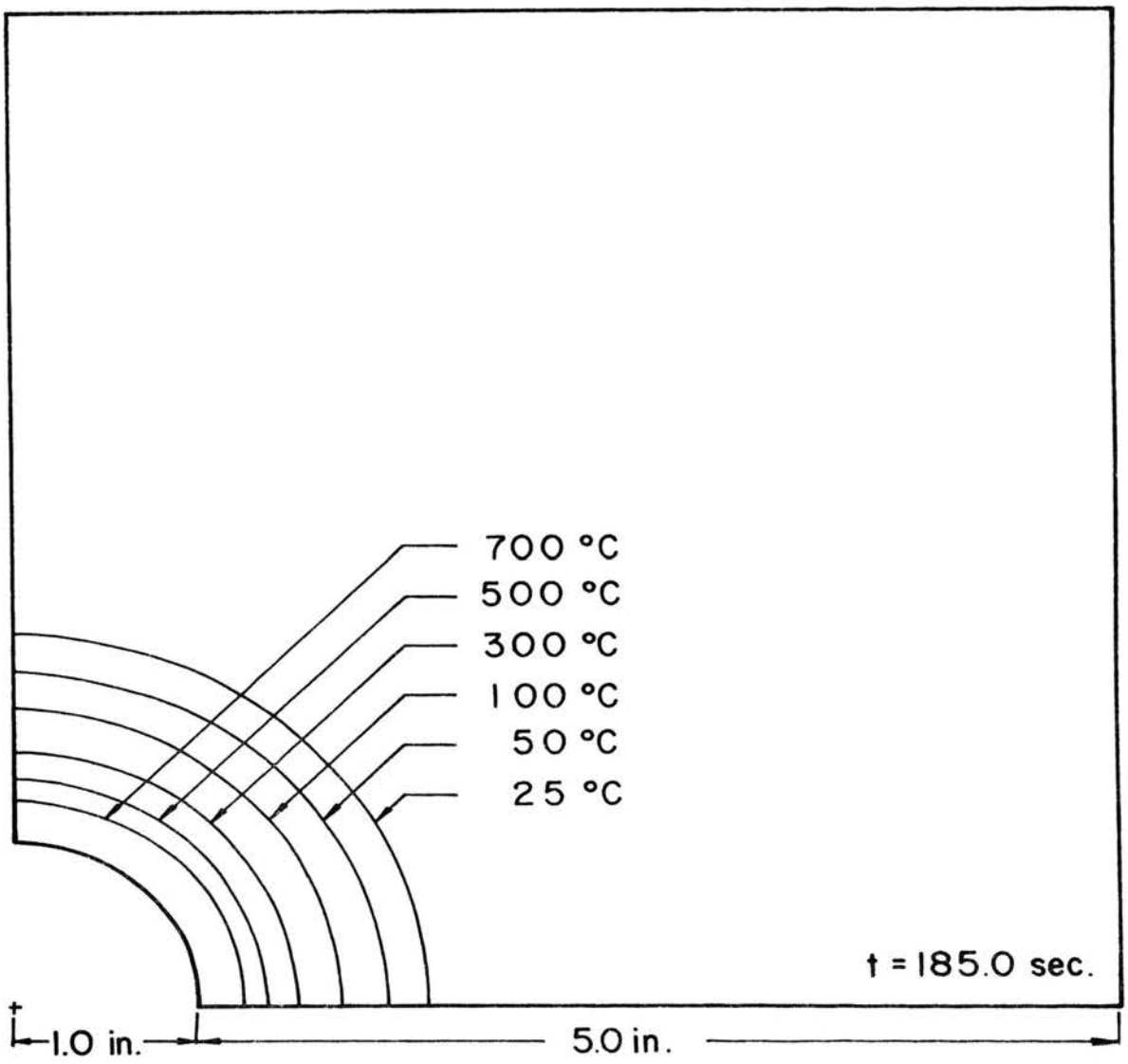

FIG. 5.4 TEMPERATURE DISTRIBUTION, MODEL 22C

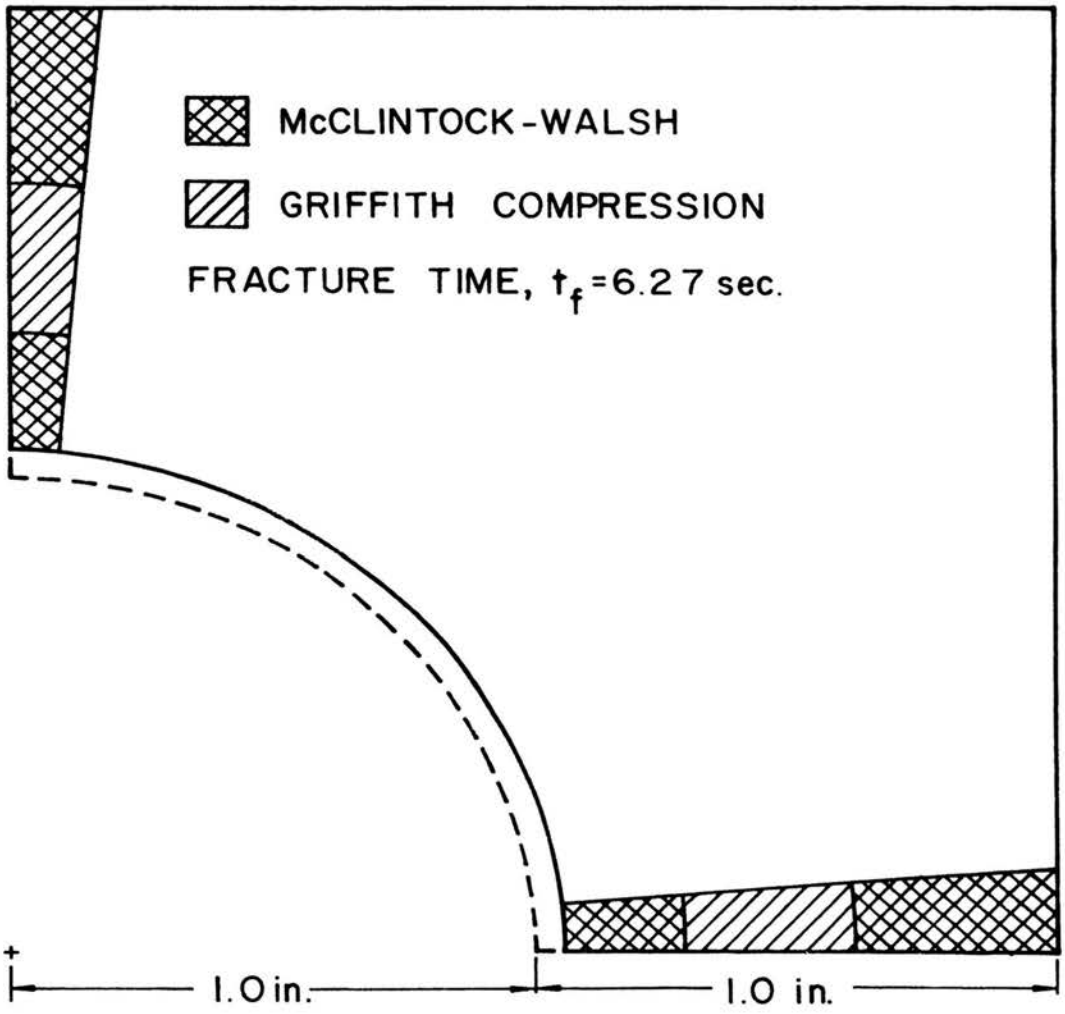

FIG. 5.5 FRACTURE ZONES, MODEL 22A

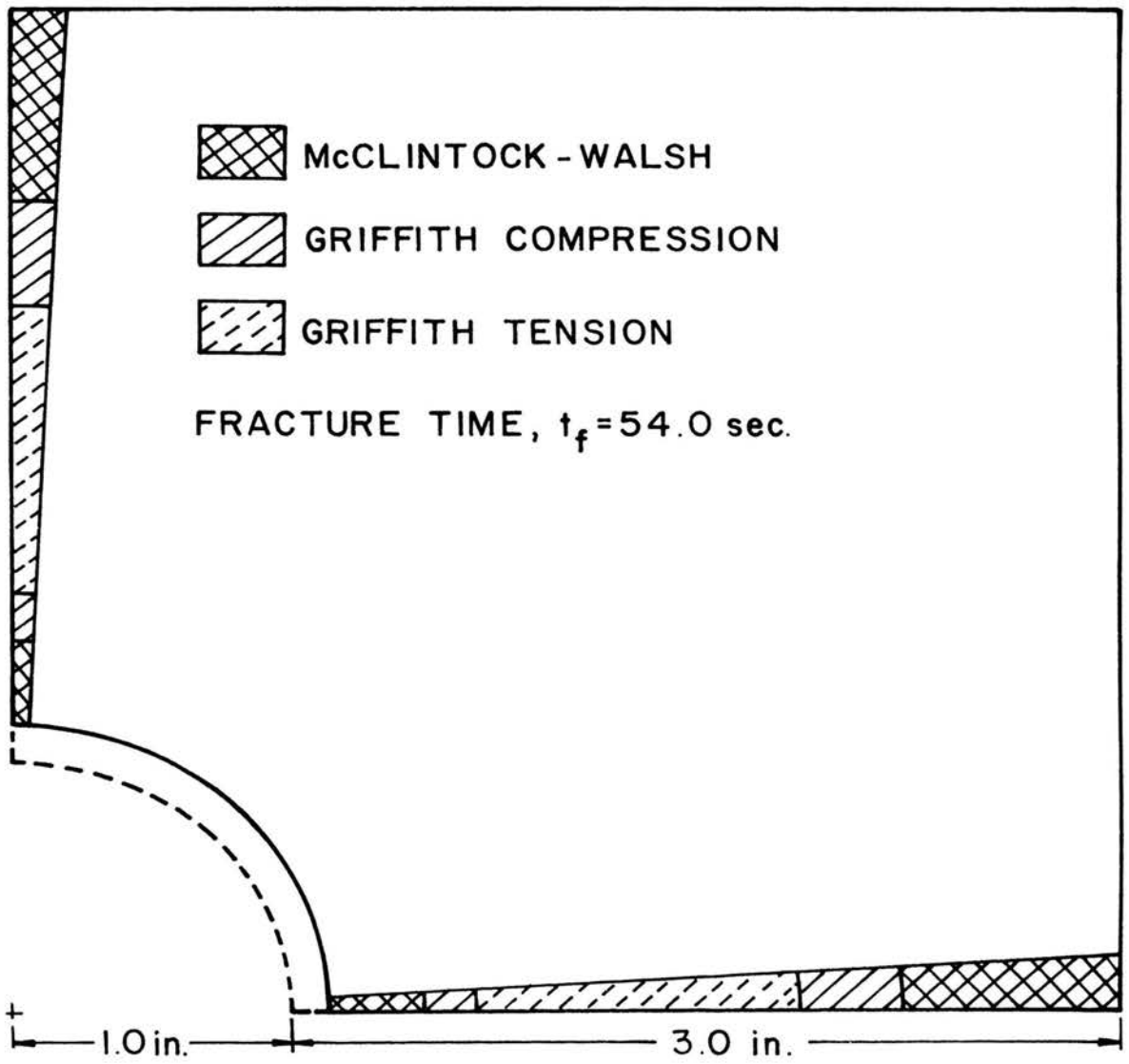

FIG. 5.6 FRACTURE ZONES, MODEL 22B

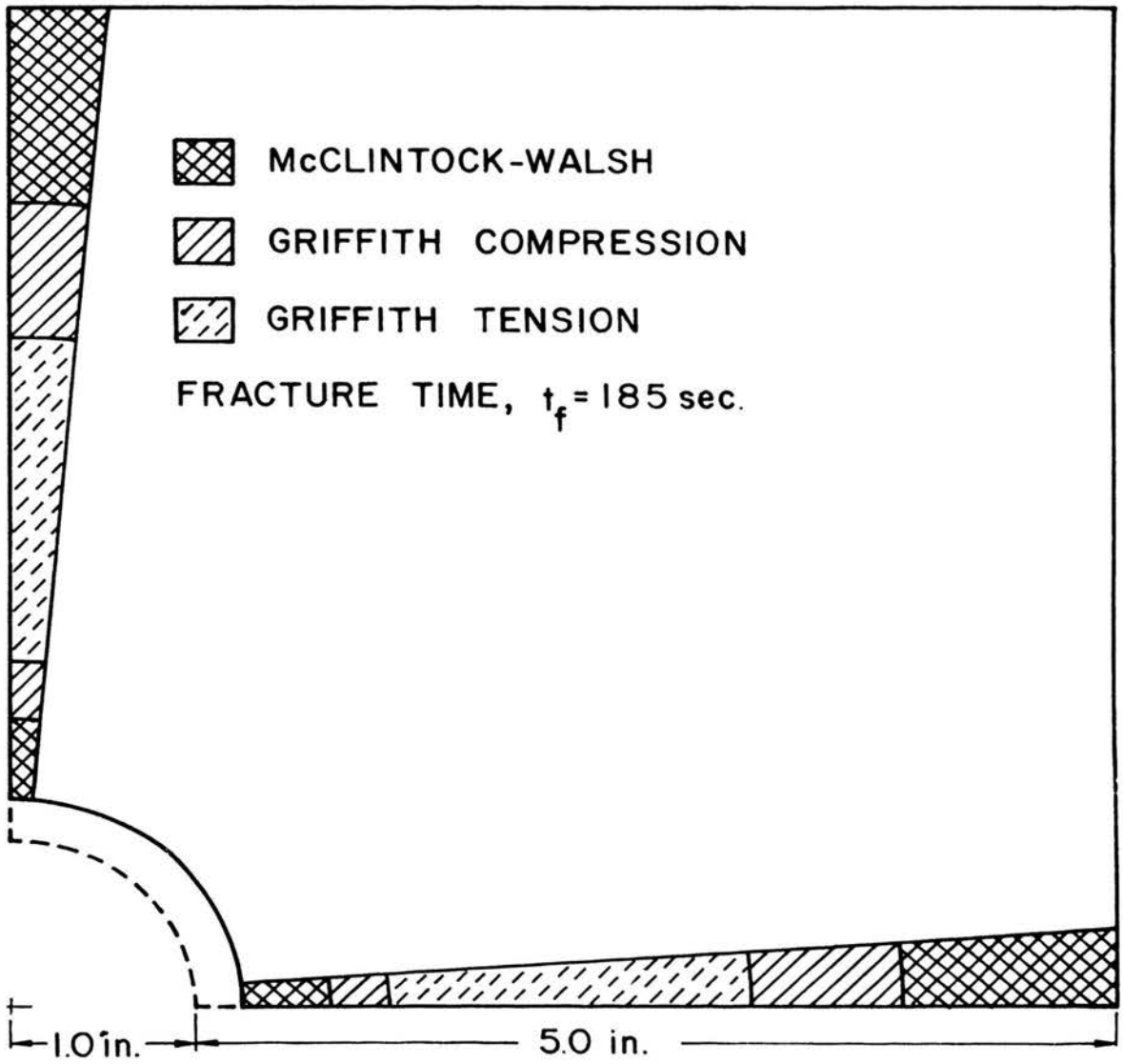

FIG. 5.7 FRACTURE ZONES, MODEL 22C

curves in Fig. 5.8 which show the fracture time versus the hole spacing plots for the hole models with different diameters.

As seen from the temperature plots for the hole models shown in Figs. 5.2 - 5.4, a major portion of the fractured volume does not experience any temperature change, and hence, the stresses in this region are due entirely to the load vector resulting from the thermally induced constraint. Thus, the explanation for the sharp increase in fracture completion time with increased hole spacing in the case of the slot models also applies to the hole models.

Comparison of Figs. 4.22 and 5.8 shows a remarkable similarity between the parallel and the perpendicular fracture characteristics, although for a given problem geometry, the perpendicular fracture time using the hole model approximation is much higher than the parallel fracture time. However, as mentioned earlier, the hole model analysis involves small hole depths without any convection depths and thus, assumes a plane stress condition. In practice, however, the holes are rather deep and the problem approaches a plane strain condition. Thus, the actual perpendicular fracture times as compared to the actual parallel fracture times will not be as high as theoretically predicted. It should also be realized that while the convection depth will greatly reduce the perpendicular fracture time as in the case of the parallel fracture, any increase in the convection depth will mean the heat source will have a greater burden against which to open cracks between the holes.

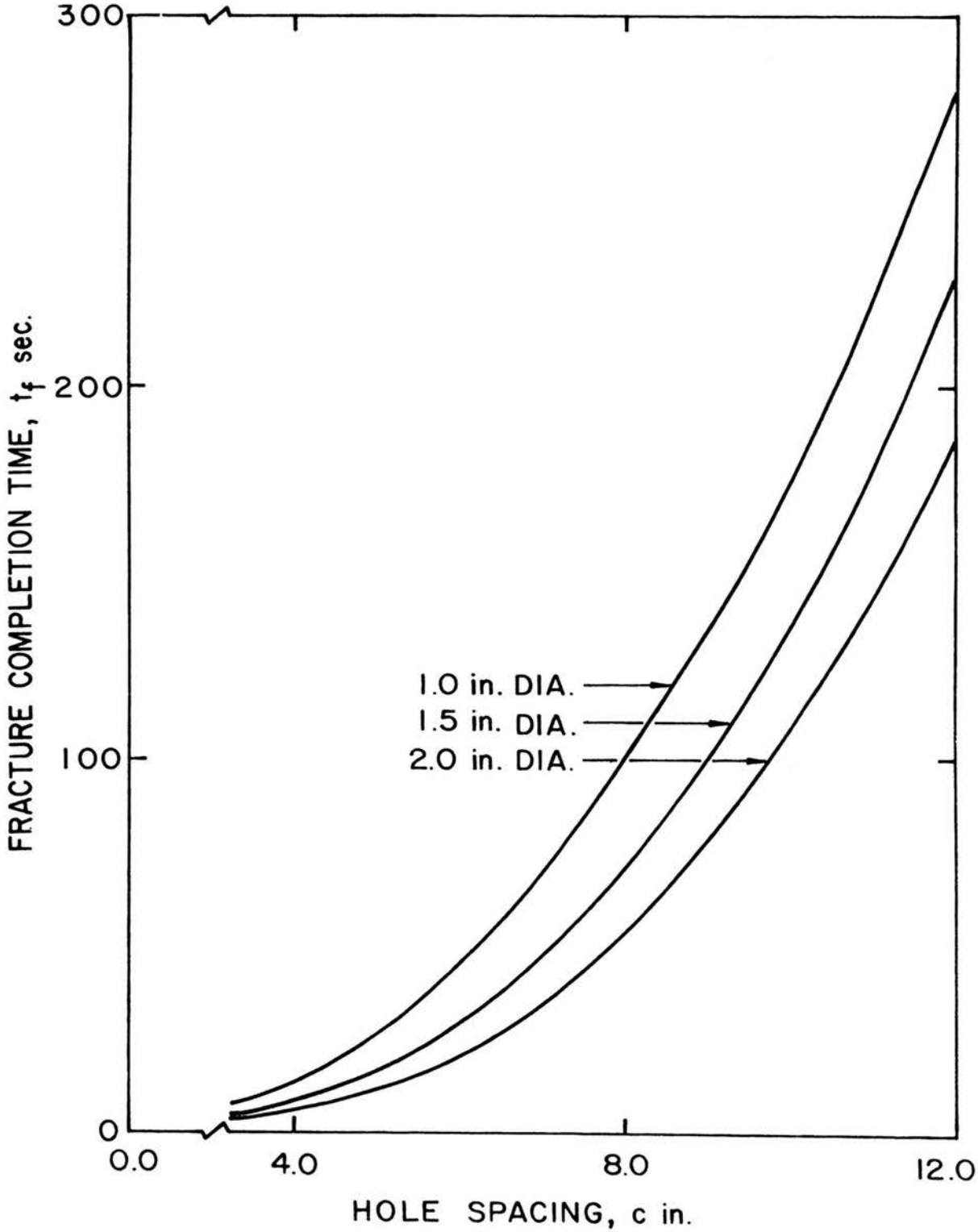

FIG.5.8 FRACTURE TIME -SPACING CURVES FOR HOLE MODELS

CHAPTER VI

CONCLUSIONS AND RECOMMENDATIONS

The close correlation between the theoretically predicted and the experimentally observed fracture patterns and the fracture length-fracture time relationships indicate that the conclusions drawn regarding the influence of various process parameters using the two two-dimensional plane models can be applied fairly accurately to the actual three-dimensional configuration. Also, for rock types with characteristics similar to Dresser basalt, the approximate fracture completion time corresponding to any given fracture length can be predicted from the data for a single test using the power relationship $t_f^* = L^{*2.7}$ between the dimensionless time and the dimensionless fracture length.

For a given geometry, the predicted fracture time is only a small fraction of the time necessary to reach the steady-state temperature distribution. The temperature field at the time of the fracture is thus highly localized, and the major portion of the fractured volume experiences only a small increase in temperature. The fracture-inducing stresses in this region are, therefore, entirely due to the load vector resulting from the thermal constraint. Since the severity of thermal constraint depends on the relative volumes of the cold and the hot zones, the fracture time is significantly influenced by both the hole spacing and the melt-free depth.

For very small melt-free depths, the fracture is characterized by mainly a compressive failure according to the McClintock-Walsh modified Griffith criterion. This fracture mode is naturally

undesirable as the compressive strength of hard rocks is many times greater than their tensile strength.

While the McClintock-Walsh compressive failure zone remains relatively unchanged in the region of the high temperature gradients, the compressive stress components in the cold zone decrease steadily with an increase in the melt-free depth. With further increase in the melt-free depth, a stage is reached when the major principal stress components become tensile. Thus, with a continuous increase in the melt-free depth, the McClintock-Walsh fracture zone in the cold region transforms first into a partial Griffith compression zone and finally into the Griffith tension zone. The effectiveness of this transformation is evident from the drastic reduction in the fracture time as the fracture now results from tensile failure.

The melt-free depth associated with the completion of the transformation of the compressive fracture into the tensile fracture mode is approximately equal to half the fracture length, that is, half the difference between the hole spacing and the hole diameter. Any further increase in this parameter has only a slight effect on the fracture time.

Another significant effect of the melt-free depth involves the location of the parallel fracture (subsurface fracture parallel to the working face). The optimum location of this fracture requires the crack initiation to occur very close to the hole base and the crack propagation in a plane approximately parallel to the hole base. From the slot model analysis, to obtain such a location, it is necessary that the thermal inclusions should be concentrated at the

very base of the holes (requiring only a small melt depth) while the melt-free depth should, at least, be equal to half the fracture length.

The hole model analysis is performed using a plane stress assumption. The actual three-dimensional fragmentation configuration, however, involves a condition somewhere between the plane stress (shallow holes heated along their entire lengths) and the plain strain (deep holes heated along their entire lengths) formulations. Also, this analysis does not involve the melt-free depth parameter which as shown from the slot model studies can be used advantageously to transform the mode of failure from compressive to tensile and thereby to greatly reduce the fracture time. Thus, it is natural to expect a predominantly compressive failure in the case of the hole models, the results of which, in view of the above considerations, are obviously representative of the upper bound of the theoretical solution.

The results of the plane analysis indicate that since the fracture initiates in the vicinity of the point of transition from the melt condition to the convection condition (along the hole depth), only small melt depths should be used. Also, in order to optimize the location of the parallel fracture and the fracture time, the melt-free depth should, at least, be equal to half the difference between the hole spacing and the hole diameter. Although any further increase in the melt-free depth shows an insignificant influence on the location and time of the parallel fracture, it will mean that the heat source will have a greater burden against which to open cracks between the

holes. The optimum depth therefore seems to be one associated with a melt-free depth equal to approximately half the difference between the hole spacing and the hole diameter.

Both the slot and the hole model analyses indicate the hole spacing to be the most influential parameter governing the fracture time. The effects of the changes in the hole diameter, on the other hand, are only secondary in nature, and can be taken into account by adjusting the hole spacing such that the fracture length remains unchanged. Thus, the effects of the hole spacing and the hole diameter can be expressed in terms of a single variable, the fracture length.

In practice, the hole diameter will be determined mainly from heater size considerations, and since the optimum hole depth, as described earlier is expressed in terms of the fracture length, the thermal fragmentation configuration can be optimized by a proper choice of the single parameter, the hole spacing.

While the power relationship, $t_f^* = L^{*2.7}$ between the dimensionless fracture time and the dimensionless fracture length (for Dresser basalt) implies faster fragmentation for smaller spacings, it is important to note that smaller spacing also means higher drilling costs as well as smaller rock volume that can be removed through each cycle of operation. The choice of an optimum spacing, therefore, will also involve factors such as the drilling rate, the cost of heating and drilling, the muck removal capacity and the overall efficiency of the actual excavation machine.

Thus, while the analysis presented here is not sufficient to enable one to optimally choose the process parameters, it does serve two very useful purposes. First, it reduces the optimal choice of various process parameters to the choice of a single parameter, the hole spacing, and also provides a relationship between the fracture time and the hole spacing. Secondly, since this investigation considers fractures due entirely to the effects of thermal inclusions, the results presented here can be used with advantage to approximately determine the effectiveness of the mechanical loading to be incorporated in designing an excavation prototype.

Recommendation for Future Work

While the analysis presented in this investigation using the two two-dimensional plane models forms the first step toward understanding the fracture characteristics of the three-dimensional solid, and also provides useful guidelines in formulating the more advanced models, it does not consider factors such as the variation in thermal properties with temperature and the interactions between the temperature and the stress fields in the two planes, parallel and perpendicular to the working face.

The effects of the three-dimensional temperature and stress fields can be approximated by using an axisymmetric cylinder model containing a single hole. This model can also be used, along with the two plane models, to investigate the significance of variations in thermal conductivity and the diffusivity of the material with temperature.

The small fracture times and the highly localized temperature field at the time of fracture indicate the insensitivity of the temperature solution to the boundary conditions in the regions not immediately surrounding the melt condition. This suggests the possibility of a closed form solution to the temperature problem using one of the numerous transformation techniques.

Results of the fracture studies indicate that, under optimum conditions, the rock fracture results from tensile failure. Also, the region undergoing tensile failure experiences only a small increase in temperature and hence, the stresses in this region are created almost entirely due to the thermal constraint resulting from restrained thermal expansion of a small heated area by a comparatively large cold area. This suggests that, of the thermoelastic properties, E, ν, and α, only the variation in α with temperature is of significance in the stress solution. Again, however, for the uncoupled theory of thermoelasticity, since the property α always appears in combination with the temperature T, the problem becomes linear. Thus, for simple geometrical shapes, such as the axisymmetric cylinder model, the stress solution could be obtained in closed form by using an Airy stress function.

BIBLIOGRAPHY

1. Thirumalai, K., "The Process of Thermal Spalling Behavior in Rocks - An Exploratory Study," Rock Mechanics - Theory and Practice, Ed. W.H. Somerton, Proceedings of the 11th Symposium on Rock Mechanics, 1970, pp. 705-727.

2. Gray, W.E., "Surface Spalling by Thermal Stresses in Rocks," Proceedings, Rock Mechanics Symposium, Univ. of Toronot, Mines Branch, Ottawa, 1965, pp. 85-106.

3. Clark, G.B., et al., "Combined Thermal Weakening and Mechanical Disintegration of Hard Rock," U. of Mo. RMERC, Annual Rept., July 1972.

4. Lauriello, P.J.J., "Thermal Fracturing of Hard Crystalline Rocks," Ph.D. Dissertation, Rutgers University, October 1971.

5. Maurer, W.C., "Novel Drilling Techniques," Pergamon Press, London, 1968.

6. Carstens, J.P., et al., "Thermal Fracture of Rock - A Review of Experimental Results," 1st. No. Amer. Rapid Excav. and Tunneling Conf., June 1972.

7. Thirumalai, K., "Potential of Internal Heating Method for Rock Fragmentation," Dynamic Rock Mechanics, Ed. G.B. Clark, Proceedings of 12th Symposium on Rock Mechanics, 1971, pp. 697-719.

8. Schumacher, B.W., and Holdbrook, R.G., "Use of Electron Beam Gun for Hard Rock Excavation," Westinghouse Electric Corp., Rept. 73-8C2-ROCUT-PI, Dec. 1972.

9. Zar, J., "The Use of a Laser for ARPA Military Geophysics Program," (Rock Mechanics and Rapid Excavation), AVCO, Semi-annual Tech. Rept. Bur. of Mines, Contract No. H-210039, Dec. 1971.

10. Carstens, J.P., and Brown, C.O., "Rock Cutting by Laser," SPE Paper 3529, October 1971.

11. Carstens, J.P., et al., "Feasibility of Flame-Jet Tunneling," United Aircraft Research Laboratories, Rept. PB 1781988, May 1968.

12. Carstens, J.P., et al., "Heat Assisted Tunnel Boring Machines," UARL Rept. No. J-970802-12, September 1970.

13. Thirumalai, K., and Chueng, J.B., "A Study of a New Concept of Thermal Hard Rock Crushing," 14th Symp. on Rock Mech., June 1972.

14. Robinson, E.S., et al., "A Preliminary Study of the Nuclear Subterrene," Rept. LA-4547, LASL, 1971.

15. Clark, G.B., et al., "An Investigation of Thermal-Mechanical Fragmentation of Hard Rock," Research Report on Contract No. USDI-H-022068, Bur. of Mines, (ARPA), October 1973.

16. Hurlbut, C.S., Jr., "Dana's Manual of Mineralogy, 18th ed.," John Wiley & Sons, Inc., 1971.

17. Clark, G.B., et al., "Rock Properties Related to Rapid Excavation," Office of High Speed Ground Transportation, Washington, D.C. Report 3-0143, March 1969.

18. Obert, L., Windes, S.L., and Duvall, W.J., "Standardized Tests for Determining the Physical Properties of Mine Rocks," U.S. Bur. Mines RI 3891, August 1946.

19. Jaeger, J.C., and Cook, N.G.W., "Fundamentals of Rock Mechanics," Methuen & Co., Ltd., 1969.

20. Robertson, E.C., "Experimental Study of the Strength of Rocks," Bull. Geol. Soc. Am., Vol. 66, Oct. 1955, pp. 1275-1315.

21. Nishihara, M., "Stress-strain Relation of Rocks," Doshisha Engineering Review, Vol. 8, No. 2, August 1957.

22. Walsh, J.B., "The Effect of Cracks on the Compressibility of Rocks," Jl. Geophys. Res., Vol. 70, No. 2, January 1965.

23. Walsh, J.B., "The Effect of Cracks on the Uniaxial Elastic Compression of Rocks," Jl. Geophys. Res., Vol. 70, No. 3, January 1965.

24. Walsh, J.B., "The Effect of Cracks in Rocks on Poisson's Ratio," Jl. Geophys. Res., Vol. 70, No. 20, October 1965.

25. Griggs, D.T., Turner, F.J., and Heard, H.C., "Deformation of Rocks at 500° to 800°C," Rock Deformation, (a symposium), Geol. Soc. Am. Memoir 79, 1960, pp. 39-104.

26. Brace, W.F., "Some New Measurements of Linear Compressibility of Rocks," Jl. Geophys. Res., Vol. 70, 1965, pp. 391-398.

27. Moavenzadeh, F., Williamson, R.B., and McGarry, F.J., "Laser Assisted Rock Fracture," PB 174245, January 1967,

28. Moavenzadeh, F., Williamson, R.B., and McGarry, F.J., "Thin Disc Technique for Analyzing Rock Fractures Induced by Laser Irradiation," PB 179-205, May 1968.

29. Moavenzadeh, F., Williamson, R.B., and Wissa, A.E.Z., "Rock Fracture Research," MIT Rept. R66-56, PB 173-638, November 1966.

30. Geller, L.B., et al., "Jet Piercing Research Project," Dept. of Mines and Mineral Surveys, Mines Branch, Ottawa, IR 62-27, 1962.

31. Birch, F., and Clark, H., "Thermal Conductivity of Rocks and Its Dependence Upon Temperature and Composition - Part I," Am. Jl. Sci., Vol. 238, No. 8, Aug. 1940, pp. 529-558.

32. Lindroth, D.P., and Krawza, W.G., "Heat Content and Specific Heat of Six Rock Types at Temperatures to 1000°C," Bu. Mines RI 7503, April 1971.

33. Birch, F., "Elasticity of Igneous Rocks at High Temperatures and Pressures," Bull. Geol. Soc. Am., Vol. 54, 1943, pp. 263-286.

34. Baidiuk, "Mechanical Properties of Rocks at High Temperatures and Pressures," Consultant Bureau, New York, 1967.

35. Wingquist, C.F., "Elastic Moduli of Rock at Elevated Temperatures," Bur. Mines RI 7269, 1969.

36. Mirkovich, V.V., "Experimental Study Relating Thermal Conductivity to Thermal Piercing of Rocks," Intl. Jl. Rock Mech. Min. Sci., Vol. 5, May 1964, pp. 205-218.

37. Norton, F.H., "A General Theory of Spalling," Jl. Am. Cer. Soc., Vol. 9, 1920, pp. 29-39.

38. Preston, F.W., "Theory of Spalling," Jl. Am. Cer. Soc., Vol. 16, No. 3, 1933, pp. 131-133.

39. Griffith, A.A., "The Theory of Rupture," Proc. 1st Intl. Congress Appl. Mech., Delft, 1924, pp. 55-63.

40. Sack, R.A., "Extension of Griffith's Theory of Rupture to Three Dimensions," Proc. Phys. Soc., 58, 1946, pp. 729-736.

41. Brace, W.F., "Brittle Fracture of Rocks," Proc. Intl. Conf., ed. W.R. Judd, American Elsevier Publishing Co., June 1963.

42. Bieniawski, Z.T., "Mechanism of Brittle Fracture of Rock, Part II - Experimental Studies," Intl. Jl. Rock Mech. Min. Sci., Vol. 4, 1967, pp. 407-423.

43. McClintock, F.A., and Walsh, J.B., "Friction on Griffith Cracks under Pressure," Proc. 4th U.S. Cong. Appl. Mech., Berkeley, 1962; ASME, New York, 1963, pp. 1015-1021.

44. Bieniawski, Z.T., "Mechanism of Rock Failure Under Compression," Report of the South African Council of Scientific and Industrial Research, No. MEG459, June 1966.

45. Hoek, E., and Bieniawski, Z.T., "Brittle Fracture Propagation in Rock under Compression," Intl. Jl. Fracture Mech., Vol. 1, No. 3, 1965, pp. 139-155.

46. Marovelli, R.L., and Veith, K.F., "Thermal Conductivity of Rock-Measurement by Transient Line Source Method," Bur. Mines RI 6604, 1965.

47. Marovelli, R.L., Chen, T.S., and Veith, K.F., "Thermal Fragmentation of Rock," Trans. Soc. Min. Engrs., Vol. 235, March 1966, pp. 1-15.

48. Marovelli, R.L., and Chen, T.S., "Analysis of Stresses in a Rock Disc Subjected to Peripheral Thermal Shock," Bur. Mines RI 6823, 1966.

49. Manson, S.S., and Smith, R.W., "Theory of Thermal Shock Resistance of Brittle Materials Based on Weibull's Statistical Theory of Strength," Jl. Am. Cer. Soc., Vol. 38, No. 1, 1955, pp. 18-27.

50. Carslaw, H.S., and Jaeger, J.C., "Conduction of Heat in Solids," 2nd ed., Oxford Univ. Press, London, 1959.

51. Baumeister, T., and Marks, L.S., "Standard Handbook for Mechanical Engineers," 7th ed., McGraw-Hill Co., New York, 1967.

52. Boley, B.A., and Weiner, J.H., "Theory of Thermal Stresses," John Wiley & Sons, Inc., 1960.

53. Paone, J., and Bruce, W.E., "Drillability Studies; Diamond Drilling," Bur. Mines RI 6324, 1963.

54. Ozisik, M.N., "Boundary Value Problems of Heat Conduction," International Textbook Company, 1968.

55. Luikov, A.V., "Methods of Solving the Nonlinear Equations of Unsteady-state Heat Conduction," Heat Transfer-Soviet Research, Vol. 3, No. 3, May-June 1971, pp. 1-51.

56. Crank, J., "The Mathematics of Diffusion," Oxford Univ. Press, London, 1956.

57. Bio, M.A., "Variational Principles in Heat Transfer," Oxford Univ. Press, London, 1970.

58. Goodman, T.R., "Application of Integral Methods to Transient Nonlinear Heat Transfer," Advances in Heat Transfer, Vol. 1, Academic Press, New York, 1964.

59. Mikhlin, S.G., "Variational Methods in Mathematical Physics," The Macmillan Company, New York, 1964.

60. Zienkiewicz, O.C., "The Finite Element Method in Structural and Continuum Mechanics," McGraw-Hill Publishing Company, 1967.

61. Wilson, E.L., and Nickell, R.E., "Application of the Finite Element Method to Heat Conduction Analysis," Nuclear Engineering and Design, Vol. 4, 1966, pp. 276-286.

62. Keith, H.D., Personal Communication, Univ. of Missouri-Rolla.

63. Jones, R.N., and Crose, J.G., "SAAS II-Finite Element Stress Analysis of Axisymmetric Solids with Orthotropic, Temperature Dependent Material Properties," Aerospace Corporation, California, 1968.

VITA

Mahendrakumar Ramkrishna Patel was born on February 6, 1947 in Amaraoti, India. In 1963, after graduating from Shri Govindram Sekseria High School at Pachora, India, he joined the Gujarat University in Ahmedabad, India from where he received the Bachelor's degree in Mechanical Engineering in June, 1968. He was awarded the Government of India National Scholarship for the years from 1965 to 1968. He came to U.S.A. in September, 1968 to join the University of Missouri-Rolla, and received his Master of Science degree in Mechanical Engineering in December 1970. He married Miss Minaxi Ramolia in October, 1971.

APPENDIX A

STRESS CODE, TRATSA - INPUT INSTRUCTIONS AND PROGRAM LISTING

This code was developed for the TRAnsient Thermoelastic Stress Analysis of plane or axisymmetric bodies with temperature-dependent material properties. The effects of displacement and stress boundary conditions, concentrated and distributed loads, and temperature changes are included. The program may be used to analyze more than one problem in a single run by inserting a change card with the code work "CHAN" in Columns 73-76 in front of each new set of problem data except the first problem.

For each problem, the following group of cards are required.

1. Identification Card (18A4):

   Cols. 2-72 This card may contain any information that the program user wants to have printed with the results to identify the problem being analyzed.

2. Control Card (7I5, 5X, F10.0, 22X, A4):

   Cols. 1-5 Number of nodal points (900 maximum)

   6-10 Number of elements (800 maximum)

   11-15 Number of different materials (5 maximum)

   16-20 Number of boundary pressure cards (100 maximum)

   25 Geometry option, 0 for axisymmetric problem, 1 for plane problem

   30 Data check option, 0 for complete analysis, 1 for checking data only

35 Stress punchout code, 1 if punchout required, 0 otherwise

40-50 Stress free or the reference temperature

73-74 Print code, NØ, to suppress data printout.

3. Material Property Information:

The following group of cards must be supplied for each different material, starting with material number one.

First card (2I5):

Cols. 1-5 Material identification number

6-10 Number of different temperatures for which properties are given (15 maximum)

One card for each temperature (4F10.0):

Cols. 1-10 Temperature

11-20 Young's modulus

21-30 Poisson's ratio

31-40 Coefficient of thermal expansion

Properties for the intermediate temperatures are obtained by linear interpolation.

Problem Geometry and Load Information

The grid geometry and the boundary conditions (concentrated loads and specified displacements) are described through the nodal point and the element card information. Distributed normal loads, if any, are to be specified through the boundary pressure cards. The nodal point coordinate can be given in either cartesian or polar form. The reference coordinate system, however, must be right-handed. To be consistent with this system, nodes defining an element must appear in

a counter-clockwise direction, and for a pressure boundary segment defined by nodes I, J, the material must be on the left while traversing from the node I to the node J.

Nodal point cards must be given in numerical sequence starting with node one. If cards are omitted, the omitted nodal points are generated at equal intervals either along a straight line or along a circular arc between the current nodal point and the last specified nodal point. For the generated nodes, the boundary condition code is set equal to 0.0.

4. Nodal Point Cards (2I5, 3F10.0, 2F5.0, 2F10.0):

Cols. 1-5 Nodal point number

10 Polar nodal point generation code, IPOLAR, defined as follows:

IPOLAR = 0 If no points are to be generated or if points are to be generated along a straight line

IPOLAR = 1 If points are to be generated along a circular arc from last previous nodal point to the present nodal point

11-20 R-coordinate (of center of arc if RAD $\neq$ 0)

21-30 Z-coordinate (of center of arc if RAD $\neq$ 0)

31-40 Radius of arc, RAD (=0 for cartesian system)

41-45 Polar angle in degrees measured counterclockwise from R-axis (=0 for cartesian system)

46-50 Boundary condition code defined as follows:

CODE = 0.0, R-load and Z-load specified

CODE = 1.0, R-displacement and Z-load specified

CODE = 2.0, R-load and Z-displacement specified

CODE = 3.0, R-displacement and Z-displacement specified

CODE = $-\theta$, S-load and N-displacement specified where SN is an orthogonal system rotated through an angle θ, $0° < \theta < 180°$, in the clockwise direction. This angle θ must always be input as a negative angle.

51-60 R-load or displacement (S-load if CODE < 0.0)

61-70 Z-load or displacement (N-displacement if CODE < 0.0)

In the printout, the R- and Z-displacements are to be interpreted as the S- and N-displacements for nodes for which CODE < 0.0.

5. Element Cards (6I5):

Cols. 1-5 Element number, N

6-10 Nodal point, I

11-15 Nodal point, J

16-20 Nodal point, K

21-25 Nodal point, L

30 Material identification number

Element cards must be given in numerical sequence starting with element number one. If element cards are omitted, the missing elements are generated by incrementing by one the preceding I, J, K,

L node numbers. The material identification code for the generated elements is set equal to the value given on the last card. The last element card must always be supplied. Triangular elements must be identified by repeating the last nodal point number, that is, I, J, K, K. To be consistent with the right-hand coordinate system, the nodes must be ordered in counter-clockwise direction around the element. The maximum permissible bandwidth of the stiffness matrix is 60; hence, the maximum difference between the nodes around an element must not exceed 29.

6. Boundary Pressure Cards (2I5, F10.0):

One card for each boundary segment subjected to normal pressure must be supplied. The boundary element must be on the left as one progresses from node I to node J. Surface tensile force is input as negative pressure. The magnitude of the pressure is based on unit length for the plane problem and on one radian segment for the axisymmetric problem.

Cols.	1-5	Nodal point, I
	6-10	Nodal point, J
	11-20	Normal pressure (assumed to be uniformly distributed)

7. Node Temperature Data:

There is no restriction on the number of temperature data set for which stress solutions are required. Each temperature data set consists of the following cards (for the research presented in the thesis, the temperature set was obtained as a punched output using a finite element conduction code):

Temperature Set Identification Card:

Cols. 1-8 Time associated with the temperature distribution as specified by the following cards:

9-80 Problem identification information. This may be same as that given in the identification card.

Node Temperature Cards (8F10.0):

Node temperatures must be given in numerical sequence starting with nodal point number one. Temperature for each node must be specified. Each card is allocated eight nodes. Thus, the temperature for nodal point number 30 will be specified in Columns 51-60 of the fourth card.

```
C     *** TRANSIENT THERMAL STRESS ANALYSIS OF ARBITRARY ***
C     *** PLANE OR AXISYMMETRIC SOLIDS WITH TEMPERATURE ****
C     ********** DEPENDENT MATERIAL PROPERTIES **********
C*************************************************************
C
      SUPPRESS UNDERFLOW MESSAGES  ***************************
      CALL ERRSET (208,256,-1,1)
      LOGICAL AXI, ERROR, QUAD, CHANGE, PUNCH, YES, FIRST
      COMMON NUMNP,NUMEL,NUMTC(5),E(15,4,5),EE(3),CODE(900),
     1T(900),Q,NAUX(900),NODE1(800),NODE2(800),NODE3(800),
     2NODE4(800),MAT(800),TELM(800),NUMPC,IBC(100),JBC(100),
     3LM(4),MTYPE,CON
      COMMON /ERASE/ R(900),Z(900),UR(900),UZ(900),PR(100),
     1HED(20)
      COMMON /LOGCAL/ AXI, ERROR, QUAD, CHANGE
      COMMON /IO/ IN,IPUNCH,IOUT,NDISK1,NDISK2,NFILE1,
     1NFILE2,NREC1
      COMMON/M2381/RR(5),ZZ(5),RCEN(800),ZCEN(800),P9(800),
     1P10(800)
      COMMON /M258/ NCODE,KODE(100),UR1(100),UZ1(100)
      COMMON/M35681/X1(6),H(6,10),CC1(9),CC2(8),HH(6,10),
     1S(10,10),TT,C11,C12,C13,C44
      COMMON /M48/ PRI1(100),PRI2(100),PRJ1(100),PRJ2(100)
      COMMON /M56/ FIRST, TLOW(5), THIGH(5)
      COMMON/M57891/A(120,60),P(10),TP(6),NUMBLK,MBAND,NDEG,
     1ND,ND2,NBSTF
      COMMON /M9/NNBAN, NLBAN, NHBAN
      DIMENSION B(1800)
      EQUIVALENCE (R(1),B(1))
      DEFINE FILE 6(3200,70,U,NREC1), 7(800,200,U,NREC2)
      DATA PHAN,PO/4HCHAN,4HNO  /
C*************************************************************
C     *** DATA SET REFERENCE NUMBERS ***
C*************************************************************
      IN=1
      IPUNCH=2
      IOUT=3
      NDISK1=4
      NDISK2=5
      NFILE1=6
      NFILE2=7
C*************************************************************
C     *** CONTROL INFORMATION AND MATERIAL PROPERTIES ***
C*************************************************************
    5 PUNCH = .FALSE.
      AXI =.TRUE.
      YES = .TRUE.
      READ (IN,10) HED,NUMNP,NUMEL,NUMMAT,NUMPC,NPP,NTEST,
     1KPUNCH,Q,HO
   10 FORMAT (20A4/7I5,5X,F10.0,22X,A4)
      IF (HO .EQ. PO) YES = .FALSE.
      IF (KPUNCH .GT. 0) PUNCH=.TRUE.
      IF (NPP .NE. 0) AXI=.FALSE.
      IF (AXI) WRITE (IOUT,20)
```

```
  20 FORMAT('1',23H AXISYMMETRIC STRUCTURE)
     IF (.NOT. AXI) WRITE (IOUT,30)
  30 FORMAT ('1',23H PLANE STRESS STRUCTURE)
     WRITE (IOUT,40) HED,NUMNP,NUMEL,NUMMAT,NUMPC,Q
  40 FORMAT (1H  20A4/
    1 31H  NUMBER OF NODAL POINTS ------ I3 /
    2 31H  NUMBER OF ELEMENTS ---------- I3 /
    3 31H  NUMBER OF DIFF. MATERIALS --- I3 /
    4 31H  NUMBER OF PRESSURE CARDS ---- I3 /
    5 31H  REFERENCE TEMPERATURE ------- F10.0)
     IF (NTEST .NE. 0) WRITE (IOUT,50)
  50 FORMAT (5X,'PROGRAM WILL NOT BE EXECUTED.',
    1' ONLY DATA WILL BE TESTED.')
     NUMTC1=1
     DO 100 M=1,NUMMAT
     READ (IN,60) MTYPE,NUMTC(MTYPE)
     NUMTM = NUMTC(MTYPE)
  60 FORMAT (2I5)
     IF (NUMTC1 .LT. NUMTM) NUMTC1=NUMTM
     READ (IN,70) ((E(I,J,MTYPE),J=1,4),I=1,NUMTM)
  70 FORMAT (4F10.0)
     WRITE (IOUT,90) MTYPE,((E(I,J,MTYPE),J=1,4),I=1,NUMTM)
  90 FORMAT (/19H  MATERIAL NUMBER =I3/
    110X,'TEMPERATURE',19X,'E',14X,'NU',14X,'ALPHA'/
    2(11X,F10.0,10X,F10.0,10X,F6.4,10X,F9.7))
     TLOW(M) = E(1,1,MTYPE)
     THIGH(M) = E(NUMTM,1,MTYPE)
 100 CONTINUE
*****************************************************************
     NODAL POINT DATA
*****************************************************************
     ERROR = .FALSE.
     RADIN=3.14159/180.
     M=1
 110 IF (M .GT. NUMNP) GO TO 190
     READ (IN,120) N,IPOLAR,RA,ZA,RAD,THETA,CODE(N),UR(N),
    1UZ(N)
 120 FORMAT (2I5,3F10.0,2F5.0,2F10.0)
     IF (N .LE. NUMNP) GO TO 125
 121 ERROR=.TRUE.
     WRITE (IOUT,122) M
 122 FORMAT (' *** NODAL POINT ERROR, NP = ',I3/)
     M=M+1
     GO TO 110
 125 N1=N-M
     IF (N1 .LT. 0) GO TO 121
     IF (RAD .EQ. 0.0) GO TO 130
     THETA=THETA*RADIN
     R(N)=RA+RAD*COS(THETA)
     Z(N)=ZA+RAD*SIN(THETA)
     GO TO 140
 130 R(N)=RA
     Z(N)=ZA
 140 IF (N1 .EQ. 0) GO TO 180
```

```
      NN=N1+1
      IF (IPOLAR .GT. 0) GO TO 160
      DR=(R(N)-R(M1))/NN
      DZ=(Z(N)-Z(M1))/NN
      DO 150 I=1,N1
      R(M)=R(M1)+DR
      Z(M)=Z(M1)+DZ
      CODE(M)=0.0
      UR(M)=0.0
      UZ(M)=0.0
      M1=M
  150 M=M+1
      GO TO 180
  160 DTH=(THETA-THST)/NN
      DO 170 I=1,N1
      THST=THST+DTH
      R(M)=RA+RAD*COS(THST)
      Z(M)=ZA+RAD*SIN(THST)
      CODE(M)=0.0
      UR(M)=0.0
      UZ(M)=0.0
  170 M=M+1
  180 M1=M
      M=M+1
      THST=THETA
      GO TO 110
  190 CONTINUE
      IF(YES)WRITE (IOUT,195)(N,R(N),Z(N),CODE(N),UR(N),
     1UZ(N), N=1,NUMNP)
  195 FORMAT ( /20X,' NODE    R-COORD    Z-COORD       CODE',4X,
     1'R-LOAD/DISP     Z-LOAD/DISP'/(I25,3F10.3,2F15.2))
C*****************************************************************
C     ELEMENT CARDS
C*****************************************************************
      IF (YES) WRITE (IOUT,200)
  200 FORMAT (//26X,' ELEMENT NO.      I      J      K      L',
     114X,'MATERIAL')
      MAXB=29
      MBAND=0
      M=0
  210 M=M+1
      READ (IN,220) N,NODE1(N),NODE2(N),NODE3(N),NODE4(N),
     1MAT(N)
  220 FORMAT (6I5)
      NM=N-M
      IF (NM) 230,270,250
  230 ERROR=.TRUE.
      WRITE (IOUT,240) M
  240 FORMAT ('*** ELEMENT CARD ERROR, ELEM = ',I3/)
      GO TO 210
  250 DO 260 I=1,NM
      M1=M-1
      NODE1(M)=NODE1(M1)+1
      NODE2(M)=NODE2(M1)+1
```

```
      NODE3(M)=NODE3(M1)+1
      NODE4(M)=NODE4(M1)+1
      MAT(M)=MAT(M1)
      IF(YES)WRITE(IOUT,280)M,NODE1(M),NODE2(M),NODE3(M),
     1NODE4(M),MAT(M)
  260 M=M+1
  270 IF(YES)WRITE(IOUT,280)N,NODE1(N),NODE2(N),NODE3(N),
     1NODE4(N),MAT(N)
  280 FORMAT (33X,I5,4I6,I12)
      LM(1)=NODE1(N)
      LM(2)=NODE2(N)
      LM(3)=NODE3(N)
      LM(4)=NODE4(N)
C*****************************************************************
C     DETERMINE THE BANDWIDTH OF THE STIFFNESS MATRIX
C*****************************************************************
      DO 310 I=1,3
      I1=I+1
      DO 310 J=I1,4
      NN=IABS(LM(I)-LM(J))
      IF (NN .LE. MAXB) GO TO 300
      WRITE (IOUT,290) N,MAXB
  290 FORMAT (/'***ELEM. ',I3,
     1', EXCEEDS ALLOWABLE NODAL POINT DIFF. =',I3)
      ERROR=.TRUE.
      GO TO 320
  300 IF (NN .GT. MBAND) MBAND=NN
  310 CONTINUE
  320 IF (M .LT. NUMEL) GO TO 210
C*****************************************************************
C     PRESSURE BOUNDARY CARDS
C*****************************************************************
      IF (NUMPC .EQ. 0) GO TO 370
      WRITE (IOUT,330)
  330 FORMAT (30H PRESSURE BOUNDARY CONDITIONS /
     125H      I      J      PRESSURE)
      DO 350 N=1,NUMPC
      READ (IN,340) IBC(N),JBC(N),PR(N)
  340 FORMAT (2I5,F10.0)
  350 WRITE (IOUT,360) IBC(N),JBC(N),PR(N)
  360 FORMAT (2I6,F12.3)
  370 IF (NTEST .NE. 0 .OR. ERROR) CALL EXIT
      MBAND=MBAND+MBAND+2
      NDEG=NUMNP+NUMNP
      NBSTF = MAXB+1
      ND = NBSTF+NBSTF
      ND2 = ND+ND
      NNBAN = ND
      NLBAN = NNBAN+1
      NHBAN = NNBAN+NNBAN
      NREC1 = 1
      CALL COORD1
      IF (NUMPC .GT. 0) CALL PRESBC
      NTIME1 = 0
```

```
      FIRST = .TRUE.
C*************************************************************
  375 READ (IN,360,END=420) (HED(I),I=1,20)
  380 FORMAT (20A4)
      IF (HED(19) .EQ. PHAN) GO TO 5
      READ (IN,381) (T(N),N=1,NUMNP)
  381 FORMAT (8F10.0)
      NTIME1 = NTIME1+1
      WRITE (IOUT,382) NTIME1,HED
  382 FORMAT ('1','TEMP. SET NO.',I3/20A4//,
     1' NODE',10X,'TEMP.',10X,'R-DISP.',10X,'Z-DISP.'/)
      IF (PUNCH) WRITE (IPUNCH,380) HED
      DO 385 N = 1, NUMEL
      N1 = NODE1(N)
      N2 = NODE2(N)
      N3 = NODE3(N)
      TELM(N) = T(N1)+T(N2)+T(N3)
      IF (N3 .EQ. NODE4(N)) GO TO 384
      N4 = NODE4(N)
      TELM(N) = (TELM(N)+T(N4))/4.0
      GO TO 385
  384 TELM(N) = TELM(N)/3.0
  385 CONTINUE
      CHANGE=.FALSE.
      IF (NTIME1 .EQ. 1 .OR. NUMTC1 .GT. 1) CHANGE=.TRUE.
      IF (CHANGE) CALL STIFF (NUMTC1)
      CALL LOAD
      CALL EQSOLV
      DO 400 N=1,NUMNP
      N2=N+N
      N1=N2-1
  400 WRITE (IOUT,410) N,T(N),B(N1),B(N2)
  410 FORMAT (I5,F15.1,2F17.8)
      CALL STRESS (PUNCH)
      FIRST = .FALSE.
      GO TO 375
  420 STOP
      END


      SUBROUTINE COORD1
      LOGICAL AXI, ERROR, QUAD, CHANGE
      COMMON NUMNP,NUMEL,NUMTC(5),E(15,4,5),EE(3),CODE(900),
     1T(900),Q,NAUX(900),NODE1(800),NODE2(800),NODE3(800),
     2NODE4(800),MAT(800),TELM(800),NUMPC,IBC(100),JBC(100),
     3LM(4),MTYPE,CON
      COMMON /ERASE/ R(900),Z(900),UR(900),UZ(900),PR(100),
     1HED(20)
      COMMON /LOGCAL/ AXI, ERROR, QUAD, CHANGE
      COMMON/M2381/RR(5),ZZ(5),RCEN(800),ZCEN(800),P9(800),
     1P10(800)
      COMMON /M258/ NCODE,KODE(100),UR1(100),UZ1(100)
      DIMENSION CODE1(4)
      NCODE=0
```

```
      DO 20 N=1,NUMNP
      NAUX(N) = N+N-2
      IF (R(N) .NE. 0.0) GO TO 10
      R(N)=0.001
      IF (AXI .AND. CODE(N) .EQ. 0.) CODE(N)=1.0
   10 IF (CODE(N) .EQ. 0. .AND. UR(N) .EQ. 0. .AND.
     1UZ(N) .EQ. 0.0) GO TO 15
      NCODE = NCODE+1
      KODE(NCODE)=N
      UR1(NCODE)=UR(N)
      UZ1(NCODE)=UZ(N)
      IF (CODE(N) .LT. 0.0) CODE(N)=CODE(N)/57.296
   15 CONTINUE
   20 CONTINUE
      DO 50 N=1,NUMEL
      N1=NODE1(N)
      N2=NODE2(N)
      N3=NODE3(N)
      N4=NODE4(N)
      RR(1)=R(N1)
      RR(2)=R(N2)
      RR(3)=R(N3)
      ZZ(1)=Z(N1)
      ZZ(2)=Z(N2)
      ZZ(3)=Z(N3)
      RR(5)=RR(1)+RR(2)+RR(3)
      ZZ(5)=ZZ(1)+ZZ(2)+ZZ(3)
      CODE1(1) = CODE(N1)
      CODE1(2) = CODE(N2)
      CODE1(3) = CODE(N3)
      IF (N3 .EQ. N4) GO TO 30
      RR(4)=R(N4)
      ZZ(4)=Z(N4)
      RR(5)=(RR(5)+RR(4))/4.0
      ZZ(5)=(ZZ(5)+ZZ(4))/4.0
      CODE1(4) = CODE(N4)
      CALL COORD2 (4,1,5,N,CODE1)
      IF (ERROR) GO TO 50
      CALL COORD2 (1,2,5,N,CODE1)
      CALL COORD2 (2,3,5,N,CODE1)
      CALL COORD2 (3,4,5,N,CODE1)
      GO TO 40
   30 RR(5)=RR(5)/3.0
      ZZ(5)=ZZ(5)/3.0
      CALL COORD2 (1,2,3,N,CODE1)
   40 RCEN(N)=RR(5)
      ZCEN(N)=ZZ(5)
   50 CONTINUE
      IF (ERROR) CALL EXIT
      RETURN
      END


      SUBROUTINE COORD2 (I1,I2,I3,N,CODE1)
```

```
      LOGICAL AXI, ERROR, QUAD, CHANGE
      REAL*8 XX(9),XM(7),R(7),Z(7),AREA
      COMMON /LOGCAL/ AXI, ERROR, QUAD, CHANGE
      COMMON /IO/ IN,IPUNCH,IOUT,NDISK1,NDISK2,NFILE1,
     1NFILE2,NREC1
      COMMON/M2381/RR(5),ZZ(5),RCEN(800),ZCEN(800),P9(800),
     1P10(800)
      COMMON/M35681/XI(6),H(6,10),CC1(9),CC2(8),HH(6,10),
     1S(10,10),TT,C11,C12,C13,C44
      DIMENSION DD(3,3),LM(3),CODE1(4)
      DATA XX/3*.125939180544B,3*.132394152788B,.225,
     10.696140478028,0.410426192314/
      R(1)=RR(I1)
      R(2)=RR(I2)
      R(3)=RR(I3)
      Z(1)=ZZ(I1)
      Z(2)=ZZ(I2)
      Z(3)=ZZ(I3)
      AREA=R(1)*(Z(2)-Z(3))+R(2)*(Z(3)-Z(1))+R(3)*(Z(1)-Z(2))
      IF (AREA .GT. 0.0) GO TO 20
      ERROR=.TRUE.
      WRITE (IOUT,10) N
10    FORMAT (26H NEGATIVE AREA ELEMENT NO. I4)
20    IF (ERROR) RETURN
      DD(1,1)=(R(2)*Z(3)-R(3)*Z(2))/AREA
      DD(1,2)=(R(3)*Z(1)-R(1)*Z(3))/AREA
      DD(1,3)=(R(1)*Z(2)-R(2)*Z(1))/AREA
      DD(2,1)=(Z(2)-Z(3))/AREA
      DD(2,2)=(Z(3)-Z(1))/AREA
      DD(2,3)=(Z(1)-Z(2))/AREA
      DD(3,1)=(R(3)-R(2))/AREA
      DD(3,2)=(R(1)-R(3))/AREA
      DD(3,3)=(R(2)-R(1))/AREA
      LM(1)=I1
      LM(2)=I2
      LM(3)=I3
      DO 30 I=1,6
      DO 30 J=1,10
30    H(I,J)=0.0
      DO 40 I=1,3
      J=LM(I)+LM(I)
      J1=J-1
      H(1,J1)=DD(1,I)
      H(2,J1)=DD(2,I)
      H(3,J1)=DD(3,I)
      H(4,J)=DD(1,I)
      H(5,J)=DD(2,I)
40    H(6,J)=DD(3,I)
      IF (CODE1(I1) .GE. 0. .AND. CODE1(I2) .GE. 0.) GO TO 60
      DO 50 J=1,2
      I=LM(J)
      IF (CODE1(I) .GE. 0.) GO TO 50
      SINA=SIN(CODE1(I))
      COSA=COS(CODE1(I))
```

```
      IJ=I+I
      IJ1=IJ-1
      DO 50 K=1,6
      TEM=H(K,IJ1)
      H(K,IJ1)=TEM*COSA+H(K,IJ)*SINA
      H(K,IJ)=-TEM*SINA+H(K,IJ)*COSA
   50 CONTINUE
   60 CONTINUE
      R(7)=(R(1)+R(2)+R(3))/3.0
      Z(7)=(Z(1)+Z(2)+Z(3))/3.0
      DO 70 I=1,3
      J=I+3
      RI7=R(I)-R(7)
      ZI7=Z(I)-Z(7)
      R(I)=RI7*XX(8)+R(7)
      R(J)=RI7*XX(9)+R(7)
      Z(I)=ZI7*XX(8)+Z(7)
   70 Z(J)=ZI7*XX(9)+Z(7)
      IF (AXI) GO TO 90
      DO 80 I=1,7
   80 XM(I)=XX(I)
      GO TO 110
   90 DO 100 I=1,7
  100 XM(I)=XX(I)*R(I)
  110 DO 120 I=1,6
  120 XI(I)=0.0
      DO 130 I=1,7
      XI(1)=XI(1)+XM(I)
      IF (.NOT. AXI) GO TO 130
      R2=R(I)*R(I)
      XMZ=XM(I)*Z(I)
      XI(2)=XI(2)+XM(I)/R(I)
      XI(3)=XI(3)+XM(I)/R2
      XI(4)=XI(4)+XMZ/R(I)
      XI(5)=XI(5)+XMZ/R2
      XI(6)=XI(6)+XMZ*Z(I)/R2
  130 CONTINUE
      AREA=0.5*AREA
      XI(1)=XI(1)*AREA
      IF (.NOT. AXI) GO TO 150
      DO 140 I=2,6
  140 XI(I)=XI(I)*AREA
  150 WRITE (NFILE1'NREC1) XI,H
      RETURN
      END


      SUBROUTINE PRESBC
      LOGICAL AXI, ERROR, QUAD, CHANGE
      COMMON NUMNP,NUMEL,NUMTC(5),E(15,4,5),EE(3),CODE(900),
     1T(900),Q,NAUX(900),NODE1(800),NODE2(800),NODE3(800),
     2NODE4(800),MAT(800),TELM(800),NUMPC,IBC(100),JBC(100),
     3LM(4),MTYPE,CON
      COMMON /ERASE/ R(900),Z(900),UR(900),UZ(900),PR(100),
```

```
     1HED(20)
      COMMON /LOGCAL/ AXI, ERROR, QUAD, CHANGE
      COMMON /M48/ PRI1(100),PRI2(100),PRJ1(100),PRJ2(100)
      RX=3.0
      ZX=3.0
      DO 40 N=1,NUMPC
      I=IBC(N)
      J=JBC(N)
      IF (.NOT. AXI) GO TO 10
      RX=2.0*R(I)+R(J)
      ZX=2.0*R(J)+R(I)
   10 PP=PR(N)/6.0
      DR=(R(J)-R(I))*PP
      DZ=(Z(I)-Z(J))*PP
      SINA=0.0
      COSA=1.0
      IF (CODE(I) .GE. 0.0) GO TO 20
      SINA=SIN(CODE(I))
      COSA=COS(CODE(I))
   20 PRI1(N)=RX*(COSA*DZ+SINA*DR)
      PRI2(N)=-RX*(SINA*DZ-COSA*DR)
      SINA=0.0
      COSA=1.0
      IF (CODE(J) .GE. 0.0) GO TO 30
      SINA=SIN(CODE(J))
      COSA=COS(CODE(J))
   30 PRJ1(N)=ZX*(COSA*DZ+SINA*DR)
      PRJ2(N)=-ZX*(SINA*DZ-COSA*DR)
   40 CONTINUE
      RETURN
      END


      SUBROUTINE STIFF (NUMTC1)
      LOGICAL AXI, ERROR, QUAD, CHANGE, FIRST
      COMMON NUMNP,NUMEL,NUMTC(5),E(15,4,5),EE(3),CODE(900),
     1T(900),Q,NAUX(900),NODE1(800),NODE2(800),NODE3(800),
     2NODE4(800),MAT(800),TELM(800),NUMPC,IBC(100),JBC(100),
     3LM(4),MTYPE,CON
      COMMON /ERASE/ R(900),Z(900),UR(900),UZ(900),PR(100),
     1HED(20)
      COMMON /LOGCAL/ AXI, ERROR, QUAD, CHANGE
      COMMON /IO/ IN,IPUNCH,IOUT,NDISK1,NDISK2,NFILE1,
     1NFILE2,NREC1
      COMMON /M258/ NCODE,KODE(100),UR1(100),UZ1(100)
      COMMON/M35681/XI(6),H(6,10),CC1(9),CC2(8),HH(6,10),
     1S(10,10),TT,C11,C12,C13,C44
      COMMON /M56/ FIRST, TLOW(5), THIGH(5)
      COMMON/M57891/A(120,60),P(10),TP(6),NUMBLK,MBAND,NDEG,
     1ND,ND2,NBSTF
      DIMENSION BDISP(1800)
        EQUIVALENCE (UR(1),BDISP(1))
      REWIND NDISK1
      DO 5 N = 1, NDEG
```

```
    5 BDISP(N) = 0.0
      DO 10 N=1,ND2
      DO 10 M=1,ND
   10 A(N,M)=0.0
      MTYPE = 0
C*****************************************************************
C     FORM STIFFNESS MATRIX A IN BLOCKS
C*****************************************************************
      NUMBLK=0
   20 NUMBLK=NUMBLK+1
      NH=NBSTF*(NUMBLK+1)
      NM=NH-NBSTF
      NL=NM+1-NBSTF
      KSHIFT=NL+NL-2
      NREC1=1
      DO 120 N=1,NUMEL
      QUAD=.TRUE.
      IF (NODE3(N) .EQ. NODE4(N)) QUAD=.FALSE.
      IF (MAT(N) .GT. 0) GO TO 40
      IF (.NOT. QUAD) GO TO 30
   25 NREC1 = NREC1+3
   30 NREC1=NREC1+1
      GO TO 120
   40 NREC2=N
      N1=NODE1(N)
      N2=NODE2(N)
      N3=NODE3(N)
      N4=NODE4(N)
      IF (N1 .GE. NL .AND. N1 .LE. NM) GO TO 50
      IF (N2 .GE. NL .AND. N2 .LE. NM) GO TO 50
      IF (N3 .GE. NL  .AND. N3 .LE. NM) GO TO 50
      IF (.NOT. QUAD) GO TO 30
      IF (N4 .LT. NL .OR. N4 .GT. NM) GO TO 25
   50 IF (FIRST) GO TO 55
      M = MAT(N)
      IF (NUMTC(M) .EQ. 1) GO TO 52

      GO TO 55
   52 READ (NFILE2'NREC2) TT,CC1,CC2,EE,C11,C12,C13,C44,HH,S
      MAT(N) = -M
      NREC1 = NREC1+1
      IF (QUAD) NREC1 = NREC1+3
      GO TO 95
   55 CALL ELMSTF (N)
      DO 60 I=1,10
      DO 60 J=1,10
   60 S(I,J)=S(I,J)*EE(1)
      IF (.NOT. QUAD) GO TO 90
C*****************************************************************
C     ELIMINATE THE FICTITIOUS CENTRAL NODE
C*****************************************************************
      S1010=S(10,10)
      DO 70 I=1,9
      CC1(I)=S(I,10)/S1010
```

```
      DO 70 J=1,9
   70 S(I,J)=S(I,J)-CC1(I)*S(10,J)
      S99=S(9,9)
      DO 80 I=1,8
      CC2(I)=S(I,9)/S99
      DO 80 J=1,8
   80 S(I,J)=S(I,J)-CC2(I)*S(9,J)
   90 CONTINUE
      WRITE(NFILE2'NREC2) TT,CC1,CC2,EE,C11,C12,C13,C44,HH,S
C*****************************************************************
C     ADD ELEMENT STIFFNESS TO TOTAL STIFFNESS
C*****************************************************************
   95 LM(1)=NAUX(N1)
      LM(2)=NAUX(N2)
      LM(3)=NAUX(N3)
      LM(4)=NAUX(N4)
      KK=0
      DO 110 I=1,4
      DO 110 K=1,2
      II=LM(I)+K-KSHIFT
      KK=KK+1
      LL=0
      DO 110 J=1,4
      IF (LM(I) .LE. LM(J)) GO TO 100
      LL=LL+2
      GO TO 110
  100 DO 110 L=1,2
      LL=LL+1
      IF (I .EQ. J .AND. K .GT. L) GO TO 110
      JJ=LM(J)+L+1-KSHIFT-II
      A(II,JJ)=A(II,JJ)+S(KK,LL)
  110 CONTINUE
  120 CONTINUE
C*****************************************************************
C     MODIFY STIFFNESS MATRIX A FOR DISPLACEMENT BC
C*****************************************************************
      DO 160 M=1,NCODE
      II=KODE(M)
      IF (II .GT. NH) GO TO 170
      IF (II .LT. NL) GO TO 160
      U=UR1(M)
      N=II+II-1-KSHIFT
      IF (CODE(II) .LT. 0.0) GO TO 150
      IF (CODE(II)-2.0) 130,150,140
  130 CALL MODIFY (KSHIFT,N,U)
      GO TO 160
  140 CALL MODIFY (KSHIFT,N,U)
  150 U=UZ1(M)
      N=N+1
      CALL MODIFY (KSHIFT,N,U)
  160 CONTINUE
  170 CONTINUE
C*****************************************************************
C     WRITE BLOCK OF MATX A ON DISK AND SHIFT UP LOWER BLOCK
```

```
C*************************************************************
      WRITE (NDISK1) ((A(N,M),M=1,MBAND),N=1,ND)
      DO 180 N=1,ND
      K=N+ND
      DO 180 M=1,ND
      A(N,M)=A(K,M)
  180 A(K,M)=0.0
C**** CHECK FOR THE LAST BLOCK ********************************
      IF (NM .LT. NUMNP) GO TO 20
C*************************************************************
C     ADD CONCENTRATED FORCES TO VECTOR B
C*************************************************************
      DO 200 N=1,NCODE
      M=KODE(N)
      IF (CODE(M) .GT. 0.0) GO TO 200
      N1=M+M-1
      BDISP(N1)=BDISP(N1)+UR1(N)
      IF (CODE(M) .LT. 0.0) GO TO 200
      N1=N1+1
      BDISP(N1)=BDISP(N1)+UZ1(N)
  200 CONTINUE
      IF (NUMTC1.EQ. 1) RETURN
C**** SET THE MATERIAL NUMBERS TO THEIR ABSOLUTE VALUES ****
      DO 210 N=1,NUMEL
  210 MAT(N)=IABS (MAT(N))
      NREC2 = 1
      FIND (NFILE2'NREC2)
      RETURN
      END


      SUBROUTINE ELMSTF (N)
      LOGICAL AXI, ERROR, QUAD, CHANGE, FIRST
      COMMON NUMNP,NUMEL,NUMTC(5),E(15,4,5),EE(3),CODE(900),
     1T(900),Q,NAUX(900),NODE1(800),NODE2(800),NODE3(800),
     2NODE4(800),MAT(800),TELM(800),NUMPC,IBC(100),JBC(100),
     3LM(4),MTYPE,CON
      COMMON /ERASE/ R(900),Z(900),UR(900),UZ(900),PR(100),
     1HED(20)
      COMMON /LOGCAL/ AXI, ERROR, QUAD, CHANGE
      COMMON /IO/ IN,IPUNCH,IOUT,NDISK1,NDISK2,NFILE1,
     1NFILE2,NREC1
      COMMON/M35681/XI(6),H(6,10),CC1(9),CC2(8),HH(6,10),
     1S(10,10),TT,C11,C12,C13,C44
      COMMON /M56/ FIRST, TLOW(5), THIGH(5)
      DIMENSION D(6,6), F(6,10)
      EQUIVALENCE (D(1),PR(1)), (F(1),PR(37))
      M=MAT(N)
      NUMTM = NUMTC(M)
      IF (.NOT. FIRST) GO TO 3
      IF (NUMTM .GT. 1) GO TO 1
      IF (M .EQ. MTYPE) GO TO 40
      GO TO 13
    1 IF (TELM(N) .GT. TLOW(M)) GO TO 3
```

```
      DO 2 J = 1, 3
    2  EE(J) = E(1,J+1,M)
      GO TO 15
    3 DO 5 I=2,NUMTM
      IF (E(I,1,M) .GE. TELM(N)) GO TO 10
    5 CONTINUE
      DO 6 J = 1, 3
    6 EE(J) = E(NUMTM,J+1,M)
      GO TO 15
   10 I1 = I-1
      DIFF=E(I,1,M)-E(I1,1,M)
      RATIO=(TELM(N)-E(I1,1,M))/DIFF
      DO 12 J=1,3
      J1 = J+1
   12 EE(J)=E(I1,J1,M)+RATIO*(E(I,J1,M)-E(I1,J1,M))
      GO TO 15
   13 DO 14 J = 1, 3
   14 EE(J) = E(1,J+1,M)
   15 IF (AXI) GO TO 20
      C11=1.0/(1.0-EE(2)*EE(2))
      C12=C11*EE(2)
      C13=0.0
      C44=0.5/(1.0+EE(2))
      GO TO 30
   20 C1=1.0-EE(2)
      C2=C1-EE(2)
      C3=C1/((1.0+EE(2))*C2)
      C11=C3
      C12=EE(2)*C3/C1
      C13=C12
      C44=0.5*C3*C2/C1
   30 CON=(C11+C12+C13)*EE(3)
      MTYPE=M
   40 TT = CON
      MAT(N)=-M
      INITIALIZE STRAIN-DISP. MATX HH & ELEM STIFFNESS MATX S
      DO 60 J=1,10
      DO 50 I=1,6
      HH(I,J)=0.0
   50 S(I,J)=0.0
      DO 60 I=7,10
   60 S(I,J)=0.0
      DO 160 N1=1,4
      FIND (NFILE1'NREC1)
      INITIALIZE
      DO 80 I=1,6
      DO 70 J=1,6
      D(I,J)=0.0
   70 F(I,J)=0.0
      DO 80 J=7,10
   80 F(I,J)=0.0
      READ (NFILE1'NREC1) XI,H
      D26=XI(1)*C12
      D35=XI(1)*C44
```

```
      D66=XI(1)*C11
      D(2,6)=D26
      D(3,5)=D35
      D(5,5)=D35
      D(6,6)=D66
      IF (AXI) GO TO 90
      D(2,2)=D66
      D(3,3)=D35
      GO TO 100
   90 C1113=C11+C13
      D(1,1)=XI(3)*C11
      D(1,2)=XI(2)*C1113
      D(1,3)=XI(5)*C11
      D(1,6)=XI(2)*C12
      D(2,2)=XI(1)*(C1113+C1113)
      D(2,3)=XI(4)*C1113
      D(2,6)=D26+D26
      D(3,3)=XI(6)*C11+D35
      D(3,6)=XI(4)*C12
  100 DO 110 I=2,6
      I1=I-1
      DO 110 J=1,I1
  110 D(I,J)=D(J,I)
      DO 130 I=1,10
      DO 130 J=1,6
      HJI=H(J,I)
      IF (HJI .EQ. 0.0) GO TO 130
      DO 120 M=1,6
  120 F(M,I)=F(M,I)+HJI*D(M,J)
  130 CONTINUE
      DO 150 I=1,10
      DO 150 J=1,6
      HJI=H(J,I)
      IF (HJI .EQ. 0.0) GO TO 150
      DO 140 M=1,10
  140 S(I,M)=S(I,M)+HJI*F(J,M)
      HH(J,I)=HH(J,I)+HJI
  150 CONTINUE
      IF (.NOT. QUAD) RETURN
  160 CONTINUE
      DO 170 I=1,6
      DO 170 J=1,10
  170 HH(I,J)=HH(I,J)/4.0
      RETURN
      END


      SUBROUTINE MODIFY (KSHIFT,N,U)
      COMMON /ERASE/ R(900),Z(900),UR(900),UZ(900),PR(100),
     1HED(20)
      COMMON/M57891/A(120,60),P(10),TP(6),NUMBLK,MBAND,NDEG,
     1ND,ND2,NBSTF
      DIMENSION BDISP(1800)
      EQUIVALENCE (UR(1),BDISP(1))
```

```
      DO 20 M=2,MBAND
      K=N-M+1
      IF (K .LE. 0) GO TO 10
      K1=K+KSHIFT
      BDISP(K1)=BDISP(K1)-A(K,M)*U
      A(K,M)=0.0
10    K=N+M-1
      IF (K .GT. ND2) GO TO 15
      K1=K+KSHIFT
      BDISP(K1)=BDISP(K1)-A(N,M)*U
      A(N,M)=0.0
15    CONTINUE
20    CONTINUE
      A(N,1)=1.0
      RETURN
      END


      SUBROUTINE LOAD
      LOGICAL AXI, ERROR, QUAD, CHANGE
      COMMON NUMNP,NUMEL,NUMTC(5),E(15,4,5),EE(3),CODE(900),
     1T(900),Q,NAUX(900),NODE1(800),NODE2(800),NODE3(800),
     2NODE4(800),MAT(800),TELM(800),NUMPC,IBC(100),JBC(100),
     3LM(4),MTYPE,CON
      COMMON /ERASE/ R(900),Z(900),UR(900),UZ(900),PR(100),
     1HED(20)
      COMMON /LOGCAL/ AXI, ERROR, QUAD, CHANGE
      COMMON /IO/ IN,IPUNCH,IOUT,NDISK1,NDISK2,NFILE1,
     1NFILE2,NREC1
      COMMON/M2381/RR(5),ZZ(5),RCEN(800),ZCEN(800),P9(800),
     1P10(800)
      COMMON /M258/ NCODE,KODE(100),UR1(100),UZ1(100)
      COMMON/M35681/XI(6),H(6,10),CC1(9),CC2(8),HH(6,10),
     1S(10,10),TT,C11,C12,C13,C44
      COMMON /M46/ PR11(100),PR12(100),PRJ1(100),PRJ2(100)
      COMMON/M57891/A(120,60),P(10),TP(6),NUMBLK,MBAND,NDEG,
     1ND,ND2,NBSTF
      DIMENSION B(1800), BDISP(1800)
      EQUIVALENCE (R(1),B(1)), (UR(1),BDISP(1))
      DO 10 N=1,NDEG
10    B(N)=BDISP(N)
      TP(1)=0.0
      TP(3)=0.0
      TP(4)=0.0
      TP(5)=0.0
      NREC1=1
      DO 120 N=1,NUMEL
      IF (TELM(N) .NE. Q) GO TO 20
      NREC1=NREC1+1
      IF (NODE3(N) .NE. NODE4(N)) NREC1=NREC1+3
      P9(N) = 0.0
      P10(N) = 0.0
      GO TO 120
20    NREC2=N
```

```
      FIND (NFILE2'NREC2)
      QUAD=.TRUE.
      N1=NODE1(N)
      N2=NODE2(N)
      N3=NODE3(N)
      N4=NODE4(N)
      IF (N3 .EQ. N4) QUAD=.FALSE.
      DO 30 I=1,10
   30 P(I)=0.0
      READ (NFILE2'NREC2) TT,CC1,CC2,EE
      TTT=TT*(TELM(N)-Q)
C*****************************************************************
C     *** FORM THERMAL LOAD VECTOR FOR ELEMENT N ***
C*****************************************************************
      DO 60 NN=1,4
      READ (NFILE1'NREC1) XI,H
      TP(2)=XI(1)*TTT
      TP(6)=TP(2)
      IF (.NOT. AXI) GO TO 40
      TP(1)=XI(2)*TTT
      TP(2)=TP(2)+TP(2)
      TP(3)=XI(4)*TTT
   40 CONTINUE
      DO 50 I=1,10
      DO 50 J=1,6
   50 P(I)=P(I)+H(J,I)*TP(J)
      IF (.NOT. QUAD) GO TO 90
   60 CONTINUE
      DO 70 I=1,9
   70 P(I)=P(I)-CC1(I)*P(10)
      DO 80 I=1,8
   80 P(I)=P(I)-CC2(I)*P(9)
   90 CONTINUE
      DO 95 I = 1, 10
   95 P(I) = P(I)*EE(1)
C*****************************************************************
C     *** ADD ELEM LOAD VECTOR TO OVERALL LOAD VECTOR, B ***
C*****************************************************************
      LM(1)=NAUX(N1)
      LM(2)=NAUX(N2)
      LM(3)=NAUX(N3)
      LM(4)=NAUX(N4)
      KK=0
      DO 100 I=1,4
      DO 100 J=1,2
      II=LM(I)+J
      KK=KK+1
  100 B(II)=B(II)+P(KK)
      P9(N)=P(9)
      P10(N)=P(10)
  120 CONTINUE
C*****************************************************************
C     *** MODIFY VECTOR B FOR PRESSURE BOND. COND. ***
C*****************************************************************
```

```
      IF (NUMPC .EQ. 0) GO TO 140
      DO 130 L=1,NUMPC
      I=IBC(L)+IBC(L)
      J=JBC(L)+JBC(L)
      I1=I-1
      J1=J-1
      B(I1)=B(I1)+PRI1(L)
      B(I)=B(I)+PRI2(L)
      B(J1)=B(J1)+PRJ1(L)
  130 B(J)=B(J)+PRJ2(L)
  140 CONTINUE
C*****************************************************************
C     *** MODIFY VECTOR B FOR DISPL. BOND. COND. ***
C*****************************************************************
      DO 180 N = 1, NCODE
      NN=KODE(N)
      IF (CODE(NN) .LT. 0.0) GO TO 170
      IF (CODE(NN)-2.0) 150,170,160
  150 N1=NN+NN-1
      B(N1)=UR1(N)
      GO TO 180
  160 N1=NN+NN-1
      B(N1)=UR1(N)
  170 N1=NN+NN
      B(N1)=UZ1(N)
  180 CONTINUE
      RETURN
      END


      SUBROUTINE EQSOLV
      LOGICAL AXI, ERROR, QUAD, CHANGE
      COMMON /ERASE/ R(900),Z(900),UR(900),UZ(900),PR(100),
     1HED(20)
      COMMON /LOGCAL/ AXI, ERROR, QUAD, CHANGE
      COMMON /IO/ IN,IPUNCH,IOUT,NDISK1,NDISK2,NFILE1,
     1NFILE2,NREC1
      COMMON/M57891/A(120,60),P(10),TP(6),NUMBLK,MBAND,NDEG,
     1ND,ND2,NBSTF
      COMMON /M9/NNBAN, NLBAN, NHBAN
      DIMENSION B(1800), B1(120)
      EQUIVALENCE (R(1),B(1)), ( PR(1),B1(1))
      IF (.NOT. CHANGE) GO TO 110
C*****************************************************************
C     REDUCE MATRIX A BY BLOCKS
      NB=0
      REWIND NDISK1
      REWIND NDISK2
      GO TO 30
C     SHIFT BLOCK OF EQUATIONS
   20 NB=NB+1
      DO 25 N=1,NNBAN
      NM=N+NNBAN
      DO 25 M=1,MBAND
```

```
      A(N,M)=A(NM,M)
   25 A(NM,M) = 0.0
C     READ NEXT BLOCK OF EQUATIONS INTO CORE
      IF (NUMBLK .EQ. NB) GO TO 40
   30 READ (NDISK1) ((A(N,M),M=1,MBAND),N=NLBAN,NHBAN)
      IF (NB .EQ. 0) GO TO 20
   40 CONTINUE
C     REDUCE BLOCK OF EQUATIONS
      DO 50 N=1,NNBAN
      C1=A(N,1)
      IF (C1 .EQ. 0.0) GO TO 50
      N1=N-1
      DO 49 L=2,MBAND
      C2=A(N,L)
      IF (C2 .EQ. 0.0) GO TO 49
      C=C2/C1
      I=N1+L
      J=0
      DO 48 K=L,MBAND
      J=J+1
      A(I,J)=A(I,J)-C*A(N,K)
   48 CONTINUE
   49 CONTINUE
   50 CONTINUE
C*****************************************************************
C     WRITE BLOCK OF REDUCED EQUATIONS ON DISK2
      WRITE (NDISK2) ((A(N,M),M=1,MBAND),N=1,NNBAN)
      IF (NB .NE. NUMBLK) GO TO 20
C     FORWARD SUBSTITUTION FOR VECTOR B
  110 REWIND NDISK2
      NB=0
      GO TO 130
C     SHIFT BLOCK OF EQUATIONS
  120 NB=NB+1
      DO 125 N=1,NNBAN
      NM=NNBAN+N
      B1(N)=B1(NM)
      B1(NM) = 0.0
      DO 125 M=1,MBAND
      A(N,M)=A(NM,M)
  125 A(NM,M) = 0.0
C     READ NEXT BLOCK OF EQUATIONS INTO CORE
      IF (NB .EQ. NUMBLK) GO TO 150
  130 READ (NDISK2) ((A(N,M),M=1,MBAND),N=NLBAN,NHBAN)
      NSTAR=(NB-1)*NNBAN
      DO 140 N=NLBAN,NHBAN
      M=NSTAR+N
  140 B1(N)=B(M)
      IF (NB .EQ. 0) GO TO 120
C     REDUCE VECTOR B - STORED IN B1
  150 DO 160 N=1,NNBAN
      C1=A(N,1)
      IF (C1 .EQ. 0.0) GO TO 160
      N1=N-1
```

```
      B1(N)=B1(N)/C1
      DO 159 L=2,MBAND
      C2=A(N,L)
      IF (C2 .EQ. 0.0) GO TO 159
      I=N1+L
      B1(I)=B1(I)-C2*B1(N)
  159 CONTINUE
  160 CONTINUE
      STORE THE REDUCED VECTOR BACK IN B
      IF (NB .EQ. NUMBLK) GO TO 180
      M=NSTAR
      DO 170 N=1,NNBAN
      M=M+1
  170 B(M)=B1(N)
      GO TO 120
*****************************************************************
      BACK - SUBSTITUTION
  180 BACKSPACE NDISK2
      NSTAR=NB*NNBAN+1
      DO 210 M=1,NNBAN
      N=NLBAN-M
      C1=A(N,1)
      IF (C1 .EQ. 0.0) GO TO 205
      N1=N-1
      DO 200 K=2,MBAND
      L=N1+K
  200 B1(N)=B1(N)-A(N,K)*B1(L)/C1
  205 NM=N+NNBAN
      B1(NM)=B1(N)
      N=NSTAR-M
      IF (N .GT. NDEG) GO TO 210
      B(N)=B1(NM)
  210 CONTINUE
      NB=NB-1
      IF (NB .EQ. 0) RETURN
      BACKSPACE NDISK2
      M=(NB-1)*NNBAN
      DO 220 N=1,NNBAN
      M=M+1
  220 B1(N)=B(M)
      READ (NDISK2) ((A(N,M),M=1,MBAND),N=1,NNBAN)
      GO TO 180
      END


      SUBROUTINE STRESS ( PUNCH)
      LOGICAL AXI, ERROR, QUAD, CHANGE, PUNCH, TWO
      COMMON NUMNP,NUMEL,NUMTC(5),E(15,4,5),EE(3),CODE(900),
     1T(900),Q,NAUX(900),NODE1(800),NODE2(800),NODE3(800),
     2NODE4(800),MAT(800),TELM(800),NUMPC,IBC(100),JBC(100),
     3LM(4),MTYPE,CON
      COMMON /ERASE/ R(900),Z(900),UR(900),UZ(900),PR(100),
     1HED(20)
      COMMON /LOGCAL/ AXI, ERROR, QUAD, CHANGE
```

```
      COMMON /IO/ IN,IPUNCH,IOUT,NDISK1,NDISK2,NFILE1,
     1NFILE2,NREC1
      COMMON/M2381/RR(5),ZZ(5),RCEN(800),ZCEN(800),P9(800),
     1P10(800)
      COMMON/M35681/XI(6),H(6,10),CC1(9),CC2(8),HH(6,10),
     1S(10,10),TT,C11,C12,C13,C44
      COMMON/M57891/A(120,60),P(10),TP(6),NUMBLK,MBAND,NDEG,
     1ND,ND2,NBSTF
      DIMENSION B(1800), SIG(9)
      EQUIVALENCE (R(1),B(1))
      LP=0
      SIGL=0
      SIG(3) = 0.0
      MPRINT=0
      TWO = .FALSE.
      DO 130 N=1,NUMEL
      NREC2=N
      FIND (NFILE2'NREC2)
      LM(1)=NODE1(N)
      LM(2)=NODE2(N)
      LM(3)=NODE3(N)
      LM(4)=NODE4(N)
      I1=0
      DO 20 I=1,4
      J=LM(I)+LM(I)
      I1=I1+1
      P(I1)=B(J-1)
      I1=I1+1
20    P(I1)=B(J)
      READ (NFILE2'NREC2)  TT,CC1,CC2,EE,C11,C12,C13,C44,HH,S
      TTT = TT*(TELM(N)-Q)
      DO 30 I=1,10
      S(9,I)=S(9,I)*EE(1)
30    S(10,I)=S(10,I)*EE(1)
      RR(1)=P9(N)*EE(1)
      RR(2)=P10(N)*EE(1)
      DO 40 J=1,8
      RR(1)=RR(1)-S(9,J)*P(J)
40    RR(2)=RR(2)-S(10,J)*P(J)
      S99=S(9,9)
      S1010=S(10,10)
      S910=S(9,10)
      S109=S(10,9)
      COM=S99*S1010-S910*S109
      IF (COM .EQ. 0.0) GO TO 50
      P(9)=(S1010*RR(1)-S910*RR(2))/COM
      P(10)=(S99*RR(2)-S109*RR(1))/COM
50    DO 60 I=1,6
      TP(I)=0.0
      DO 60 J=1,10
60    TP(I)=TP(I)+HH(I,J)*P(J)
      RR(1)=TP(2)
      RR(2)=TP(6)
      RR(3)=(TP(1)+TP(2)*RCEN(N)+TP(3)*ZCEN(N))/RCEN(N)
```

```
      RR(4)=TP(3)+TP(5)
*****************************************************************
      CALCULATE STRESS COMPONENTS R,Z,T,RZ
      SIG(1)=(C11*RR(1)+C12*RR(2)+C13*RR(3)-TTT)*EE(1)
      SIG(2)=(C12*RR(1)+C11*RR(2)+C13*RR(3)-TTT)*EE(1)
      IF (AXI) SIG(3)=((RR(1)+RR(2))*C13+C11*RR(3)-TTT)*EE(1)
      SIG(4)=C44*RR(4)*EE(1)
      EFFECTIVE STRESS AND EFFECTIVE STRAIN
      A1=SIG(1)-SIG(2)
      A2=SIG(2)-SIG(3)
      A3=SIG(3)-SIG(1)
      A4=SIG(4)*SIG(4)
      SIG(5)=SQRT (0.5*(A1*A1+A2*A2+A3*A3+6.0*A4))
      A5=SIG(1)+SIG(2)
      IF (.NOT. AXI) RR(3)=-A5*EE(2)/EE(1)
      B1=RR(1)-RR(2)
      B2=RR(2)-RR(3)
      B3=RR(3)-RR(1)
      SIG(6)=0.4714*SQRT((B1*B1+B2*B2+B3*B3)+1.5*RR(4)*RR(4))
      PRINCIPAL STRESSES
      A1=A1/2.0
      A5=A5/2.0
      B1=SQRT (A1*A1+A4)
      SIG(7)=A5+B1
      SIG(8)=A5-B1
      SIG(9)=28.648*ATAN2(SIG(4),A1)
*****************************************************************
      WRITE STRESSES
      IF (MPRINT) 90,70,90
   70 WRITE (IOUT,80)
   80 FORMAT('1'/' ELEM     RCEN    ZCEN',5X,'TEMP.',7X,
     1'R-STRESS  Z-STRESS  T-STRESS RZ-STRESS',7X,
     2'E-STRESS  E-STRAIN  MAX ST.    MIN ST. ANGLE'/)
      MPRINT=50
   90 MPRINT=MPRINT-1
      WRITE(IOUT,100)N,RCEN(N),ZCEN(N),TELM(N),(SIG(I),I=1,9)
  100 FORMAT (I5,1X,2F7.3,F10.0,5X,4F10.0,5X,F10.0,F10.7,
     12F10.0,F6.1)
      FIND THE LARGEST EFFECTIVE STRESS
      IF (SIGL .GE. SIG(5)) GO TO 105
      SIGL=SIG(5)
      LP=N
  105 IF (.NOT. PUNCH) GO TO 130
      IF (TWO) GO TO 110
      TWO = .TRUE.
      NSAVE = N
      RSAVE = RCEN(N)
      ZSAVE = ZCEN(N)
      SAVE7 = SIG(7)
      SAVE8 = SIG(8)
      GO TO 130
  110 TWO = .FALSE.
      WRITE(IPUNCH,120) NSAVE,RSAVE,ZSAVE,SAVE7,SAVE8,
     1N,RCEN(N),ZCEN(N),SIG(7),SIG(8)
```

```
  120 FORMAT (2(I6,2F7.2,2F10.0))
  130 CONTINUE
      IF (PUNCH .AND. TWO) WRITE(IPUNCH,120)
     1NSAVE,RSAVE,ZSAVE,SAVE7,SAVE8
      WRITE (IOUT,140) SIGL,LP
  140 FORMAT(/' LARGEST EFF. STRESS =',F12.0,
     1', AND IT OCCURS IN ELEM NO.',I4)
      RETURN
      END
```

*** JCL FOR DIRECT ACCESS & SEQUENTIAL FILES 4-7 ***

```
//G.FT04F001 DD UNIT=2314,SPACE=(TRK,(60,10)),
// DCB=(RECFM=VBS,LRECL=3516,BLKSIZE=3520)
//G.FT05F001 DD UNIT=2314,SPACE=(TRK,(60,10)),
// DCB=(RECFM=VBS,LRECL=3516,BLKSIZE=3520)
//G.FT06F001 DD UNIT=2314,SPACE=(280,(3200)),
//   DCB=DSORG=DA
//G.FT07F001 DD UNIT=2314,SPACE=(800,(800)),
//   DCB=DSORG=DA
```

APPENDIX B

FRACTURE CODE - INPUT INSTRUCTIONS AND PROGRAM LISTING

The fracture predictions are based on the Griffith and the McClintock-Walsh modified Griffith fracture criteria as given by Eqs. (2.1 - 2.5). These equations involve the uniaxial tensile strength, σ_t, the uniaxial compressive strength, σ_c, and the fracture surface coefficient of friction, μ_f of the material, and the maximum and the minimum principal stress components. These stress components with their associated element centroids are obtained as punched output using the stress code, TRATSA. This data, along with the problem outline cards and the plot scale information are input into the fracture code according to the format given below. The output of the fracture code is in the plot form which is then used to predict the approximate fracture zones. The fracture intensity levels (FIL) are plotted at the centroids of the fractured elements. The maximum to the minimum FIL for the McClintock-Walsh fracture mode (Eq. 2.4) is denoted by numerals 0-9. The letters A-H and S-Z are used to describe the fracture governed by the original Griffith criteria, Eqs. (2.1) and (2.2), respectively.

1. Name Card (8A4, 40X, A4):

   Cols. 1-32 Programmer's name

   73-76 Code word, NAME (must be punched)

The programmer's name given in the first thirty-two columns of this card is plotted on the output. Although the fracture code can

be used to analyze more than one set of data in one run, the name card must be put only once as the first card of all the data sets.

For each data set, the following cards are required.

2. Control card (7F7.2, 1X, 2F10.0, 2I5):

Cols. 1-7 Minimum R-coordinate to be plotted

8-14 Maximum R-coordinate to be plotted

15-21 Minimum Z-coordinate to be plotted

22-28 Maximum Z-coordinate to be plotted

29-35, 36-42 Horizontal and vertical dimensions of the page size of the plot. The order is not important.

43-49 Fracture surface coefficient of fracture, μ_f

51-60 Uniaxial compressive strength, σ_c

61-70 Uniaxial tensile strength, σ_t

71-75 Number of elements used in the stress analysis

76-80 Number of nodes defining the plot outline (49 maximum), NNGRID

3. Plot Outline Cards:

These cards are to be supplied only when NNGRID $\neq$ 0. The format is the same as that used for the nodal point cards in the stress code, TRATSA. The boundary condition information is, however, not necessary.

The control card and the plot outline cards must always be supplied for the first data set. The control card for any other data set may be omitted if all of the information for that set is identical with that of the previous set. For partial similarity, the control card may be modified as follows:

For identical fracture plot outline, Cols. 1-42 and Cols. 76-80 may be left blank.

For identical material properties, μ_f, σ_c, and σ_t, Cols. 43-70 may be left blank.

For identical stress analysis grids, Cols. 71-75 may be left blank.

With the exception of the first data set, any time a control card is supplied, a card with code word, NEW in Cols. 73-75 must precede.

The maximum page size of the fracture plot is determined by the plotter specifications. If the page dimensions are not supplied, the page size is defaulted to 8.5" x 11.0" and the grid is drawn leaving a minimum total margin of 2.8" in both directions.

4. Stress Output Set(s):

A stress output set consists of an Auxiliary Identification card followed by the element stress results. This deck is obtained through the stress code, TRATSA, and is to be input without any modification.

```
C      ***     FRACTURE  PATTERN  PLOTTER     ****************
C
       LOGICAL NPOS,ROTAT,SKIP,WITHIN
       COMMON /GRD/ R1(50),Z1(50),RR1(50),HED(20),NGRID,RMIN,
      1RMAX,ZMIN,ZMAX,ASZ,BSZ,SCAL
       COMMON /FRAC/ SIGMAX(800),SIGMIN(800),RCEN(800),
      1ZCEN(800),EMU1,EMU2,SIGC,SIGT,SIGT8,THETA,WITHIN(800)
       DIMENSION PNAME(8)
       DATA PNAME/32HPATEL, MAHENDRA R.                  /
       DATA PAME,PEW,PHAN,NUMEL,NREAD,NWRITE/4HNAME,4HNEW ,
      14HCHAN,0,1,3/
C**** CORRECTIVE ACTION FOR ILLEGAL DECIMAL CHARACTER INPUT
       CALL ERRSET (215,1,1,2)
C      ***    HEADING     ************************************
       NPOS=.TRUE.
       READ (NREAD,20) (HED(I),I=1,20)
   20  FORMAT (20A4)
       IF (HED(19) .NE. PAME) GO TO 40
       DO 30 I=1,8
   30  PNAME(I)=HED(I)

   40  IF (NPOS) CALL PENPOS (PNAME,32,0)
       NPOS=.FALSE.
       WRITE (NWRITE,60)
   60  FORMAT (/20X,'***  FRACTURE  PATTERNS  PLOTS  ***'/)
C      ***  GRID  OUTLINE  CARDS  ****************************
   65  READ (NREAD,70) RMI,RMX,ZMI,ZMX,ASIZ,BSIZ,EMU,SIGCC,
      1SIGTT,NEWEL,NNGRID
   70  FORMAT (7F7.2,1X,2F10.0,2I5)
       IF (EMU .EQ. 0.0) GO TO 80
       SIGC = SIGCC
       SIGT = SIGTT
       SIGT8 = -8.0*SIGT
       EMU3 = SQRT (1.0+EMU*EMU)
       EMU1 = EMU/EMU3
       EMU2 = (EMU3+EMU)/(EMU3-EMU)
   80  IF (NEWEL .EQ. 0) GO TO 90
       NUMEL = NEWEL
       SKIP = .FALSE.
   90  IF (NNGRID .EQ. 0) GO TO 125
       NGRID1 = NNGRID
C**** READ AND GENERATE GRID OUTLINE NODE CARDS ************
       CALL NODES (NGRID1,R1,Z1,NREAD)
       NGRID = NGRID1+1
       R1(NGRID) = R1(1)
       Z1(NGRID) = Z1(1)
       RMIN=RMI
       RMAX=RMX
       ZMIN=ZMI
       ZMAX=ZMX
       ASZ = 8.2
       BSZ = 5.7
       IF (ASIZ .EQ. 0.0) GO TO 122
       ASZ = ASIZ
```

```
      BSZ = BSIZ
      IF (ASZ .GE. BSZ) GO TO 121
      ASZ = BSIZ
      BSZ = ASIZ
  121 ASZ = ASZ-2.8
      BSZ = BSZ-2.8
  122 ROTAT = .FALSE.
      RDIF = RMAX-RMIN
      ZDIF = ZMAX-ZMIN
      ADIF = RDIF
      BDIF = ZDIF
      IF (ADIF .GE. BDIF) GO TO 124
      ADIF = ZDIF
      BDIF = RDIF
      ROTAT = .TRUE.
      DO 123 I = 1, NGRID
  123 RR1(I) = -R1(I)
  124 SCAL1 = ASZ/ADIF
      SCAL2 = BSZ/BDIF
      SCAL = SCAL1
      IF (SCAL2 .LT. SCAL1) SCAL = SCAL2
      ASZ = ADIF*SCAL
      BSZ = BDIF*SCAL
  125 CONTINUE
C     *** NEW STRESS DATA SET ***************************
      READ (NREAD,20) (HED(I),I=1,20)
  150 WRITE (NWRITE,170) (HED(I),I=1,18)
  170 FORMAT (/10X,18A4)
      IF (HED(19) .EQ. PHAN) SKIP = .FALSE.
      IF (SKIP) GO TO 185
      DO 175 N = 1, NUMEL, 2
      N1 = N+1
  175 READ (NREAD,176) RCEN(N),ZCEN(N),SIGMAX(N),SIGMIN(N),
     1RCEN(N1),ZCEN(N1),SIGMAX(N1),SIGMIN(N1)
  176 FORMAT (2(6X,2F7.2,2F10.0))
      DO 178 N = 1, NUMEL
      WITHIN(N) = .TRUE.
      IF (ZCEN(N) .LT. ZMIN .OR. ZCEN(N) .GT. ZMAX)GO TO 177
      IF (RCEN(N) .LT. RMIN .OR. RCEN(N) .GT. RMAX)GO TO 177
      GO TO 178
  177 WITHIN(N) = .FALSE.
  178 CONTINUE
      SKIP = .TRUE.
      IF (.NOT. ROTAT) GO TO 180
      THETA = -90.0
      DO 179 N = 1, NUMEL
      RSAVE = RCEN(N)
      RCEN(N) = ZCEN(N)
  179 ZCEN(N) = -RSAVE
      GO TO 188
  180 THETA = 0.0
      GO TO 188
  185 DO 186 N = 1, NUMEL,2
      N1 = N+1
```

```
  186 READ (NREAD,187) SIGMAX(N),SIGMIN(N),SIGMAX(N1),
     1SIGMIN(N1)
  187 FORMAT (2(20X,2F10.0))
  188 CONTINUE
C**** PLOT THE GRID OUTLINE, AND HEADING ********************
      CALL GRID (ROTAT)
C     ***  PLOT  FRACTURE  PATTERNS   **********************
      CALL FRACTR (NUMEL,NWRITE)
      CALL ENDPLT
C     ***  CHECK  FOR  NEW  SET  OF  STRESS  DATA   ********
      READ (NREAD,20,END=190) (HED(I),I=1,20)
      IF (HED(19) .EQ. PEW) GO TO 65
      GO TO 150
  190 CALL LSTPLT
      STOP
      END


      SUBROUTINE NODES (N,R,Z,NREAD)
      DIMENSION R(50),Z(50)
      RADIN=0.0174533
      M=1
   10 IF (M .GT. N) RETURN
      READ (NREAD,15) NA,IPOLAR,RA,ZA,RAD,THETA
   15 FORMAT (2I5,3F10.0,F5.0)
      NAM=NA-M
      IF (RAD .EQ. 0.0) GO TO 16
      THETA=THETA*RADIN
      R(NA)=RA+RAD*COS(THETA)
      Z(NA)=ZA+RAD*SIN(THETA)
      GO TO 17
   16 R(NA)=RA
      Z(NA)=ZA
   17 IF (NAM .EQ. 0) GO TO 25
      NDIFF=NAM+1
      IF (IPOLAR .GT. 0) GO TO 19
      DR=(R(NA)-R(M1))/NDIFF
      DZ=(Z(NA)-Z(M1))/NDIFF
      DO 18 I=1,NAM
      R(M)=R(M1)+DR
      Z(M)=Z(M1)+DZ
      M1=M
   18 M=M+1
      GO TO 25
   19 DTH=(THETA-THST)/NDIFF
      DO 20 I=1,NAM
      THST=THST+DTH
      R(M)=RA+RAD*COS(THST)
      Z(M)=ZA+RAD*SIN(THST)
   20 M=M+1
   25 M1=M
      M=M+1
      THST=THETA
      GO TO 10
      END
```

```
      SUBROUTINE GRID (ROTAT)
      LOGICAL ROTAT
      COMMON /GRD/ R1(50),Z1(50),RR1(50),HED(20),NGRID,RMIN,
     1RMAX,ZMIN,ZMAX,ASZ,BSZ,SCAL
C**** PLOT THE GRID OUTLINE **********************************
      IF (ROTAT) GO TO 10
C**** NATURAL ORIENTATION ************************************
      CALL NEWPLT (1.0,2.0,ASZ+2.8)
      CALL ORIGIN (RMIN,ZMIN)
      XINN = ASZ+0.6
      RMAXX = XINN/ SCAL+RMIN
      CALL XSCALE (RMIN,RMAXX,XINN)
      YINN = BSZ+0.6
      ZMAXX = YINN/SCAL +ZMIN
      CALL YSCALE (ZMIN,ZMAXX,YINN)
      CALL XAXIS (0.)
      CALL YAXIS(0.0)
      CALL NUM (0.0,-0.20,0.105,RMIN,0.0,2)
      CALL SYM (ASZ+0.8,-0.05,0.105,'R',0.0,1)
      CALL NUM (ASZ,-0.20,0.105,RMAX,0.0,2)
      CALL NUM (-0.095,0.0,0.105,ZMIN,90.0,2)
      CALL SYM  (0.05,BSZ+0.8,0.105,'Z',90.0,1)
      CALL NUM (-0.095,BSZ,0.105,ZMAX,90.0,2)
      CALL XYPLT (R1,Z1,NGRID,1,-1)
      GO TO 20
C**** ROTATE THE GRID THRU 90 DEGREES, CLOCKWISE ************
   10 CONTINUE
      CALL NEWPLT (1.0,8.5,ASZ+2.8)
      CALL ORIGIN (ZMIN,-RMIN)
      XINN = ASZ+0.6
      ZMAXX = XINN/SCAL +ZMIN
      CALL XSCALE (ZMIN,ZMAXX,XINN)
      YINN = BSZ+0.6
      RMAXX = YINN/SCAL +RMIN
      RRMIN = -RMAXX
      RRMAX = -RMIN
      CALL YSCALE (RRMIN,RRMAX,YINN)
      CALL XAXIS (0.0)
      CALL YAXIS(0.0)
      CALL NUM(0.0,0.095,0.105,ZMIN,0.0,2)
      CALL SYM (ASZ+0.8,-0.05,0.105,'Z',0.0,1)
      CALL NUM (ASZ,0.095,0.105,ZMAX,0.0,2)
      CALL NUM (-0.20,0.0,0.105,RMIN,-90.0,2)
      CALL SYM (-0.05,-BSZ-0.8,0.105,'R',-90.0,1)
      CALL NUM (-0.20,-BSZ,0.105,RMAX,-90.0,2)
      CALL XYPLT (Z1,RR1,NGRID,1,-1)
   20 CONTINUE
C**** PLOT HEADING AND LEGEND ********************************
      NHT = ASZ*2.2
      HIGHT = 0.007*NHT
      XX=0.1
      YY=-0.7
      IF (ROTAT) YY=0.58
      CALL SYM (XX,YY,HIGHT,HED,0.0,72)
```

```
      RETURN
      END


      SUBROUTINE FRACTR (NUMEL,NWRITE)
      LOGICAL WITHIN
      COMMON /FRAC/ SIGMAX(800),SIGMIN(800),RCEN(800),
     1ZCEN(800),EMU1,EMU2,SIGC,SIGT,SIGT8,THETA,WITHIN(800)
      DIMENSION DIFFM(400),RM(400),ZM(400),DIFFT(400),
     1RT(400),ZT(400),DIFFC(400),RC(400),ZC(400),D(11)
C     ***  INITIALIZE  ***************************************
      DMAXM = 0.0
      DMINM = 1.0 E10
      NM = 0
      DMAXT = 0.0
      DMINT = 1.0 E10
      NT = 0
      DMAXC = 0.0
      DMINC = 1.0 E10
      NC = 0
C     ***************************************************************
      DO 40 N = 1, NUMEL
      IF (.NOT. WITHIN(N)) GO TO 40
      SMIN = SIGMIN(N)
      SMAX = SIGMAX(N)
      IF (SMIN .GE. 0.0) GO TO 20
      IF (SMAX .LE. 0.0) GO TO 5
      C1 = SMIN+SMAX
      C2 = SMAX-SMIN
      C=C1+C2*EMU1
      IF (C .GT. 0.0) GO TO 10
C     ***  CHECK FOR MC-CLINTOCK - WALSH FRACTURE  *********
    5 RHS = SMAX*EMU2+SIGC
      IF (SMIN .GT. RHS) GO TO 40
      DIFF = RHS-SMIN
      IF (DIFF .GT. DMAXM) DMAXM = DIFF
      IF (DIFF .LT. DMINM) DMINM = DIFF
      NM = NM+1
      DIFFM(NM) = DIFF
      RM(NM) = XSTOIN(RCEN(N))
      ZM(NM) = YSTOIN(ZCEN(N))
      GO TO 40
C     ***  CHECK FOR GRIFFITH FRACTURE CRITERION  **********
   10 CC = 3.0*SMAX+SMIN
      IF (CC .GE. 0.0) GO TO 20
C     ***  GRIFFITH - COMPRESSION  *************************
      C = C2*C2/C1
      IF (C .GT. SIGT8) GO TO 40
      DIFF = SIGT8-C
      IF (DIFF .GT. DMAXC) DMAXC = DIFF
      IF (DIFF .LT. DMINC) DMINC = DIFF
      NC = NC+1
      DIFFC(NC) = DIFF
      RC(NC) = XSTOIN(RCEN(N))
```

```
      ZC(NC) = YSTOIN(ZCEN(N))
      GO TO 40
C     ***  GRIFFITH - TENSION  ****************************
   20 IF (SMAX .LT. SIGT) GO TO 40
      DIFF = SMAX-SIGT
      IF (DIFF .GT. DMAXT) DMAXT = DIFF
      IF (DIFF .LT. DMINT) DMINT = DIFF
      NT = NT+1
      DIFFT(NT) = DIFF
      RT(NT) = XSTOIN(RCEN(N))
      ZT(NT) = YSTOIN(ZCEN(N))
   40 CONTINUE
C     *** PLOT  FRACTURE  INTENSITY  LEVELS  ***************
C     ***  MC-CLINTOCK WALSH  ****************************
C     ***  MAX TO MIN FIL. DENOTED BY NUM. 0 THRU 9  *******
      IF (NM .EQ. 0) GO TO 65
      DINC = (DMAXM-DMINM)/10.0
      D(1) = DMINM
      DO 50 I = 2, 10
   50 D(I) = D(I-1)+DINC
      D(11) = DMAXM
      WRITE (NWRITE,51) DMINM,DMAXM,DINC
   51 FORMAT (19X,'MCCLINTOCK-WALSH, MIN,MAX,INCR :',3F10.0)
      DO 60 I = 1,NM
      DIFF = DIFFM(I)
      DO 55 J = 2, 10
      IF (D(J) .GE. DIFF) GO TO 56
   55 CONTINUE
      J = 11
   56 NSYM = 123-J
      CALL SYM (RM(I),ZM(I),0.07,NSYM,THETA,-1)
   60 CONTINUE
C     ***  GRIFFITH TENSION  ******************************
C     ***  MAX TO MIN FIL. DENOTED BY LETTERS A THRU H  ****
   65 IF (NT .EQ. 0) GO TO 85
      DINC = (DMAXT-DMINT)/8.0
      D(1) = DMINT
      DO 70 I = 2, 8
   70 D(I) = D(I-1)+DINC
      D(9)  = DMAXT
      WRITE (NWRITE,71) DMINT,DMAXT,DINC
   71 FORMAT (19X,'GRIFFITH TENSION, MIN,MAX,INCR :',3F10.0)
      DO 80 I = 1,NT
      DIFF = DIFFT(I)
      DO 75 J = 2, 8
      IF (D(J) .GE. DIFF) GO TO 76
   75 CONTINUE
      J = 9
   76 NSYM = 74-J
      CALL SYM (RT(I),ZT(I),0.07,NSYM,THETA,-1)
   80 CONTINUE
C     ***  GRIFFITH COMPRESSION  **************************
C     ***  MAX TO MIN FIL. DENOTED BY LETTERS S THRU Z  ****
   85 IF (NC .EQ. 0) RETURN
```

```
      DINC = (DMAXC-DMINC)/8.0
      D(1) = DMINC
      DO 90 I = 2, 8
   90 D(I) = D(I-1)+DINC
      D(9)  = DMAXC
      WRITE (NWRITE,91) DMINC,DMAXC,DINC
   91 FORMAT (19X,'GRIFFITH COMP.  , MIN,MAX,INCR :',3F10.0)
      DO100 I = 1,NC
      DIFF = DIFFC(I)
      DO 95 J = 2, 8
      IF (D(J) .GE. DIFF) GO TO 96
   95 CONTINUE
      J = 9
   96 NSYM = 107-J
      CALL SYM (RC(I),ZC(I),0.07,NSYM,THETA,-1)
  100 CONTINUE
      RETURN
      END
```

APPENDIX C

FIELD TEST RESULTS*

The Rock Mechanics and Explosives Research Center at the University of Missouri-Rolla has been conducting extensive field research on the thermal fragmentation of in situ rock. The tests are being conducted on Missouri red granite at a quarry near Graniteville, Missouri and are designed to lead to the development of a prototype excavation machine.

The choice of the process parameters for the field tests is mainly governed by practical aspects such as availability of equipment, limitations in their application, and the economy of the overall operation. For the theoretical analysis using a numerical treatment, however, the governing factor involves computer time and storage considerations. The typical dimensions used for the theoretical studies were thus two to three times smaller than those used in the field tests. Also, the rock type used for the theoretical analysis was Dresser basalt as all the properties of Missouri red granite were not available. A one-to-one comparison of the theoretical and the field test results is obviously not possible. Nevertheless, the field test results on a qualitative basis were found to be in good agreement with the predicted fracture patterns as well as the fracture length-fracture time characteristics.

Due to equipment limitations, most of the tests were conducted using a maximum of three heater holes drilled in a row parallel to a

---

*For details, see [15].

free surface as shown in the bottom half of Fig. C.1. The free surface was found necessary for rock displacement relief. The fracture pattern for this test configuration consisted of perpendicular cracks across the holes and subsurface cracks parallel to the working face and passing approximately through the center of the inclusions. This fracture pattern is in good agreement with the one predicted theoretically.

A second test configuration involved a total of four heater holes drilled at the corners of a square as shown in the top center of Figs. C.1 and C.2. Although this test configuration, too, is somewhat different from the one theoretically analyzed, the results of test data available thus far were found to compare quite well with the theoretical predictions.

For the particular test which used only thermal energy for fragmentation the hole spacing used was 18.0 in. The heater holes were 24.0 in. deep and approximately 2.25 in. in diameter. The fracture length was thus approximately 15.75 in. The distance between the free surfaces and the nearest hole centers was 10.0 in. The heat was supplied by electric arcs between two one-half inch diameter carbon electrodes placed near the bottom of the holes. The arc temperature is estimated at about 10,000°F, and justifies the use of a melted surface boundary condition in the theoretical analysis.

For the test parameters described above, hairline fractures on the work face across the holes and parallel to the free surfaces were visible after about 12 minutes. The fractures parallel to the work face were seen almost simultaneously. After 29 minutes the test was

FIG. C.1 THREE - AND FOUR-HOLE FIELD TEST CONFIGURATIONS

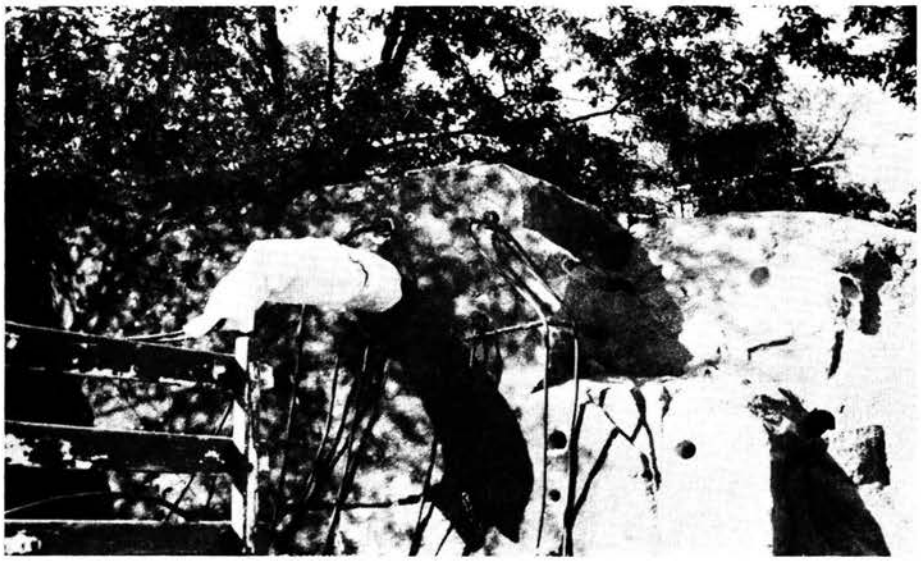

FIG. C.2 FOUR-HOLE FIELD TEST AND TYPICAL RESULTING EXCAVATION

FIG. C.3 VIEW OF AN EXCAVATION AFTER REMOVAL OF A FRAGMENTED BLOCK

stopped as the fracturing was complete. The fractured block was removed from the parent material with the help of pry bars. A close-up and an overall view of the excavation after the removal of the blocks are shown in Figs. C.3 and C.2, respectively. This typical fracture pattern is in good agreement with that predicted theoretically.

It is important to note that the theoretical predictions regarding the fracture patterns remain unchanged regardless of the rock type, although the fracture times may vary considerably from one rock type to another. This is demonstrated by the results of the laboratory tests conducted on single blocks of Missouri red granite and Dresser basalt using approximately centered single holes, about 10.0 in. deep.

Rock Type	Block Dimensions	Power (kw)	Fracture Time
Missouri red granite	24" x 24" x 20"	6	9 min.
Missouri red granite	24" x 24" x 24"	5	6 min.
Dresser basalt	30" x 30" x 24"	6	3 min.

Although the block dimensions are not identical, the above results indicate that the fracture time for Missouri red granite is larger than that of Dresser basalt by a factor of 3 at least. Nevertheless, the fracture patterns observed during the field tests on Missouri red granite show good agreement with those predicted theoretically using the properties of Dresser basalt. This indicates that while the fracture time is considerably influenced by the rock type properties, the fracture pattern is governed by the loading configuration alone.